6
CONCLUSIONS

This report describes the technical bases for relaxation of inspection requirements based on the surface stress improvement provided by peening. Given that the applicable requirements outlined in Table 1-1 (including the peening performance criteria) are met, this report defines appropriate inspection requirements and intervals for Alloy 82/182 DMWs and Alloy 600 RPVHPNs that have been treated by SSI methods for the purpose of mitigating PWSCC. The deterministic and probabilistic calculations show that, given an SSI process that meets the applicable performance criteria, inspection of the peened components at the schedules specified in Table 4-1 and Table 4-3 is appropriate after SSI treatment.

The deterministic and probabilistic analyses discussed in Section 5 and Appendix A and Appendix B conservatively model the effects of peening on PWSCC. These analyses show that the peening provides large benefits in terms of preventing initiation of new PWSCC and that any cracks that could be present after pre-peening inspections and repairs are effectively addressed by inspections subsequent to peening. Section 6.1 and Section 6.2 summarize the main bases for the effectiveness of peening mitigation and for the relaxed in-service inspection requirements. Section 6.3 lists the application-specific information needed to support inspection relief.

6.1 Bases for Effectiveness of Peening

An application-specific qualification report is used to demonstrate that peening of a specific set of Alloy 82/182 DMWs or Alloy 600 RPVHPNs will be effective to mitigate PWSCC. From a general perspective, the water jet and laser peening processes described in MRP-267R1 are concluded to be effective based on the following:

- There is extensive industrial experience that shows that peening of many types is effective at inhibiting the initiation of both fatigue and stress corrosion cracks. For this reason, peening of many types is used in various industrial applications to improve resistance to these modes of cracking.
- Over 25 years of service experience with shot peening of steam generator tubes has shown that the peening provides large benefits with regard to mitigation of PWSCC of the tubes.
- As described in MRP-267R1 [4], extensive laboratory tests have been performed of samples exposed to peening processes being considered for use on DMWs and RPVHPNs. These tests have shown that these peening processes do not result in growth of any pre-existing flaws during peening, and that they prevent growth of flaws with depths less than the depth of the compressive stress field developed by peening.
- Extensive testing, including examination of many peened samples and test blocks, has been performed of peening processes as described in MRP-267R1 [4]. No adverse effects have been identified in this testing. Peening has been extensively used in Japanese PWRs and BWRs for 14 years with no reported adverse effects to the peened components. Additionally,

shot peening has been widely used since the mid-1980s in steam generator tubes as a PWSCC mitigation method, with no adverse effects being identified.

6.2 Bases for Appropriate Relaxation of Inspection Requirements After Peening

Appropriate relaxed in-service inspection requirements for Alloy 82/182 DMWs and Alloy 600 RPVHPNs that have been mitigated by peening are shown in Table 4-1 and Table 4-3, respectively. The main bases for concluding that the defined relaxations of the in-service inspection requirements are appropriate are as follows:

- The deterministic and probabilistic analyses discussed in Section 5 and Appendix A and Appendix B show that risks of leakage and nozzle ejection are reduced for mitigated components inspected at the relaxed schedule in comparison to the risks for unmitigated components inspected at currently required schedules.
- The probabilistic analyses include significant conservatisms such that the benefits of peening tend to be under predicted. Among other conservatisms, the nominal input values for peening bases cases correspond to the bounding performance criteria for the minimum peening residual stress effect. These conservatisms provide confidence that the combination of SSI using peening coupled with the relaxed schedule for inspections will ensure that nuclear safety, as well as defense in depth, is maintained.

6.3 Application-Specific Information Supporting Inspection Relief

The licensee shall provide the following technical information to support requests for inspection relief based on peening surface stress improvement meeting the applicable performance criteria:

- Identification of the components to be given surface stress improvement peening treatments, together with identification of the specific areas to be treated.
- Identification of the specific equipment and processes that will be used for each area of each component.
- Identification of any limitations in the accessibility of the treated surface for the peening equipment and process.
- Identification of the specific changes in inspection requirements that are requested based on application of surface stress improvement by peening.
- A reference to the peening process qualification report.

The peening process shall be qualified and the qualification shall be documented in a qualification report. In accordance with applicable QA requirements (Section 2.1), the qualification report shall be reviewed by the licensee as part of the pre-implementation approval for peening mitigation.

The following technical information shall be included in the peening process qualification report:

- Discussion of how the specific processes that will be used have been demonstrated to be effective per the criteria discussed in this report, including surface stress magnitude, compressive residual stress depth, and sustainability of the stress effect. Included shall be a

description of the demonstration testing of peening of specimens or test sections representative of the geometry, accessibility, and surface condition of the component to be peened.

- Discussion of how the specific processes that will be used have been demonstrated to result in no adverse effects.
- Essential variables with associated ranges of acceptable values for the specific application, plus a description of the process controls to ensure that the essential variables will be within their acceptable ranges.
- Discussion of the specific process or controls that will ensure that the coverage requirements are met with a high degree of confidence, including what overlap of peening beyond the susceptible material is required.
- Description of plans for addressing contingencies, such as equipment failure, during performance of peening.

An application- specific post-peening report shall be developed to document the performance of peening and verification that the peening effect met the applicable performance criteria. The following information shall be included in the post-peening report:

- Description of the components that were peened
- Identification of personnel and equipment used for the peening, together with qualification information for the equipment and personnel
- Results of the pre-peening NDE
- Description of any repairs or other disposition of reported indications made in response to the pre-peening inspections
- Verification that the required peening coverage was obtained and that the peening process essential variables were maintained within their acceptable ranges
- Listing and descriptions of any problems or unusual events that occurred during the peening, and how these were handled
- Dispositioning of any criteria that were not met as a corrective action

6.4 Consideration for Pre-Mobilization

It may be prudent to pre-mobilize a response to a flaw detection in the pre-peening inspection, depending on industry and plant-specific experience. If there is a reasonable likelihood that shallow flaws could be present, preparations may be made to remove them if they are detected, e.g., by grinding and polishing. If there is a reasonable likelihood of flaws being present that are too deep to be removed by grinding and polishing, other mitigation measures may be considered or preparations may be made for local removal and repair of such flaws (e.g., by grinding and welding).

7
REFERENCES

1. ASME Code Case N-770-1, "Alternative Examination Requirements and Acceptance Standards for Class 1 PWR Piping and Vessel Nozzle Butt Welds Fabricated With UNS N06082 or UNS W86182 Weld Filler Material With or Without Application of Listed Mitigation Activities," Section XI, Division 1, American Society of Mechanical Engineers, New York, Approval Date: December 25, 2009.
2. ASME Code Case N-729-1, "Alternative Examination Requirements for PWR Reactor Vessel Upper Heads With Nozzles Having Pressure-Retaining Partial-Penetration Welds," Section XI, Division 1, American Society of Mechanical Engineers, New York, Approval Date: March 28, 2006.
3. ASME Code Case N-722-1, "Additional Examinations for PWR Pressure Retaining Welds in Class 1 Components Fabricated with Alloy 600/182/82 Materials," Section XI, Division 1, American Society of Mechanical Engineers, New York, Approval Date: January 26, 2009.
4. *Materials Reliability Program: Technical Basis for Primary Water Stress Corrosion Cracking Mitigation by Surface Stress Improvement (MRP-267, Revision 1)*, EPRI, Palo Alto, CA: 2012. 1025839. [Freely Available at www.epri.com]
5. ASME Boiler and Pressure Vessel Code 2013, Section III, ASME, 2013.
6. ASME Boiler and Pressure Vessel Code 2013, Section XI, ASME, 2013.
7. Section titled "Peening," page 891, *ASM Metals Handbook*, Ninth Edition, Volume 6, "Welding, Brazing and Soldering," ASM, 1983.
8. Letter from A. Byk (ASME) to D. Weakland (Ironwood Consulting, LLC), "ASME BPVC, Section III, Division 1, NB-4422, Peening (1968 Edition through the 2011 Addenda)," 12-1192, dated August 22, 2012.
9. Letter from R. Crane (ASME) to D. Weakland (Ironwood Consulting, LLC), "ASME BPVC, Section XI, IWA-4621(c) and IWA-4651(g), 1989 Edition through the 2013 Edition," 12-1238, dated November 8, 2012.
10. *Materials Reliability Program Generic Evaluation of Examination Coverage Requirements for Reactor Pressure Vessel Head Penetration Nozzles, Revision 1 (MRP-95R1NP)*, EPRI, Palo Alto, CA: 2004. 1011225. [NRC ADAMS Accession No.: ML043200602]
11. *Materials Reliability Program: An Assessment of the Control Rod Drive Mechanism (CRDM) Alloy 600 Reactor Vessel Head Penetration PWSCC Remedial Techniques (MRP-61)*, EPRI, Palo Alto, CA: 2003. 1008901. [Freely Available at www.epri.com]
12. R. Smith, "Reactor Vessel Head CRDM Nozzle Repairs with Abrasive Water Jet Remediation," AREVA presentation at *Industry – NRC 2010 Meeting on PWSCC Mitigation*, Rockville, MD, July 13, 2010. [NRC ADAMS Accession No.: ML102020677]

13. Letter from U.S. Nuclear Regulatory Commission to G. Hamrick, "Shearon Harris Nuclear Power Plant, Unit 1 -Relief Request 13R-11 For Reactor Vessel Closure Head Penetration Nozzles Repair Inservice Inspection Program -Third 10-Year Interval (TAC No. MF1876)," dated September 13, 2013. [NRC ADAMS Accession No.: ML13238A154]

14. *Materials Reliability Program: Reactor Vessel Closure Head Penetration Safety Assessment for U.S. PWR Plants (MRP-110NP): Evaluations Supporting the MRP Inspection Plan,* EPRI, Palo Alto, CA: 2004. 1009807-NP. [NRC ADAMS Accession No.: ML041680506]

15. *Materials Reliability Program: Reevaluation of Technical Basis for Inspection of Alloy 600 PWR Reactor Vessel Top Head Nozzles (MRP-395).* EPRI, Palo Alto, CA: 2014. 3002003099. [Freely Available at www.epri.com]

16. D. Rudland, J. Broussard, et al., "Comparison of Welding Residual Stress Solutions for Control Rod Drive Mechanism Nozzles," *Proceedings of the ASME 2007 Pressure Vessels & Piping Division Conference: PVP2007,* San Antonio, Texas, July 2007.

17. *Materials Reliability Program: Development of Probability of Detection Curves for Ultrasonic Examination of Dissimilar Metal Welds (MRP-262, Revision 1) – Typical PWR Leak-Before-Break Line Locations,* EPRI, Palo Alto, CA: 2009. 1020451. [Freely Available at www.epri.com]

18. Section titled "Shot Peening," page 131, *ASM Handbook,* Volume 5, "Surface Engineering," ASM, 1994.

19. Letter from B. C. Rudell (Exelon) and A. Demma (EPRI) to U.S. NRC, "Response to the NRC Request for Additional Information (RAI) related to Electric Power Research Institute (EPRI) MRP-335, Revision 1, "Topical Report for Primary Water Stress Corrosion Cracking Mitigation by Surface Stress Improvement [Peening]" (TAC No. MF2429)," MRP 2014-027, dated October 10, 2014. [NRC ADAMS Accession No.: ML14288A370]

20. *Materials Reliability Program: Prediction of Relaxation of Peening Residual Stresses in Alloy 600 (MRP-397).* EPRI, Palo Alto, CA: 2014. 3002003955. [Freely available at www.epri.com]

21. *Materials Reliability Program: Primary System Piping Butt Weld Inspection and Evaluation Guidelines (MRP-139, Revision 1),* EPRI, Palo Alto, CA: 2008. 1015009. [Freely Available at www.epri.com]

22. *Materials Reliability Program: Inspection Plan for Reactor Vessel Closure Head Penetrations in U.S. PWR Plants (MRP-117),* EPRI, Palo Alto, CA: 2004. 1007830. [Freely Available at www.epri.com]

23. *Materials Reliability Program: Reactor Vessel Head Nozzle and Weld Safety Assessment (MRP-103NP),* EPRI, Palo Alto, CA: 2004. 1009402. [NRC ADAMS Accession No.: ML041680477]

24. *Materials Reliability Program: RV Head Nozzle and Weld Safety Assessment for Westinghouse and Combustion Engineering Plants (MRP-104NP),* EPRI, Palo Alto, CA: 2004. 1009403. [NRC ADAMS Accession No.: ML041680483]

25. *Materials Reliability Program: Probabilistic Fracture Mechanics Analysis of PWR Reactor Pressure Vessel Top Head Nozzle Cracking (MRP-105NP)*, EPRI, Palo Alto, CA: 2004. [NRC ADAMS Accession No.: ML041680489]

26. *Materials Reliability Program (MRP) Crack Growth Rates for Evaluating Primary Water Stress Corrosion Cracking (PWSCC) of Thick-Wall Alloy 600 Materials (MRP-55) Revision 1*, EPRI, Palo Alto, CA: 2002. 1006695. [Freely Available at www.epri.com]

27. *Materials Reliability Program Crack Growth Rates for Evaluating Primary Water Stress Corrosion Cracking (PWSCC) of Alloy 82, 182, and 132 Welds (MRP-115)*, EPRI, Palo Alto, CA: 2004. 1006696. [Freely Available at www.epri.com]

28. *3-D Finite Element Software for Cracks: User's Manual v2.7.* Structural Reliability Technology – FEA Crack.

29. *Materials Reliability Program: Technical Basis for Reexamination Interval Extension for Alloy 690 PWR Reactor Vessel Top Head Penetration Nozzles (MRP-375).* EPRI, Palo Alto, CA: 2014. 3002002441. [Freely Available at www.epri.com]

30. *Materials Reliability Program: Effects of Surface Peening on the Inspectability of Nondestructive Evaluation*, EPRI, Palo Alto, CA: 2013. 3002000656.

31. *Materials Reliability Program: Study of New Mitigation Technique Effects on Nondestructive Evaluation Inspectability*, EPRI, Palo Alto, CA: 2014. 3002002952.

A
PROBABILISTIC ASSESSMENT CASES FOR ALLOY 82/182 DISSIMILAR METAL WELDS IN PRIMARY SYSTEM PIPING

A.1 Scope of Assessment

The probabilistic modeling presented in this appendix explicitly considers two example large-diameter Alloy 82/182 dissimilar metal welds in PWR primary system piping: a reactor vessel outlet nozzle operating at reactor hot-leg temperature and a reactor vessel inlet nozzle operating at reactor cold-leg temperature. The reactor vessel outlet and inlet nozzles are considered to be the main candidates for peening where access limitations may preclude other types of mitigation from the exterior (i.e., mechanical stress improvement and weld overlay). However, considering the range of sensitivity cases included (including the effect of variability in pipe loads), it is concluded that the examination requirements of Section 4 are also valid for other Alloy 82/182 piping butt weld locations, including large-diameter reactor coolant pump suction and discharge nozzles in B&W- and CE-designed plants, reactor vessel safety injection nozzles in two-loop Westinghouse-designed plants, and reactor vessel core flood nozzles in B&W-designed plants. These other cited locations operate at or below reactor cold-leg temperature. The calculations presented in this appendix showed large improvement in the leakage probability versus the case without peening and with inspections performed per intervals applicable to unmitigated welds.

A.2 Probabilistic Modeling Methodology

The integrated probabilistic modeling framework that is used to study the effect of peening DMW components on PWSCC combines the individual models discussed in Sections A.3 through A.6. Namely, this integrated probabilistic modeling framework is used to predict leakage criterion statistics, which are discussed in Section A.7, over the operating lifetime of the unit. Results generated with this model are given in Section A.9, using the inputs and uncertainties discussed in Section A.8.

The DMW probabilistic model described in this appendix applies a framework similar to that of the xLPR probabilistic software tool ([1], [2]), which is currently under development under sponsorship of NRC and EPRI.[11] For example:

[11] This project, known as xLPR for Extremely Low Probability of Rupture, is developing a fully probabilistic, fracture-mechanics-based computational tool to evaluate the rupture probability of reactor coolant piping. In the xLPR Pilot Study [2] concluded in 2011, the project was focused on evaluating pipe rupture probabilities within Alloy 82/182 dissimilar metal welds located in lines licensed for leak-before-break (LBB) as allowed under General Design Criterion 4, "Environmental and Dynamic Effects Design Bases," of Appendix A, "General Design Criteria for Nuclear Power Plants," to 10 CFR 50.

- Uncertainty propagation is handled by sampling input and parameter values from appropriately selected probability distributions (with appropriately selected bounds) in the main model loop, prior to the time looping structure. It is noted that for simplicity the model discussed in this report does not treat differently epistemic (i.e., due to incomplete knowledge) and aleatory (i.e., due to random variation) uncertainties.
- Event scheduling for a given weld, including operating, mitigation, inspection, and PWSCC initiation times, is developed in the main loop prior to entering the time looping structure.
- If one or more of the predicted PWSCC initiation times, adjusted for differences in stress and temperature, are less than the final operating time and the peening time (if applied), the time looping structure is entered. Each active flaw is allowed to grow until it coalescences with another active flaw, it achieves through-wall crack growth, it is detected and repaired, or it reaches the end of the operation partially through-wall.
- Initiations, leaks, repairs, among other events, are tracked as a function of operating cycle for each Monte Carlo realization and summary statistics are compiled at the end of each Monte Carlo run.

However, there are also several key differences between the DMW probabilistic model and xLPR Version 2.0:

- The DMW model described in this report takes a simplified approach of modeling through-wall penetration but not pressure boundary rupture. Growth after through-wall penetration, crack opening displacement and leak rate, and component stability are not explicitly modeled. However, by demonstrating a greatly reduced probability of through-wall penetration, the results demonstrate a reduced risk of large flaws that could compromise structural integrity.
- As the cracking degradation concern in Alloy 82/182 piping butt welds is dominated by PWSCC initiation and growth, fatigue initiation and growth are not modeled in the DMW model described in this report. xLPR Version 2.0 predictions are expected to confirm the marginal effect of fatigue on leakage risks in piping butt weld components.
- xLPR Version 2.0 includes treatment for accident conditions, such as seismic loading. These accident conditions are of interest in xLPR primarily for their contribution to stability risks. As stated above, the DMW probabilistic model presented in this report does not consider stability risks explicitly and therefore modeling of accident loads is not critical.
- PWSCC initiation modeling is similar between both probabilistic models. Both utilize semi-empirical model forms with key coefficients calibrated with field data for PWSCC detections in butt weld components in domestic plants. Both utilize circumferential discretization in order to model multiple flaw formation. However, in addition to the Weibull initiation model, the xLPR Version 2.0 model includes two additional initiation model forms. Furthermore, the xLPR initiation model factors in temporal variation using a Miner's rule approximation for damage accumulation. This approach enables the treatment of changing surface stresses or temperature. The DMW probabilistic model described in this report treats only one key temporal change—the change in surface stresses at the time of peening—but otherwise does not treat temporal variation. Studies with temporal variation were not of importance for this report.

- The probabilistic model discussed in this report utilizes the weld residual stress profile model form from the xLPR Pilot Study—third or fourth order polynomials fit to a set of constraints on the value of stresses at various through-wall positions. In xLPR Version 2.0, the weld residual stress profile progressed to a piecewise linear model with stress defined at up to 26 points through the component thickness. While the xLPR Version 2.0 model affords more flexibility in the definition of weld residual stress, the primary characteristics of the weld residual stress (i.e., ID surface stress, OD surface stress, tensile-compressive crossover point, and force balance in the case of axial stresses) are well captured in the DMW model.
- The DMW model described in this report includes more detail for modeling peening stress profiles. This includes explicit definition of the peening stress profile with surface compressive stress and penetration characteristics, treatment of stress redistribution, and implementation of a partial crack closure methodology. xLPR Version 2.0 allows the specification of a surface stress component with the capability to mimic the effect of peening on PWSCC initiation, but stress profiles have not been developed within xLPR to mimic the penetration of the peening stress effect into the component thickness.
- The probabilistic model discussed in this report has the added capability (relative to the xLPR tool) of allowing correlation of selected input parameters during runtime. Specifically, multi-dimensional normal deviates are computed using a covariance matrix Cholesky-decomposition-based approach as discussed in *Numerical Recipes* [3]. For a given pair of correlated input parameters, a Pearson product-moment correlation coefficient, which provides a measure of the strength of the linear relationship between two variables, is specified and the pair of correlated random deviates is then used to sample the relevant input parameter distributions. The Pearson coefficient provides a measure of the strength of the linear relationship between two variables where a value of 1 indicates a perfect positive correlation (i.e., a perfect linear correlation with a positive slope), a value of -1 indicates a perfect negative correlation (i.e., a perfect linear correlation with a negative slope), and a value of 0 indicates that there is no linear relationship between the given variables.
- It is noted that for convenience of analysis, the probabilistic model described in this report has been designed to simulate up to three distinct DMWs (i.e., welds with different geometries, temperatures, inspection and mitigation schedules, etc.) during a single Monte Carlo run.

In similar fashion to the structure of the xLPR tool, the model is made up of a main loop with an internal time looping structure. Inside the time looping structure, a flaw looping structures are included to account for multiple flaws and their potential interaction. A high level presentation of the main loop of the probabilistic model for a given weld is presented in Figure A-1 and a more detailed presentation of the time looping structure is given in Figure A-2. The remainder of this section provides an end-to-end description of a DMW Monte Carlo run.

The initial conditions for the run are defined prior to entering the main loop. These initial conditions include all input parameters that remain constant throughout the run, such as the number and length of operating cycles, the frequency of inspections, certain weld geometry attributes, and the times of mitigation.

Following the definition of the initial conditions the main loop is entered. The main loop is cycled for each Monte Carlo realization and is exited once all of the user-specified Monte Carlo

realizations have been completed. After exiting the main loop, the program evaluates the results of the run, outputs certain information relevant to the study, and terminates the run.

At the beginning of each Monte Carlo realization, the values of the distributed inputs (detailed in Section A.8) are determined by random sampling. The distributions for each of the distributed inputs are user-defined. The program then calls the load models (detailed in Section A.3) to determine the relevant circumferential or axial loads (including peening loads if peening is scheduled before the end of the plant operational period).

Once all stresses have been determined from the load model, the program invokes the initiation model (detailed in Section A.4) to predict the initiation times at all potential flaw sites. The flaw initiation times are compared to the "initiation end time": the final operating time or, if peening is scheduled, the peening application time. It is assumed that flaws may not initiate on the component surface after the application of peening. The current Monte Carlo realization is terminated if all of the predicted initiation times exceed the "initiation end time". If not, the initiation model assigns initiation conditions to each flaw with an initiation time occurring before the "initiation end time." These flaws are "scheduled to initiate". Subsequently, the Monte Carlo realization enters the time looping structure.

The time looping structure is composed of an outer cycle-by-cycle loop with a nested within-cycle loop. The cycle-by-cycle loop may be terminated if all flaws that have been "scheduled to initiate" have been repaired. If this occurs, the program exits the time loop structure, stores relevant information, and cycles to the next Monte Carlo realization.

The within-cycle loop is entered if there is an active flaw whose initiation time is less than the time of the end of the current operating cycle. Immediately prior to entering the within-cycle loop, any peening application that is scheduled for the current cycle is invoked resulting in new stress profiles utilized to predict crack growth.

If no flaw initiations occur prior to the end of the current sub-step in the within-cycle loop, the sub-step is skipped. Otherwise, at the beginning of each sub-step, the stress intensity factor for each active flaw is calculated based on the geometry of the flaw and the stress profile at the beginning of the sub-step. During each sub-step, all active flaws are grown using the flaw propagation model (detailed in Section A.5) that determines the flaw propagation rate and increases the depth and length of the flaw at a constant rate for the duration of the sub-step.

Before completing a given sub-step, the program checks if any flaw has reached through-wall, and if so, the cycle number is stored for a statistical summary generated at the end of Monte Carlo run. The exception to this is if a flaw achieves through-wall crack growth before a user-defined past inspection time for which it is assumed that no flaws have leaked or been detected (i.e., credit is taken for the fact that the modeled DM weld has not leaked or had detected cracks up to a user defined time); in this case, the Monte Carlo realization is restarted with newly sampled values. For DM welds, when through-wall growth occurs (and its timing does not contradict the results of the assumed past inspection), the current realization is terminated and the program returns to the start of the main loop (contrary to RPVHPNs whose simulation continues to check for nozzle ejection).

At the end of each sub-step, if multiple flaws are active, the coalescence model (detailed in Section A.5.4) is used to consolidate circumferential flaws that are determined to be close enough to coalesce.

When all sub-steps during a given cycle have been completed, the program determines if an ultrasonic examination (UT) is to be performed at the end of the current cycle. If so, the UT inspection models (detailed in Section A.6) are called appropriately. If a flaw is detected, and its detection time does not contradict the results of the assumed past inspection, the flaw is repaired and the cycle number is stored for a statistical summary generated at the end of the Monte Carlo simulation; the examination continues to any other active flaws. In a similar fashion to a through-wall occurrence, if any flaw detection result contradicts the results of the assumed past inspection, the code exits the time looping structure without saving any results and restarts the current Monte Carlo realization from the beginning of the main loop. If a flaw is not detected, it remains active. After all scheduled inspections, the code returns to the cycle-by-cycle loop and continues to the next cycle or returns to the main loop if the cycle-by-cycle loop is complete.

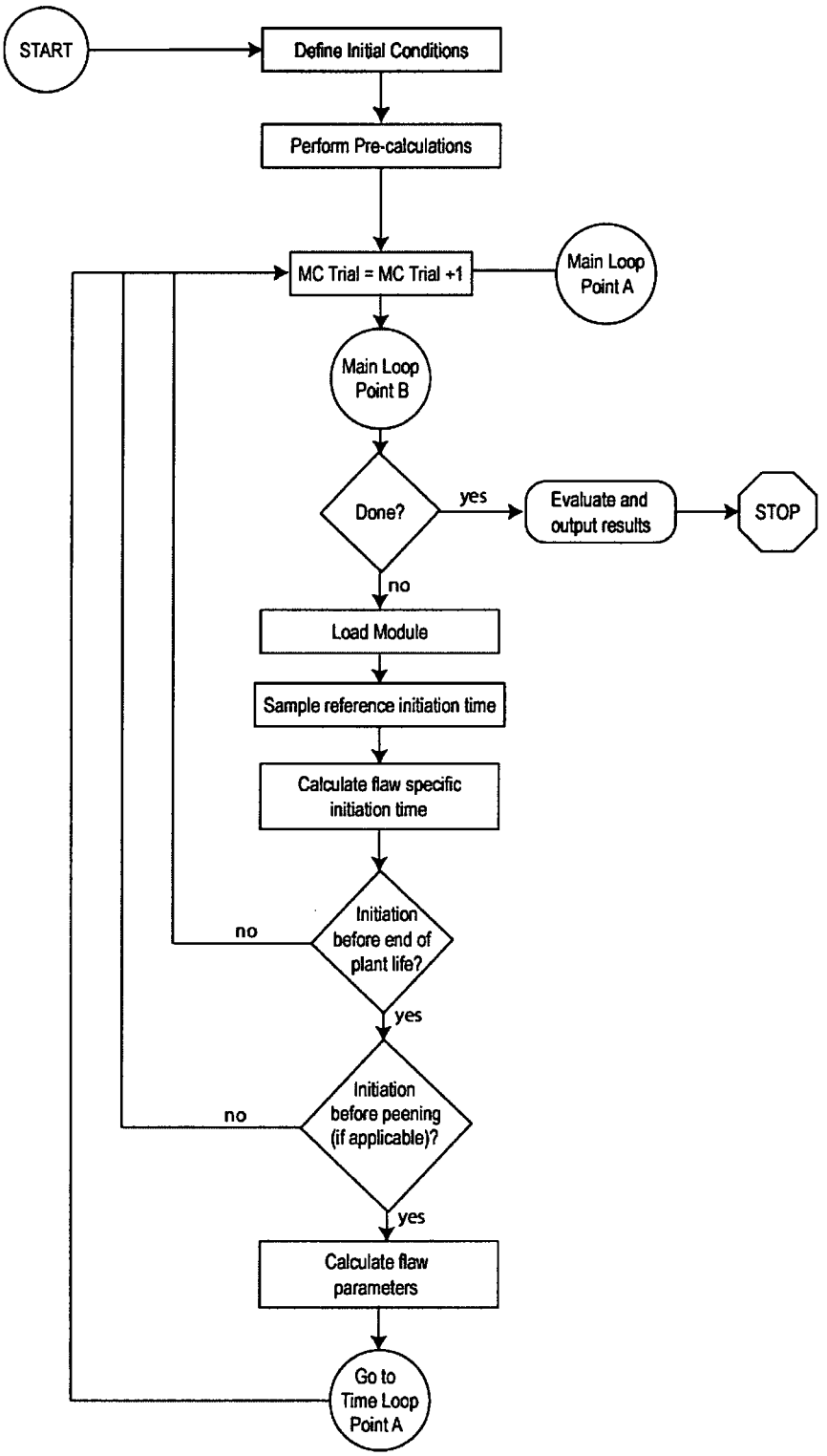

Figure A-1
DM Weld Probabilistic Model Flow Chart: Main Loop

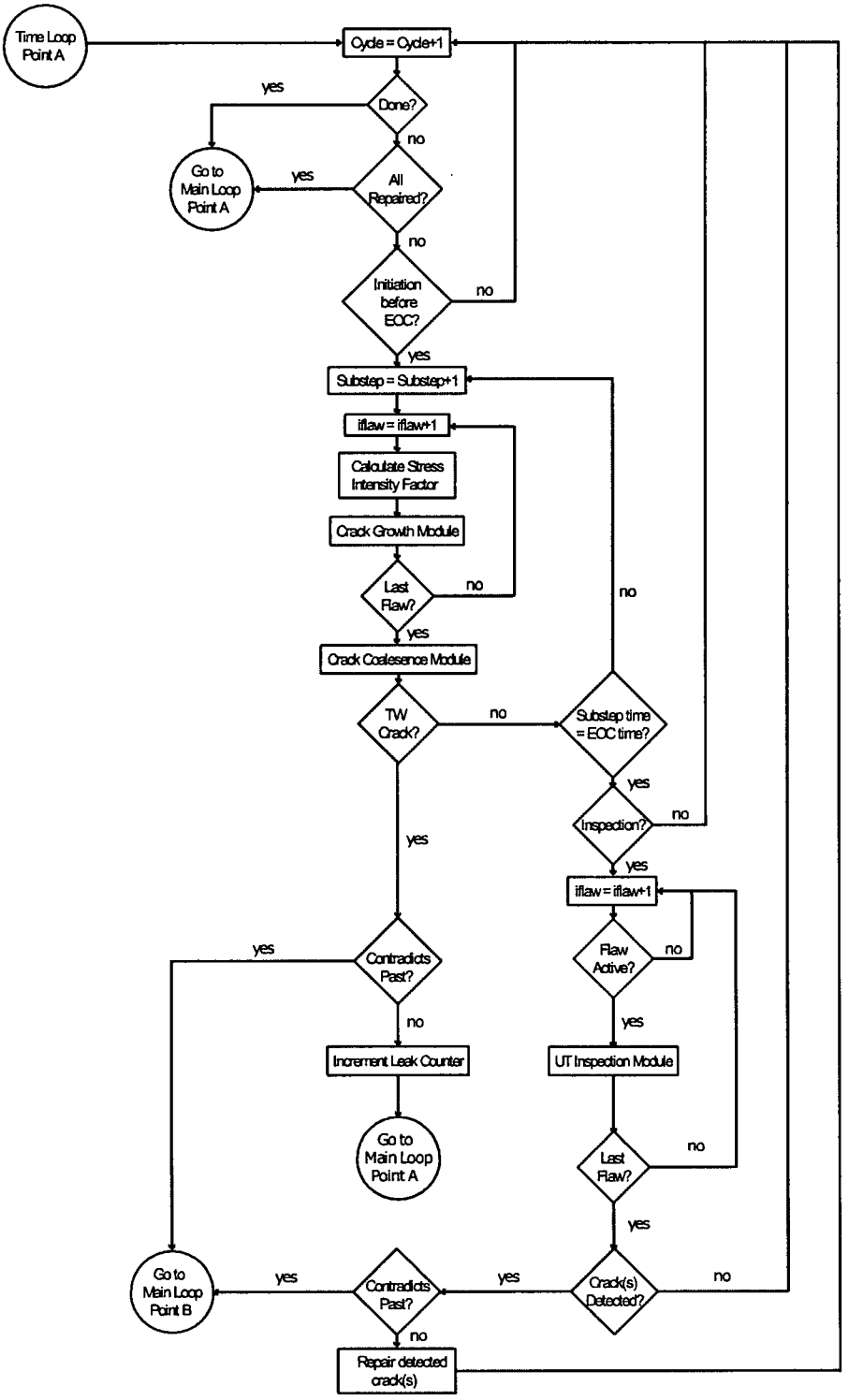

Figure A-2
DM Weld Probabilistic Model Flow Chart: Detail of Time Loop

A.3 Load and Stress Model

Load models are used to calculate the stress in the DM weld component during each Monte Carlo realization. The crack initiation and crack growth models utilize this information. Separate load models are used for hoop stresses (driving axial cracks) and axial stresses (driving circumferential cracks).[12]

The load models account for welding residual stresses, internal pressure, and piping loads (dead weight, thermal expansion, and thermal stratification, if applicable). In addition, a peening residual stress model is introduced for modeling crack growth during cycles after a peening application. The load models differentiate between residual stress and operational stress (which can all be combined to obtain total stress) as well as membrane stress and bending stress; the initiation and growth models use these differentiations at various steps.

The DM weld load models described in this report use many of the same general methodologies used by the xLPR Pilot Study program [2]. Significant differences between the models used in this study and those used in the xLPR Pilot Study include the following:

- Both axial and circumferential cracks are considered in this analysis. Because this study concentrates on the probability of through-wall crack growth and leakage rather than the probability of rupture, it was necessary to include axial flaws in the analysis.
- Peening residual stresses are modeled. The peening models are based on the bounding stress conditions meeting the performance criteria of Section 4. These models are pertinent because the main goal of this report is to assess the impact of peening on component performance with respect to leak mitigation (and ejection mitigation for RPVHPNs).
- No seismic loads (which affect crack stability but not subcritical crack growth) are considered in the analysis reported here. For simplicity, the failure criterion in the current study was selected to be a through-wall crack. Therefore, demonstrated crack stability during seismic events is not relevant.
- Thermal stratification loads are not included in this study. The xLPR Pilot Study investigated PWSCC degradation for a pressurizer surge nozzle, and thus included thermal stratification loads.

In the same manner as for the xLPR Pilot Study, it is assumed that the residual stress profile does not vary around the circumference (i.e., all residual stresses are axisymmetric).

The methodologies for calculating stresses due to internal pressure and piping loads (operational loads), component welding, and peening are discussed in Sections A.3.1, A.3.2, A.3.3, respectively. Considerations for the effects of temperature and load cycling are discussed in Section A.3.4. The load model for initiation and growth is summarized fully in Section A.3.5.

A.3.1 Internal Pressure and Piping Loads

Pipe stresses due to internal pressure, in the hoop and axial directions, are calculated using thin-walled cylindrical shell equations:

[12] The subscripts "h" and "a" will be used to differentiate between hoop and axial stresses.

$$\sigma_{P,h} = \frac{PD_i}{2t} \quad [A\text{-}1]$$

$$\sigma_{P,a} = \frac{PD_i^2}{(D_i + 2t)^2 - D_i^2} \quad [A\text{-}2]$$

where P is the normal operating pressure, D_i is the pipe inner diameter, and t is the pipe thickness.

For both axial and circumferential cracks, a crack face pressure stress equal to the operating pressure, P, is superimposed after initiation.

Other piping loads include dead weight and pipe thermal expansion. These loads act to create a longitudinal force component, torsion, and two orthogonal bending moments. These loads do not affect the hoop stress.

The axial membrane stresses due to deadweight and normal thermal expansion are calculated:

$$\sigma_{DW,a} = \frac{F_{DW}}{A} \quad [A\text{-}3]$$

$$\sigma_{NTE,a} = \frac{F_{NTE}}{A} \quad [A\text{-}4]$$

where F_{DW} and F_{NTE} are the axial loads due to dead weight and normal thermal expansion, respectively, and A is the cross-sectional area of the pipe.

The bending stress is calculated using the bending moment and torsion components of the dead weight and normal thermal expansion piping loads (i.e., M_x (torsion) and M_y and M_z (bending)). The load model determines an effective moment (M_{eff}) as a Von Mises combination of the bending and torsional loads:

$$M_{eff} = \sqrt{M_y^2 + M_z^2 + \left[\frac{\sqrt{3}}{2} M_x\right]^2} \quad [A\text{-}5]$$

(For the calculation results presented in this appendix, the effective pipe moment acting on the weld cross section is an assumed input rather than calculated from components through this equation. Sensitivity cases are used to assess the effect of the magnitude of the effective moment, given its variability for actual plant components.)

Then, using the effective moment, the OD bending stress at any azimuthal angle (φ) is approximated as:

$$\sigma_B(\varphi) = \frac{M_{eff} R_o}{I} \cos(\varphi) \quad [A\text{-}6]$$

$$I = \frac{\pi\left(R_o^4 - R_i^4\right)}{4} \qquad \text{[A-7]}$$

where R_o is the pipe outer diameter and I is the moment of inertia of the pipe cross-sectional area. Given this definition, φ=0° is the location of maximum tensile stress due to bending and φ=180° is the location of maximum compressive stress due to bending.

A.3.2 Welding Residual Stress Before Peening

The through-thickness residual stress profile is affected by local weld repairs and weld starts and stops. Thus, these processes can affect the susceptibility of the weld to initiation of PWSCC and the growth of PWSCC flaws through the weld, and as such must be modeled. In this analysis of DM welds, as in the xLPR Pilot Study, welding residual stress profiles are assumed to be axisymmetric and varying through-wall. The through-wall WRS profiles in the axial and hoop directions are detailed in the remainder of this section.

The axial load model uses a third-order polynomial function of through-wall fraction to approximate the axial WRS profile:

$$\sigma_{WRS,a}\left(\frac{x}{t}\right) = \sigma_{0,WRS,a} + \sigma_{1,WRS,a}\left(\frac{x}{t}\right) + \sigma_{2,WRS,a}\left(\frac{x}{t}\right)^2 + \sigma_{3,WRS,a}\left(\frac{x}{t}\right)^3 \qquad \text{[A-8]}$$

where x is through-wall depth from the inner diameter, $\sigma_{0,WRS,a}$ is the ID axial WRS stress, and $\sigma_{1,WRS,a}$, $\sigma_{2,WRS,a}$, and $\sigma_{3,WRS,a}$ are curve-fit parameters.

The model solves for the three curve-fit parameters using three constraints (identical to those used in the xLPR Pilot Study) resulting in a system of three linear equations:

1. The OD axial WRS ($\sigma_{OD,WRS,a}$) is defined:

$$\sigma_{WRS,a}(1) = \sigma_{OD,WRS,a} \qquad \text{[A-9]}$$

2. A through-wall fraction at which axial WRS is zero (X_c) is defined:

$$\sigma_{WRS,a}(X_c) = 0 \qquad \text{[A-10]}$$

3. The axial WRS is constrained to equilibrate through the thickness of the wall considering the effect of curvature. Using the axisymmetric assumption, that is:

$$\int_0^t \sigma_{WRS,a}\left(\frac{x}{t}\right)(R_i + x)\,dx = 0 \qquad \text{[A-11]}$$

The circumferential load model uses a fourth-order polynomial function of through-wall percentage to approximate the hoop WRS profile:

$$\sigma_{WRS,h}\left(\frac{x}{t}\right)=\sigma_{0,WRS,h}+\sigma_{1,WRS,h}\left(\frac{x}{t}\right)+\sigma_{2,WRS,h}\left(\frac{x}{t}\right)^2+\sigma_{3,WRS,h}\left(\frac{x}{t}\right)^3+\sigma_{4,WRS,h}\left(\frac{x}{t}\right)^4 \quad [A\text{-}12]$$

where $\sigma_{0,WRS,h}$ is the ID hoop WRS stress, and $\sigma_{1,WRS,h}$, $\sigma_{2,WRS,h}$, $\sigma_{3,WRS,h}$ and $\sigma_{4,WRS,h}$ are curve-fit parameters.

The model solves for the four curve-fit parameters using four constraints resulting in a system of four linear equations:

1. The OD hoop WRS ($\sigma_{OD,WRS,h}$) is defined:

$$\sigma_{WRS,h}(1)=\sigma_{OD,WRS,h} \quad [A\text{-}13]$$

2. The location of minimum hoop WRS (X_{min}) is defined:

$$\left[\frac{d}{dx}\sigma_{WRS,h}\left(\frac{x}{t}\right)\right]_{\frac{x}{t}=X_{\min}}=0 \quad [A\text{-}14]$$

3. The minimum hoop WRS ($\sigma_{min,WRS,h}$) is defined:

$$\sigma_{WRS,h}(X_{\min})=\sigma_{min,WRS,h} \quad [A\text{-}15]$$

4. The derivative of hoop WRS is assumed to be zero at the ID, effectively:

$$\sigma_{1,WRS,h}=0 \quad [A\text{-}16]$$

A.3.3 Residual Stress After Peening

As discussed in the body of this report, peening has the effect of adding a thin region of compressive stress at the surface of its application. This compressive region both prevents crack initiation and arrests the growth of cracks that are located within the compressive stress zone (when the effects of operating stresses are considered). For modeling purposes, a single outage in the operating life of the plant can be selected for the application of peening. After the application, it is assumed that no new cracks initiate and the growth of existing cracks occurs in the presence of the post-peening residual stress (PPRS) profile described below.

As with WRS, the peening stress profile is assumed to be axisymmetric and varying through-wall. The through-wall PPRS, in both the hoop and axial directions, is modeled using a piecewise stress equation that captures the minimum depth of the compressive residual stress layer and the limiting magnitude of the residual plus normal operating stress as detailed in Section 4. The assumed PPRS profile shape is depicted in Figure A-3 and is described in the remainder of this section (using the symbols presented in the figure).

For modeling purposes, the post-peening profile is separated into four general regions: the compressive region (nearest to the peened surface), the first transition region, the second transition region, and the "minimally affected" region (farthest from the peened surface). These regions are presented out of spatial order below for pedagogical reasons:

Region 1: The Compressive Region

The compressive region is the thin region near the application surface where the hoop and axial residual stresses are compressive. This region is characterized by a surface stress ($\sigma_{0,PPRS}$) and a penetration depth ($x_{1,PPRS}$). In this region, the PPRS profile varies linearly from the surface stress at the application surface to neutral stress at the penetration depth, as is reflected in the following equation:

$$\sigma_{PPRS}(x) = \sigma_{0,PPRS} + \left(\frac{\sigma_{0,PPRS}}{x_{1,PPRS}}\right)x \qquad 0 \le x \le x_{1,PPRS} \qquad \text{[A-17]}$$

Note that the argument to the PPRS equations is absolute depth as opposed to the non-dimensional depth used by the WRS equations. This reflects the notion that the peening profile is insensitive to the thickness of the peening component (for thicknesses characteristic of components studied here).

The same surface stress and peening depth are applied to the axial and hoop directions. This reflects the assumption that the peening-induced pressure waves travel without dependence on their orientation to the peened component. Vendor-supplied data, including orthogonal stress profiles from the same peened component, support this assumption.

It is noted that the peening profile data from vendors uncovered a slight trend between the residual surface stress after peening and the residual surface stress prior to peening. This effect, described in Section 3.3.3, can be included in the model as a linear adjustment to the sampled PPRS surface stress value that is dependent on the residual surface stress before the peening application. This effect is not included for base case results because the bounding stress effect meeting the performance criteria is used.

Region 4: The "Minimally Affected" Region

The "minimally affected" region is the portion of the PPRS profile that is far enough (greater than the "minimally affected depth", $x_{3,PPRS}$) from the application surface that it does not experience a stress improvement. This region takes up the majority of the thickness of the component and is described by the following equations:

$$\sigma_{PPRS,a}(x) = \sigma_{WRS,a}\left(\frac{x}{t}\right) + A_a \qquad x_{3,PPRS} < x \le t$$
$$\sigma_{PPRS,h}(x) = \sigma_{WRS,h}\left(\frac{x}{t}\right) + A_h \qquad x_{3,PPRS} < x \le t \qquad \text{[A-18]}$$

The additive terms A_a and A_h are force balance terms included to ensure the effective residual force on the peened through-wall element does not change due to peening (accounting for curvature for the axial stress case). Under the axisymmetric assumption, that is:

$$\int_0^t \sigma_{WRS,a}\left(\frac{x}{t}\right)(R_i+x)\,dx = \int_0^t \sigma_{PPRS,a}(x)(R_i+x)\,dx = 0$$
$$\int_0^t \sigma_{WRS,h}\left(\frac{x}{t}\right)dx = \int_0^t \sigma_{PPRS,h}(x)\,dx \qquad \text{[A-19]}$$

This modeling convention assumes that any residual tension removed near the application surface is redistributed through the wall-thickness of the peened component. Validation of this assumption is included in Appendix C.

Regions 2 and 3: The Transition Regions

The two transition regions are used to connect the compressive region stresses with the "minimally affected" region stresses, preserving stress continuity through-wall. Because little information is available to describe this transition, a simple approach is taken.

The first transition region uses a linear equation to connect the neutral stress location at the penetration depth to the pre-peening residual stress at the "transition depth" ($x_{2,PPRS}$). The general equation for this is:

$$\sigma_{PPRS,d}(x) = \left(\frac{x - x_{1,PPRS}}{x_{2,PPRS} - x_{1,PPRS}}\right)\cdot\sigma_{WRS,d}\left(\frac{x_{2,PPRS}}{t}\right) \qquad x_{1,PPRS} < x \le x_{2,PPRS} \qquad \text{[A-20]}$$

where the subscript *d* indicates a placeholder for the subscript *a* (axial) or the subscript *h* (hoop).

The second transition region uses a linear equation to connect the pre-peening residual stress at the "transition depth" to the "minimally affected" region at the "minimally affected depth". The general equation for this is:

$$\sigma_{PPRS,d}(x) = \left(\sigma_{WRS,d}\left(\frac{x_{3,PPRS}}{t}\right) + A_d - \sigma_{WRS,d}\left(\frac{x_{2,PPRS}}{t}\right)\right)\cdot\left(\frac{x - x_{2,PPRS}}{x_{3,PPRS} - x_{2,PPRS}}\right) + \sigma_{WRS,d}\left(\frac{x_{2,PPRS}}{t}\right) \qquad x_{2,PPRS} < x \le x_{3,PPRS} \qquad \text{[A-21]}$$

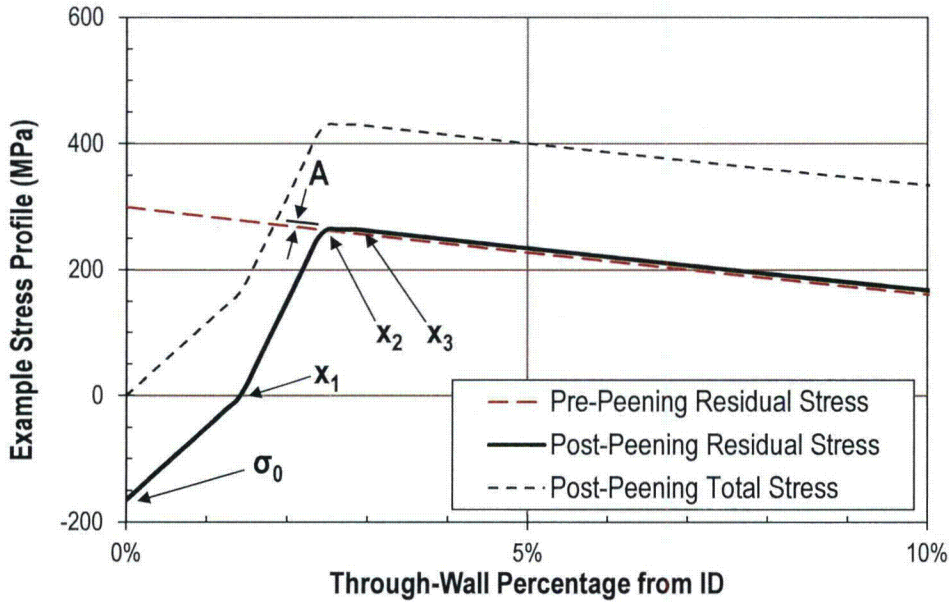

Figure A-3
Example Post-Peening Residual Stress Profile near Surface of Circumferential Crack in a DMW Component (Repeat of Figure 5-2)

A.3.4 Effect of Operating Temperature and Load Cycling

Residual stress relaxation can occur in reactor components due to temperature and load cycling effects. This relaxation is characterized by a reduction of residual stress magnitudes as a function of operating time. As the bounding stress profile defined in Section 4 is applied to this analysis, no stress relaxation effects are applied to the base-case probabilistic model. The performance criteria of Section 4.2.8 require that the effects of thermal relaxation and load cycling (shakedown) be considered when demonstrating that the bounding stress effect meeting the performance criteria will be obtained for the remaining service life of the component.

A best-fit time-dependent model is applied to peening and welding residual stresses in a sensitivity case presented later to quantify the dependence of predicted results on the stress relaxation model:

$$\sigma_{PPRS,d}\left(x,\Delta t_{peen}\right)=\sigma_{PPRS,d}\left(x,\Delta t=0\right)\cdot\exp[-m\cdot\Delta t_{peen}] \qquad [A\text{-}22]$$

where Δt_{peen} is the time elapsed since peening (in EFPYs) and m is the empirical stress relaxation exponent.

The final (relaxed) surface stress is based on the minimum acceptable peening performance criteria defined in Section 4. The relaxation factor is based on vendor-supplied data for peened samples subjected to strain cycling and/or elevated temperatures [4]. These analyses are detailed in Section A.8.5. Using the model form described in Equation [A-22], the initial surface stress is then evaluated by back-extrapolating the final (relaxed) stress state to the stress state just after peening.

A.3.5 Summary of Load Model

The models discussed in the previous sections can be combined to obtain total stress applicable to crack initiation or crack growth, before or after peening, and applicable to axial or circumferential cracks.

The DM weld *initiation* model considers only the surface (ID) stress and does not include crack face pressure. Prior to peening, this results in the following equations for axial and circumferential cracks:

$$\sigma_{ID,a}(\varphi) = \sigma_{P,a} + \sigma_{DW,a} + \sigma_{NTE,a} + \sigma_{0,WRS,a} + \frac{R_i}{R_o}\sigma_B(\varphi) \quad \text{[A-23]}$$

$$\sigma_{ID,h} = \sigma_{P,h} + \sigma_{0,WRS,h} \quad \text{[A-24]}$$

After peening, it is assumed that initiation cannot occur. That is, it is assumed that the compressive residual surface stress introduced by peening is sufficient to prevent the total surface stress during operation from reaching approximately +20 ksi (+140 MPa) tensile (which is a conservative threshold for initiation of PWSCC [5]).

The growth model requires total stress as a function of through-wall depth. Prior to peening, the total stresses for axial and circumferential cracks are:

$$\sigma_{tot,a}(x,\varphi) = \sigma_{P,a} + \sigma_{DW,a} + \sigma_{NTE,a} + \frac{R_i + x}{R_o}\sigma_B(\varphi) + \sigma_{WRS,a}\left(\frac{x}{t}\right) + P \quad \text{[A-25]}$$

$$\sigma_{tot,h}(x) = \sigma_{P,h} + \sigma_{WRS,h}\left(\frac{x}{t}\right) + P \quad \text{[A-26]}$$

After peening, the total stresses for axial and circumferential cracks are:

$$\sigma_{tot,a}(x,\varphi) = \sigma_{P,a} + \sigma_{DW,a} + \sigma_{NTE,a} + \frac{R_i + x}{R_o}\sigma_B(\varphi) + \sigma_{PPRS,a}(x) + P \quad \text{[A-27]}$$

$$\sigma_{tot,h}(x) = \sigma_{P,h} + \sigma_{PPRS,h}(x) + P \quad \text{[A-28]}$$

Note that at most azimuthal locations on the pipe, the pressure and thermal loads that occur during operation result in a tensile contribution to stress. Superimposing these tensile operating stresses with the post-peening residual stress profile results in a reduced compressive stress and a reduced compressive layer depth at the peened surface stress. This is effectively captured in the equations above.

A.4 Crack Initiation Model

This study employs a statistical Weibull approach for predicting crack initiation and allows adjustments for operating temperature and surface stress, two factors commonly considered

significant for crack initiation prediction. Furthermore, the model allows for initiation of multiple flaws with axial or circumferential orientations.

A.4.1 Spatial Discretization of Crack Sites

In a similar fashion to the xLPR Pilot Study, to account for the possibility of multiple cracks, the DM weld component is divided into a 19 (N_{crack}) crack initiation locations. Because this study also analyzes axial cracks, each of the 19 crack *locations* is given both an axial and circumferential crack *site*. This results in 38 total crack sites at which initiation is modeled.

The program sets the crack locations simply by dividing the 360 degrees of the pipe ID into N_{crack} equal arc lengths. By convention, the first crack location is centered at zero degrees, resulting in the following equation for the arc length centers (in radians):

$$\hat{\varphi}_i = \frac{2\pi}{N_{crack}}(i-1) \quad i = 1,..,N_{crack} \qquad \text{[A-29]}$$

where the subscript i will be used throughout the remainder of this appendix to denote the different crack locations.

After initiation, crack location is randomly sampled within its respective arc length.

A.4.2 Initiation Time for First Crack

A Weibull model has been selected for use in predicting the time of first initiation of PWSCC in DM welds. The use of this statistical model reflects systematic and statistical variations in material properties and environmental conditions from part to part. Furthermore, this statistical model captures the fact that the time between PWSCC initiation, for the population's first DM weld component and its last DM weld component, is quite long (several decades and even centuries). A number of distributions can be used to model failures, but the Weibull distribution is one of the most commonly used in reliability engineering since it can model a variety of data and life characteristics [6].

The two-parameter Weibull cumulative distribution function is given as follows:

$$F(t) = 1 - e^{-\left(\frac{t}{\theta}\right)^{\beta}} \qquad \text{[A-30]}$$

where F is the cumulative fraction of components with a PWSCC initiation and t is the corresponding operating time. The Weibull slope, or shape parameter, β, is related to the rate at which degradation spreads through a given component population such as steam generator tubing. The Weibull characteristic time parameter, θ, provides a measure of the time scale for the degradation mode of interest. Specifically, the Weibull characteristic time is the time required to reach a cumulative failure fraction of 0.632 (i.e., the time required for 63.2% of the items in a given population to fail).

The Weibull slope, β, an arbitrary failure fraction, F_1, (e.g., 0.1%, 1%, 10%, 63.2%, etc.), and the time at which this arbitrary failure fraction is reached, t_1, are provided as inputs to the probabilistic model. The value of θ is then determined during runtime using Equation [A-30].

The process by which β, F_1, and t_1 are fit to existing data for first crack initiation in DM welds is discussed in Section A.8.2.

Once β and θ are known for the current Monte Carlo realization, they can be used to sample a reference initiation time in EDY (t_{ref}). This sampled initiation time can be adjusted to account for temperature, material condition, and feedwater chemistry. In this study, the initiation time is adjusted for temperature (to convert to EFPY) using the widely accepted Arrhenius relationship:

$$t_f = t_{ref} \times e^{\left(\frac{Q_i}{R}\right)\left(\frac{1}{T}-\frac{1}{T_{ref}}\right)} \qquad \text{[A-31]}$$

where T is the absolute operating temperature, Q_i is the apparent thermal activation energy for crack initiation, R is the universal gas constant, and T_{ref} is the Arrhenius model absolute reference temperature.

The result, t_f, is the time of the first PWSCC on the component for the current Monte Carlo realization. As a convention, this time is attributed to the crack located at the point of maximum tensile stress. If this point happens to be at a circumferential crack site, it will be at the location maximum tensile bending stress; if this point happens to be at an axial crack site, all of which experience the same tensile stress, the crack site is arbitrary (and the axial crack site located at 0° is selected). As described in the next section, the multiple flaw initiation model uses the first initiation time to predict the initiation times of the remaining crack sites.

A.4.3 Initiation Time for Multiple Cracks

A Weibull model has been selected for use in predicting times of initiation of multiple PWSCC cracks in a single DM weld component. The use of this statistical model reflects systematic and statistical variations in material properties and environmental conditions from location to location on a single component. An adjustment is made for surface stress at each location to capture the known dependence of PWSCC initiation susceptibility on surface stress.

The multiple crack initiation Weibull model uses a new Weibull slope, β_{mult}, or a new rate at which PWSCC degradation spreads to multiple sites on a component after the first crack initiation. This rate, when used to predict a time of initiation at each crack site independently, results in more rapid crack initiation than the time to first initiation model. This reflects the premise that there may be a distinct, but random, event or condition that, after its onset, promotes more rapid PWSCC. This behavior has been observed in industry. The selection of a value for β_{mult} is discussed in Section A.8.2.6.

As in the previous section, a defined cumulative fraction at a defined time is necessary to complete the Weibull model. Since the time provided by Equation [A-31] is indicative of the time of first PWSCC initiation across all $2N_{crack}$ crack sites, it is associated with the cumulative probability (F_{1st}) given in Equation [A-32] below:

$$F_{1st} = \frac{1-0.3}{2N_{crack}+0.4} \qquad \text{[A-32]}$$

The shape parameter for the multiple flaw Weibull model, θ_{mult}, is calculated from β_{mult}, t_f, and F_{1st} above using Equation [A-30]. Then, an initiation time for each remaining crack site, $t_{ref,i,d}$, is sampled from the resulting Weibull distribution. Sampled initiation times are truncated at t_f such that no cracks form prior to the crack at the site experiencing the largest tensile surface stress (i.e., if the initiation time sampled from the multiple flaw model is less than that of the first flaw, it is resampled).

Employing the surface stresses calculated by the load model (Equations [A-23] and [A-24]), each initiation time is adjusted for surface stress effects using an empirical stress-dependent factor ($S_{factor,i}$):

$$t_{f,i,d} = \frac{t_{ref,i,d}}{S_{factor,i,d}} \qquad \text{[A-33]}$$

$$S_{factor,i,a} = \left(\frac{\sigma_{ID,a}(\hat{\varphi}_i)}{\sigma_{ref}} \right)^n$$

$$S_{factor,i,h} = \left(\frac{\sigma_{ID,h}}{\sigma_{ref}} \right)^n \qquad \text{[A-34]}$$

where the stress exponent n and reference stress σ_{ref} are empirical parameters. Note that initiation times for sites with a compressive (negative) surface stress are not modeled with the above equations and instead the stress adjustment factor is considered to be zero; i.e., the initiation times are set to infinity; i.e., cracks are not allowed to initiate orthogonal to a compressive stress field.

By convention, the reference stress, σ_{ref}, is set equal to the stress at the site of maximum tensile stress. This constrains the stress adjustment factor in Equation [A-34] to be less than or equal to one, across all crack sites, and effectively shifts initiation times for sites with lower stresses further into the future. This normalizing convention has been selected over using a constant reference stress across all Monte Carlo realizations (as has been done in other studies) because it is assumed that the variation in the multiple flaw Weibull initiation models already includes the effects due to varying surface stresses throughout in-service DM welds. Thus, to apply Equation [A-33] with a *constant* reference stress would be to "double-count" the variation due to component surface stress and, furthermore, would require an arbitrary selection of σ_{ref}.

A.4.4 Crack Initialization

In this context, crack initialization refers to assigning of initial conditions to each crack at its initiation time. These conditions include size, location, and capacity for growth. Orientation of an initiated crack, which has been part of initialization in other studies, is inherently addressed in the spatial discretization procedure discussed in Section A.4.1.

Initial crack depth is sampled from a distribution of positive, non-zero, crack through-wall percentages. This reflects both that the Weibull initiation models discussed above were fit to industry data recording first detection of crack indications and that crack detection is only

possible for finite crack sizes. Initial crack lengths are attained by scaling the initial depth by a sampled aspect ratio.

Crack center location, φ_i, which is important in this study for modeling growth and coalescence of *circumferential* cracks only, is sampled uniformly on the arc length of each initiated crack, defined in Section A.4.1.

Finally, growth capacity for each crack is modeled using sampled growth variation terms, f_{weld} and $f_{ww,i}$, discussed in more detail in Section A.5.3. It is generally accepted by PWSCC experts that components and locations that are more susceptible to PWSCC initiation tend to have higher flaw propagation rates, even after normalizing for temperature and stress effects [7]. This tendency is modeled by correlating the weld-to-weld growth variation, f_{weld}, with the reference time of first PWSCC initiation, t_{ref}, and similarly by correlating the within-weld variation for each crack, $f_{ww,i}$, with the corresponding multiple flaw reference initiation time, $t_{ref,i}$.

A.5 Crack Growth Model

This study employs a model to allow the prediction of PWSCC growth rate as a function of crack geometry, component loading, and other conditions. Assuming that cracks maintain a semi-elliptical shape as they grow through-wall, the model predicts growth rates of the surface tips (in the length direction) and the deepest point (in the depth direction) of the crack.

The model predicts growth rates for partially through-wall cracks. As discussed in Section A.7, a through-wall growth (i.e., leakage) event is treated as the end condition in this study of DM welds, so growth prediction does not proceed to necessitate a through-wall crack growth model (contrary to the analysis of RPVHPNs).

Growth is simulated by integrating the crack growth rates over time. This integration is done numerically by discretizing each cycle into many sub-cycles and advancing growth linearly over each sub-cycle, using the crack geometry and stress profile at the beginning of each sub-cycle to predict growth rate (i.e., a forward Euler method).

The dependence of PWSCC on component loading (i.e., stresses near and orthogonal to the crack) requires the calculation of stress intensity factors at the crack points of interest. Sections A.5.1 and A.5.2 discuss the stress intensity factor calculation methods for a crack subject to a polynomial stress profile and a crack subject to a general stress profile, respectively. These solutions are based on the results of finite element parametric analyses for circumferential and axial cracks; these analyses are based on the superposition method of linear-elastic fracture mechanics.

The crack growth rate model, which factors in stress intensity factor, temperature, and various other effects, is discussed in Section A.5.3.

Finally, Sections A.5.4 and A.5.5 discuss special considerations made for predicting growth given geometry characteristics specific to a DM weld component and a stress profile characteristic of a peened component (i.e., with a compressive stress region near the surface), respectively.

A.5.1 Stress Intensity Factor Calculation Using Influence Coefficient Method

Welding Research Council (WRC) Bulletin 471 [8] describes the calculation of stress intensity factor, K, for a circumferentially or axially oriented surface crack on a pipe of arbitrary size using the influence coefficient method. The method described may be applied to a crack subjected to: a) a stress profile acting orthogonally to the crack face (i.e., axial stresses for circumferential cracks and hoop stresses for axial cracks) that is defined by a polynomial function in the direction of the crack depth and is uniform along the crack length, and/or b) stresses due to global bending loads, which are by definition not uniform over the crack length. (In this study, global bending loads are only considered for the growth of circumferential cracks.)

Before the application of peening, the axial and hoop residual stresses may be approximated by polynomial functions, as demonstrated in Equations [A-25] and [A-26], and so the influence coefficient method is used due to its simplicity and computational efficiency. After peening, the more general weight function method, which is described in the next section, must be employed.

The general form of the stress intensity factor calculation (for a surface crack with depth a on a pipe with thickness t) by way of the influence coefficient method is:

$$K = \left[\sigma_0 G_0 + \sigma_1 G_1 \left(\frac{a}{t}\right) + \sigma_2 G_2 \left(\frac{a}{t}\right)^2 + \sigma_3 G_3 \left(\frac{a}{t}\right)^3 + \sigma_4 G_4 \left(\frac{a}{t}\right)^4 + G_{gb}\sigma_{gb} \right] \sqrt{a\pi} \qquad \text{[A-35]}$$

where the G terms are the influence coefficients specific to the crack and component geometries and the point on the crack, σ_0 through σ_4 are the polynomial coefficients of the through-wall stress profile (in units of stress), and σ_{gb} is the nominal bending stress due to a bending moment acting in the direction indicated in Figure A-4 (i.e., the bending moment is assumed to be directed such that the crack center is at the azimuthal location of maximum tensile or compressive stress). While the bending direction indicated in Figure A-4 only applies to two distinct azimuthal locations on a pipe, stress intensity factors at all locations are calculated with Equation [A-35] using bending stress approximated as a function of azimuthal angle per Equation [A-6]. This is the same simplification made in the xLPR Pilot Study.

The influence coefficients are interpolated from tables built by way of linear-elastic finite element parametric analyses. Table 15 and 39 in Marie, et al. [9] provides such look-up tables for the surface tip and deepest points of cracks of interest to the study of PWSCC in DM weld components: semi-elliptical, axial or circumferential surface cracks on the inner diameter of a pipe. Higher order influence coefficients (e.g., G_2, G_3, and G_4) may be calculated with weight function coefficients as discussed in Section 6.3 in WRC Bulletin 471 [8].

The look-up tables for the crack types of interest require three non-dimensional terms: the ratio of the pipe inner radius to pipe thickness (R_i/t), the ratio of crack half-length to crack depth (c/a), and the ratio of crack depth to pipe thickness (a/t). Table A-1 describes the lower and upper bounds of the look-up tables provided in Marie, et al. [9] and the protocol used for extrapolation of the look-up tables.

Table A-1
Interpolation and Extrapolation Criteria for Influence Coefficient Lookup

	R_i / t	c / a	a / t
Lower Bound	1	1	0
Lower Truncation Protocol	Error message is given. Extrapolation is not reliable below R_i/t=1.	Value of c/a=1 is used. Extrapolation is not reliable below c/a=1.	Error message is given. Negative depth indicates error.
Upper Bound	1000	16	0.8
Upper Truncation Protocol	User is instructed to use R_i/t=1000. Solution is converged to a flat plate	Value of c/a=16 is used. Extrapolation is not reliable above c/a=16.	Linear extrapolation of look-up table is executed.

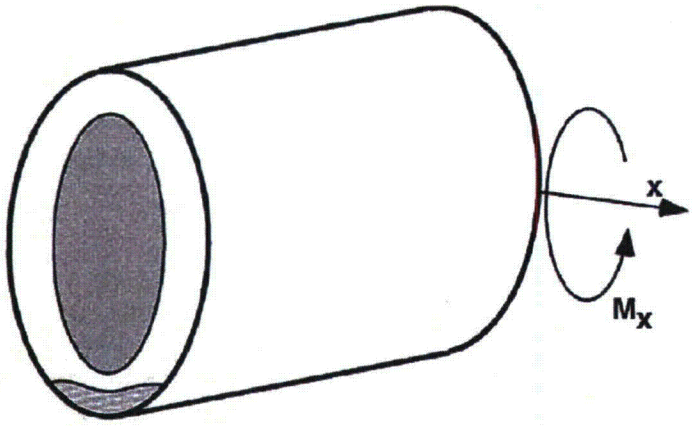

Figure A-4
Crack Location Relative to Bending Moment Assumed for Stress Intensity Factor Calculation [8]

A.5.2 Stress Intensity Factor Calculation Using the Weight Function Method

Section 6 in WRC Bulletin 471 [8] describes the calculation of stress intensity factor, K, for a circumferentially or axially oriented surface crack on a pipe of arbitrary size using the weight function method, a generalization of the influence coefficient method discussed in the previous section. The weight function method may be applied to a crack subjected to a stress profile acting orthogonally to the crack face (i.e., axial stresses for circumferential cracks and hoop stresses for axial cracks) that is defined by an arbitrary function in the direction of the crack depth and is uniform along the crack length.

The general form of the stress intensity factor calculation by way of the weight function method is:

$$K = \int_0^a h(x,a)\sigma(x)dx \qquad \text{[A-36]}$$

where x is the distance from the surface, $h(x,a)$ is the weight function, and $\sigma(x)$ is the stress profile function. (The weight function is dependent on the crack and component geometries and

the location on the crack although this is not demonstrated explicitly by its argument list for the sake of conciseness.)

For the purpose of predicting crack growth under the semi-elliptical crack shape assumption, the two points of interest on the crack are the deepest point (denoted by the subscript 90) and the surface tip points (denoted by the subscript 0). The general weight functions for these two points, respectively, are:

$$h_{90} = \frac{2}{\sqrt{2\pi(a-x)}}\left[1 + M_1\left(1-\frac{x}{a}\right)^{1/2} + M_2\left(1-\frac{x}{a}\right) + M_3\left(1-\frac{x}{a}\right)^{3/2} + M_4\left(1-\frac{x}{a}\right)^2\right] \quad \text{[A-37]}$$

$$h_0 = \frac{2}{\sqrt{\pi x}}\left[1 + N_1\left(\frac{x}{a}\right)^{1/2} + N_2\left(\frac{x}{a}\right) + N_3\left(\frac{x}{a}\right)^{3/2} + N_4\left(\frac{x}{a}\right)^2\right] \quad \text{[A-38]}$$

where the M and N terms are simple algebraic equations of the influence coefficients discussed in the previous section [10].

The weight function method is powerful because it allows the estimation of stress intensity factors for an arbitrary through-wall stress profile function. This capability is required in this study because the post-peening stress profile cannot accurately be represented by a polynomial.

There are several approaches to evaluating the integral in Equation [A-36]. If the functional form of the stress profile is available, the integral may be solvable analytically. This approach has been implemented for the four-region piecewise polynomial stress profile defined for post-peening in this study (Equations [A-27] and [A-28]). This method is similar to approximating any arbitrary stress profile with piecewise linear equation, resulting in a closed-form solution [10], as is being used in xLPR Version 2.0.

To experiment with different stress profiles, without having to derive the analytical weight function indefinite integral for each, a numerical integration procedure is also available. An adaptive, open, degree-2, Newton-Cotes integration algorithm with a 1% convergence termination criteria is employed to estimate the weight function integral numerically (see Section 4.1 of *Numerical Recipes* [3]). The use of an integral transformation discussed in Section 4.4 of *Numerical Recipes* [3] accelerates convergence by concentrating the integrand evaluations in areas with the most rapid change (i.e., near the vertical asymptotes of the weight functions given in Equations [A-37] and [A-38]).

Due to the mathematical and programming complexities of the implemented weight function solution modules, verification studies were performed to compare stress intensity factor solutions against FEA Crack [11], for various crack geometries and stress profiles.

It is noted that the weight function method cannot be applied accurately for estimating stress intensity factors due to bending because the bending stress profile is by definition not uniform along the crack length. So, after the application of peening, the contribution of the global bending load to the stress intensity factor continues to be evaluated with the influence coefficient method (as discussed in the previous section) and is superimposed with those stress intensities

due to axisymmetric membrane stresses. Accordingly, for circumferential cracks, Equation [A-36] becomes:

$$K = \int_0^a h(x,a)\sigma(x)dx + G_{gb}\sigma_{gb}\sqrt{a\pi} \qquad \text{[A-39]}$$

A.5.3 MRP-115 Crack Growth Rate Model for Alloy 82/182

The model selected in this study to estimate PWSCC crack growth in Alloy 182 weld metal is the model presented in MRP-115 [7].

The crack growth model provides a way to predict the extension of crack length and depth due to PWSCC. The model is relatively simple and incorporates the major factors affecting flaw growth rate: temperature and stress intensity factor. Temperature effects are incorporated through a widely accepted Arrhenius term and stress effects are incorporated through a standard power-law dependence, as presented below:

$$\frac{\delta}{\delta t}(d) = e^{-\frac{Q_g}{R}\left(\frac{1}{T}-\frac{1}{T_{ref}}\right)} \alpha f_{weld} f_{ww} \left(K_I - K_{Ith}\right)^b \qquad \text{[A-40]}$$

where

d = general crack dimension (e.g., depth or length)

Q_g = thermal activation energy for crack growth

R = universal gas constant

T = absolute temperature at location of crack

T_{ref} = absolute reference temperature used to normalize data

α = power-law coefficient

f_{weld} = common factor applied to all specimens fabricated from the same weld to account for weld wire/stick heat processing and for weld fabrication

f_{ww} = "within weld" factor that accounts for the variability in crack growth rate for different specimens fabricated from the same weld

K_I = crack-tip stress intensity factor at location of interest

K_{Ith} = crack-tip stress intensity factor threshold, below which the crack growth rate is zero

b = stress intensity factor exponent

This model is analogously applied to predict depth growth (substituting the K_{90} stress intensity factor term for the K_I term above) and length growth (substituting the K_0 stress intensity factor term for the K_I term above).

The estimation of crack growth versus time requires the solution of the above ordinary differential equation. This is achieved numerically by discretizing each plant operating cycle into many sub-cycles and advancing growth linearly over each sub-cycle, using the crack geometry and stress profile at the beginning of each sub-cycle to predict growth rate (i.e., a forward Euler method). The use of 12 sub-cycles per calendar year has been demonstrated to converge sufficiently to actual solution (e.g., a solution that uses twice as many sub-cycles) for a variety of initial conditions, temperatures, and stress profiles.

Various parameters in the above equation are empirical in nature and their derivation for crack growth in Alloy 82/182 is described in Section A.8.3. These include the absolute reference temperature T_{ref}, the growth activation energy Q_g, the power-law coefficient α, the crack-tip stress intensity factor threshold K_{Ith}, and the stress intensity factor exponent b.

Two additional factors, f_{weld} and f_{ww}, are included in the crack growth model to describe the aleatory uncertainty in the crack growth rate model (i.e., uncertainty due to the unknowns that differ each time we run the same experiment). The within-weld variation, f_{ww}, is a value sampled for each flaw site from a distribution reflective of the growth rate variation observed in laboratory studies of cracks in a controlled weld. Similarly, the weld-to-weld growth rate variation, f_{weld}, is a value sampled for each weld from a distribution reflective of the growth rate variation observed in laboratory studies of cracks in identically controlled welds, after accounting for the within-weld variation. The derivation of these distributions is described in Section A.8.3.

As discussed in Section A.4.4, the sampled growth variation terms may be correlated with sampled initiation times to simulate the premise that components and locations that are more susceptible to PWSCC initiation tend to have higher flaw propagation rates.

A.5.4 Special Considerations for Crack Growth on a DM Butt Weld Geometry

This section discusses the special constraints and interactions applied to cracks growing on a DM weld component. These constraints and interactions are imposed by a set of modeling "rules" used to approximate known physical behaviors. While these physical behaviors are complex in nature, the simple set of rules is applied in the probabilistic model in order to capture the most essential growth characteristics.

As discussed in Section A.4.1, both axial and circumferential cracks are allowed to initiate on the inner diameter of the DM weld. Axial cracks are constrained such that they cannot grow beyond the defined width of the weld geometry. Circumferential cracks are constrained such that they cannot grow beyond the defined inner circumference of the weld geometry. In the case that an axial, or circumferential, crack grows beyond the defined maximum length (weld width or inner circumference of the weld) before growing through-wall in the depth direction, its length is truncated.

In accordance with the approach of xLPR Version 2.0, all initiated circumferential cracks are assumed to initiate and grow on the same axial plane. For cracks with little to no circumferential overlap (Example Configuration A in Figure A-5), this assumption will lead to a single large flaw at the expense of two axially offset flaws, slightly increasing the probability of leakage and susceptibility to rupture. For cracks with substantial circumferential overlap (Example Configuration B in Figure A-5), this assumption would tend to result in a slightly reduced

probability of leakage and susceptibility to rupture as one of two cracks may grow more quickly than the other. However, given the large variability in weld residual stress and crack growth rates assumed in the probabilistic analyses, the coplanar simplification is appropriate. Also in accordance with the approach of xLPR Version 2.0, it is assumed that axial cracks do not interact with each other, or with circumferential cracks.

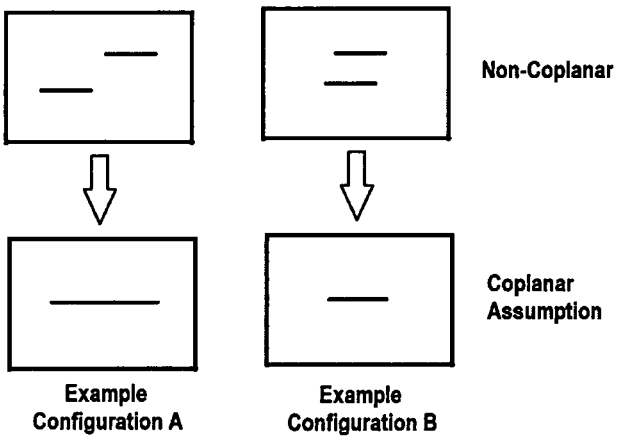

Figure A-5
Example of Configurations Illustrating Impact of Coplanar Flaw Assumption

Given the coplanar assumption for circumferential cracks, it was necessary to develop a coalescence model, or a set of coalescence rules, to describe the crack interaction on this plane. These are described in the remainder of this section.

Coalescence is modeled at the completion of each sub-cycle growth prediction, if multiple circumferential cracks are active. Coalescence is considered to occur if, at the completion of a given sub-cycle, two adjacent cracks (call them cracks A and B) overlap or are close enough such that the dividing section of weld material collapses. While the phenomena of weld section collapse is highly complex, the collapse distance, $\Delta c_{threshold}$, is modeled here as a user-defined ratio, $1/F_{coalescence}$, of the maximum depth of cracks A and B:

$$\Delta c_{threshold} = \frac{\max\{a_A, a_B\}}{F_{coalescence}} \qquad [A\text{-}41]$$

where the subscripts A and B denote the two adjacent cracks. The same methodology is discussed in ASME Section XI [12], where $F_{coalescence}$ is defined as 2.0.

If coalescence occurs, the following rules are used to consolidate the original cracks into a single resulting crack:

- The resulting crack is assumed to take on a semi-elliptical shape immediately following coalescence, with a depth equal to the maximum depth of cracks A and B and a length such that the original cracks A and B are fully circumscribed.
- The within-weld variation factor for the resulting cracks is calculated using a depth-weighted average of cracks A and B:

$$f_{ww,i} = \frac{a_A f_{ww,A} + a_B f_{ww,B}}{a_A + a_B} \qquad \text{[A-42]}$$

  The within-weld variation is thought to be a function of varying material and chemical conditions. During coalescence, the resultant within-weld variation factor is considered to be dependent on the within-weld factors of the original cracks. This is because the resultant crack will grow in a combination of the material and chemical conditions of the original cracks. The depth-weighted average in Equation [A-42] gives preference toward the deeper crack, which on average is expected to have the higher of the two within-weld factors.

The coalescence of cracks is repeated until there are no active cracks close enough to one another (although it would be extremely rare for more than two cracks to coalescence during a given sub-cycle given the initiation rates discussed previously).

A.5.5 Special Considerations for Crack Growth on a Peened Surface

This section discusses special considerations made for predicting growth in a component with a stress profile characteristic of a peened component, i.e., with a compressive stress region near the surface. The traditional stress intensity factor calculation methods discussed in Sections A.5.1 and A.5.2 assume a crack that is fully-open and semi-elliptical, while in fact, given a compressive stress region near the surface, these assumptions may not be realistic. Two deviations from these assumptions, and how they are addressed from a modeling standpoint, are discussed in this section; they are crack closure and sub-surface, often resembling a "balloon" shape, crack growth. Both of these topics have been investigated in detail in other empirical, numerical, and analytical studies.

As has been emphasized throughout this report, peening produces a compressive layer near the surface that prevents crack initiation and slows growth of shallow cracks. During operation after the application of peening, the depths of the compressive layer in the axial and hoop directions, $x_{comp,a}$ and $x_{comp,h}$, are given by the following equations:

$$x_{comp,a} = x_{1,PPRS}\left(1 - \frac{\sigma_{oper,a}}{\sigma_{0,PPRS}}\right)$$
$$x_{comp,h} = x_{1,PPRS}\left(1 - \frac{\sigma_{oper,h}}{\sigma_{0,PPRS}}\right) \qquad \text{[A-43]}$$

where $\sigma_{oper,a}$ and $\sigma_{oper,h}$ are terms that include all the operational stresses on the peened location of interest; if the operational stress is tensile, it has the effect of moving the compressive layer depth nearer to the surface.

Cracks with depths less than the compressive layer depth during operation will close entirely at the time of peening. Such cracks do not have any stresses acting to open their crack faces and thus are assumed to arrest. This is consistent with the results of laboratory experimentation of crack growth in a peened component [4].

Cracks with depths greater than the compressive layer may have partial closure, i.e., they are open at their deep crack tip, but may be closed near the surface due to the compressive layer (see Figure A-6). At locations where crack closure occurs, a contact stress is created that is considered to be equal and opposite to the local stresses. If the stress required to keep the crack closed is superimposed with the contact stresses (as in Figure A-6) it can be shown that the only stresses that contribute to crack stress intensity factor are those acting in regions where the crack remains open. As a corollary, if closure is not accounted for, stress intensity factors may be under-estimated, and in some cases they may be predicted to be negative or zero when in fact they are positive.

Beghini and Bertini [13] present a methodology for accounting for crack closure under the assumption of elastic deformation of the crack face. This methodology has been implemented in this study. Because the methodology is iterative in nature and requires a substantial computational effort, it is not applied for the simulation base case. A sensitivity study is presented later to demonstrate the effect of crack closure on leakage probability.

A second special consideration for crack growth near a compressive surface stress is "balloon" crack growth: growth of PWSCC below the compressive layer near the surface, while growth is arresting in the compressive layer. For cracks with depths greater than the compressive layer depth, the effect of the peening stresses on the crack growth is inaccurately modeled solely by growing the crack at the surface (in length) and at the deepest point (in depth). Although the length of the crack at the peened surface may be held fixed, the sub-surface crack length (deeper than the compressive layer) can continue to grow.

To assess balloon-shaped growth, analyses were conducted using the finite element software FEA Crack to produce high fidelity predictions for crack growth, allowing for non-semi-elliptical growth (e.g., growth resembling a balloon), as seen in Figure A-7. (While the FEA Crack program simulates fatigue crack growth, advancing the crack front over load cycles instead of time, the resultant shape progression is reflective of the advancement of a PWSCC flaw.) The crack shape results of these analyses were compared to two limiting cases; the first case did not allow crack length growth while the second allowed crack length growth uninhibited by peening. An example comparison of crack front shapes predicted using the different methods is shown in Figure A-8. As expected, the balloon growth approximation bounds the length of the FEA predicted crack shape, given the same crack depth.

In a related study [14], it is demonstrated that crack growth below a PWSCC resistant weld inlay may be closely approximated by assuming a semi-elliptical shape below the inlay, driving growth with the deepest and surface points of sub-inlay portion of the crack (referred to as "idealized crack growth"). The idealized crack growth results in accurate time to through-wall crack growth relative to the actual crack growth predicted with FEA.

Considering these results, the "balloon" crack growth phenomenon is approximated conservatively by allowing crack length growth independent of peening (i.e., using only the pre-

peening stresses). A sensitivity study is presented later to demonstrate the effect of fixing length growth after peening.

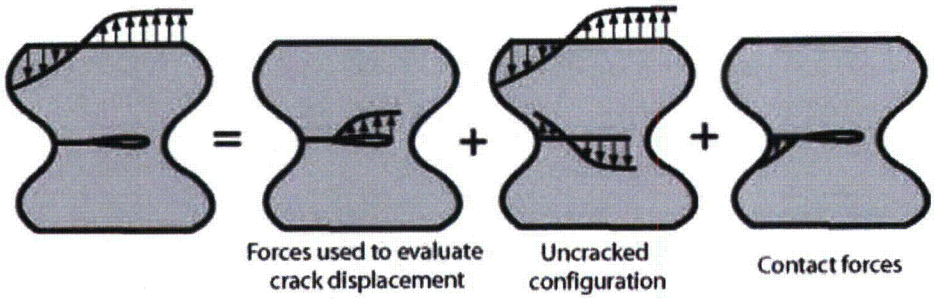

Figure A-6
Demonstration of Stresses Superposition for Partially Closed Crack

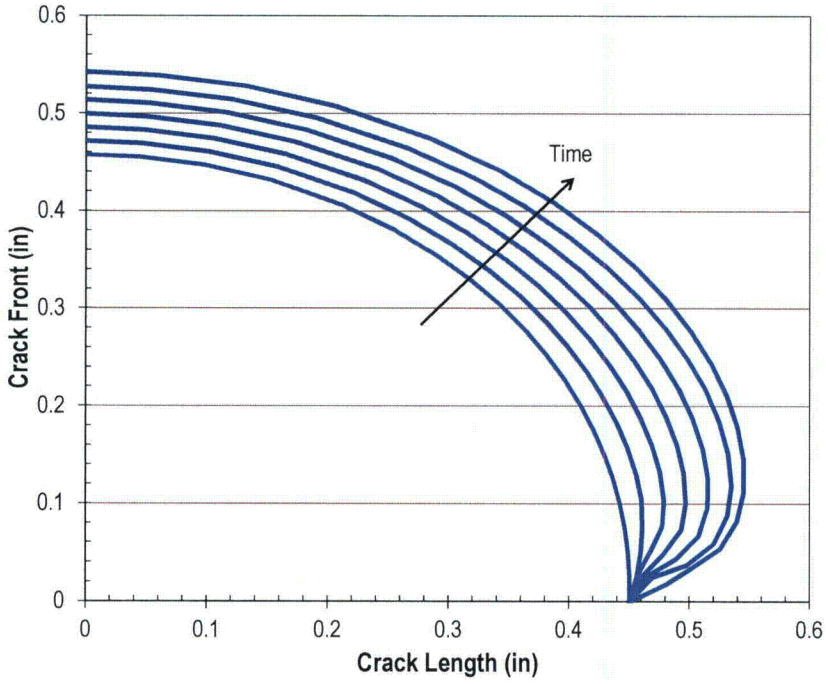

Figure A-7
Example of "Balloon" Crack Growth over Time Calculated with FEA Crack

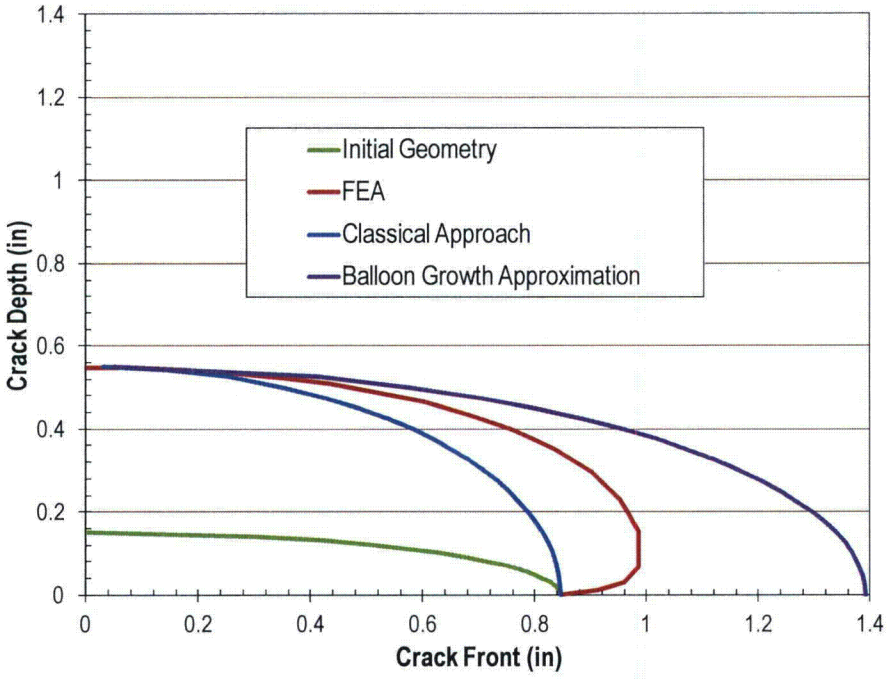

Figure A-8
Example of Crack Front Shapes Predicted in a Peened Component with: a) FEA, b) Classical Analytical Methods, or c) the Balloon Growth Approximation (Repeat of Figure 5-3)

A.6 Examination Model

This section describes the models applied to simulate ultrasonic examinations of DM welds. Similar to the xLPR study, this study uses probability of detection (POD) curves to estimate the likelihood of a crack being detected, given its size. These models are essential for predicting leakage probabilities since cracks that lead to leaks are often those that go undetected during one or more scheduled examinations.

Section A.6.1 discusses how examinations are scheduled, before and after peening. Section A.6.2 describes the inspection models, i.e., how POD is calculated, factoring for the geometry of the crack. Finally, Section A.6.3 describes the detection and repair modeling rules.

A.6.1 Examination Scheduling

UT examination scheduling for DM welds (prior to peening) is required per ASME Code Case N-770-1 [15]. Specifically, a Performance Demonstration Initiative (PDI) qualified volumetric inspection is required once every five years for unmitigated hot leg DM welds and once every seven years for hot leg cold leg DM welds. The time of the first modeled UT inspection is set by the user.

When peening is applied, different examination scheduling requirements and options are included in the model. First, during the peening application outage, immediately prior to peening, a UT inspection can be modeled to simulate a pre-peening inspection.

A follow-up UT examination is included before entering the relaxed in-service inspection (ISI) schedule. In the comparative studies presented later, the follow-up inspection time is varied between 1, 2, or 3 cycles after the peening application for the RVON and 1, 2, 3, or 6 cycles after the peening application for the RVIN. Conservatively, the second follow-up UT examination for the RVON is not credited, and the new ISI schedule is entered after the first follow-up.

After the follow-up examination, a new ISI schedule is used. The central goal of this probabilistic modeling effort is to demonstrate that the ISI inspection interval after peening can be elongated compared to N-770-1 requirements without increasing the probability of leakage over the entire plant service life. Accordingly, several different ISI intervals will be tested after peening and compared to predictions for unmitigated components.

A.6.2 Inspection Modeling

For modeling UT inspections of cracks in DM welds, a modified version of the POD model from MRP-262 [16] will be used. This model is based on POD data for inspections of realistic DMW mockups containing well-characterized, representative cracks. However, the POD model applied in this probabilistic assessment assumes a POD of zero for flaws less than 10% through–wall.

The modified MRP-262 model from is comprised by a POD curve that is a function of the through-wall fraction of the crack, as given in the following equation:

$$POD\left(\frac{a}{t}\right)=\begin{cases} 0 & 0\le\frac{a}{t}<0.1 \\ \dfrac{e^{\beta_1+\beta_2\left(\frac{a}{t}\right)}}{1+e^{\beta_1+\beta_2\left(\frac{a}{t}\right)}} & 0.1\le\frac{a}{t}\le 1 \end{cases} \qquad \text{[A-44]}$$

where β_1 and β_2 are fit parameters determined by regression analysis of inspection data from the mockups containing circumferential flaws. The specific values of these fit parameters are given in Section A.8.4. The resulting set of POD curves is demonstrated in Figure A-9.

The model defined in Equation [A-44] is based on experiments which included circumferential cracks only. Experience gathered during UT detection qualification suggests that POD may be lower in general for axial cracks. Accordingly, for axial cracks, an optional POD reduction factor, $f_{UT,axial}$, may be applied to the POD predicted by Equation [A-44].

The model defined in Equation [A-44] is based on experiments including cracks ranging from 10% to 100% through-wall. As the data documented in MRP-262 do not include flaws shallower than 10% of the wall thickness, a POD of zero is conservatively applied for cracks with depths less than 10% through-wall. (The model also includes the ability to linearly extrapolate the POD between the origin, i.e. 0% POD for an infinitesimal crack, and the POD given by Equation [A-44] for a 10% through-wall crack; this option is invoked in a sensitivity case.)

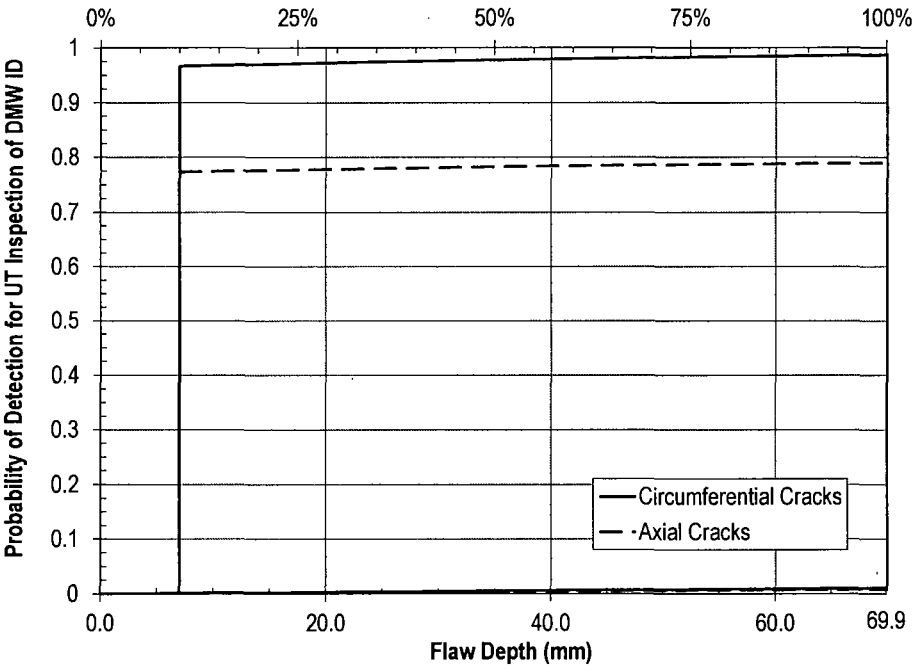

Figure A-9
Mean Assumed UT Inspection POD Curve for DMW Cracking from the ID

A.6.3 Detection and Repair Modeling

After a POD has been calculated, given the size of the crack of interest, detection may be simulated by sampling a random value between zero and one, referred to as the detection sample. If the detection sample is less than or equal to the POD, the crack is predicted to be detected; if not, the crack is predicted to be undetected for the current examination.

If the detection sample is sampled independently of previous samples, it reflects the premise that inspection success is uncorrelated, from examination to examination. Alternatively, the examination model allows for the correlation of successive detection samples for a given flaw. This is equivalent to assuming that each crack has some ambiguous features which may make it harder or easier to detect than the general population.

Credit can be taken for the condition that the unit(s) of interest have had no flaw detections before some user-defined past inspection time. If a flaw is predicted to be detected before this user-defined past inspection time, the Monte Carlo realization is rejected and repeated with newly sampled inputs. If a flaw is predicted to be detected after this past inspection time, that flaw is repaired (removed entirely from the flaw site), but the DM weld component stays in service and other flaws remain active.

A.7 Through-Wall Flaw (Leakage) Criterion

At the end of each Monte Carlo realization, the probabilistic model discussed in this report stores a limited number of metrics related to the extent of flaw growth and the repair status of the weld, including the timing of related events. Most importantly, during each realization, the code tracks

if at least one flaw reaches through-wall crack growth (i.e., leakage) and, if so, the number of the cycle of the first through-wall crack growth.

Similar to detection, credit can be taken for the condition that the unit(s) of interest have had no leakages before some user-defined past inspection time. If a flaw is predicted to grow through-wall before this user-defined past inspection time, the Monte Carlo realization is rejected and repeated with newly sampled inputs, and the leak is not counted toward the metric discussed above.

Flaws modeled using the xLPR tool are able to reach through-wall crack growth either by propagating through the entire thickness of the component wall or by net section collapse of a critical surface flaw. Specifically, if the xLPR tool determines that the bending load on a given surface flaw exceeds the calculated net section collapse bending load, the surface flaw will transition to a through-wall flaw. For simplicity, the probabilistic model described in this report does not address the net section collapse failure mode and a given flaw may only reach through-wall crack growth if it propagates through the entire thickness of the wall before it is repaired.

A.8 Probabilistic Model Inputs

The probabilistic modeling framework for DMWs accepts both deterministic and distributed inputs. The values of the deterministic inputs are constant for every Monte Carlo realization. The values of the distributed inputs are determined by sampling probability distributions (e.g., normal distribution, log-normal distribution, triangular distribution, etc.) during each Monte Carlo realization. The probabilistic model accepts an array of eight inputs that is used to define the distribution of each distributed input. Each input array contains the following information:

- The value of the parameter to be used when conducting deterministic assessments;
- The distribution type to be sampled during probabilistic assessments (e.g., normal distribution);
- Parameter values defining the distributions (up to four, e.g., the mean and standard deviation of a normal distribution);
- Lower and upper truncation limits used to impose bounds on the sampled values.

The inputs selected for use in the probabilistic model are discussed in Section A.8.1 through A.8.5. All inputs to the probabilistic model for the reactor vessel outlet nozzle (hot leg, RVON) and reactor vessel inlet nozzle (cold leg, RVIN) are tabulated in this section.

A.8.1 Component Geometry, Operating Time, Temperature, and Loads

The choice of inputs for component geometry, operating time, temperature, and component loading are discussed in this section. These inputs are given for two component cases for which results will be presented: a reactor vessel outlet nozzle (hot leg) in a Westinghouse plant and a reactor vessel inlet nozzle (cold leg) in a Westinghouse plant. These inputs are tabulated in Table A-2.

A.8.1.1 Component Geometry

In similar fashion to the xLPR pilot study, the component specific parameters (i.e., wall thickness, outer diameter, and weld width) were taken as deterministic inputs. The values selected are for the outer diameter and the wall thickness are based on information provided in MRP-44, Part 1 [17] and are given in Table A-2.

A.8.1.2 Operating Time

Both DM weld components are simulated from plant startup until the end of the plant operational service period. This is considered to occur approximately 80 years after startup (i.e., a 40-yr original license and two 20-yr license renewals). Cumulative statistics are provided at the end of the plant operational service period.

Both DM weld components are simulated with 18-month operating cycles at a capacity factor of 0.97. These values are representative of U.S. PWRs.

As discussed in the modeling sections, credit can be taken for the fact that the simulated component has not experienced leaks or repairs before some user-defined outage. Monte Carlo realizations that predict leaks or repairs before the user-defined outage are rejected and rerun with new samples. As defined in Section A.9, average leakage frequencies and cumulative probabilities of leakage are averaged over the total number of Monte Carlo realizations that are active (have not yet leaked) following the hypothetical time of peening.

As a sensitivity case, a user-defined outage (before which no leaks or repairs have occurred) will be set. All statistics presented in this study apply conditionally to Alloy 182 reactor vessel outlet/inlet nozzles that have experienced no leaking or repairs to date, but otherwise have characteristics similar to those defined in Table A-2. For this sensitivity case, the number of rejected and rerun Monte Carlo realizations is reported, which provides further insight on this modeling assumption.

A.8.1.3 Temperature

Uncertainty in the component temperature is incorporated into the model by using a normal distribution. The temperature distributions used for the RVON and RVIN base cases are included in Table A-2. The means of these distributions reflect bounding reactor hot-leg and cold-leg temperatures for U.S. PWRs. The uncertainty in the temperatures represents a number of factors including temperature streaming and measurement uncertainty. The standard deviations have been selected such that the 95% confidence band is ±5.1°C (±9.2°F) for the RVON and ±1°C (±1.8°F) for the RVIN.

A.8.1.4 Loads

The input parameters specific to the DM weld loading are summarized in Table A-3 and are further discussed below.

Like the xLPR Pilot study, relevant operational loads are taken as deterministic inputs. The values selected are considered to be representative of the loads in the actual components as described in MRP-307 [18]. Additionally, a tensile axial load of 100 kips (445 kN) was assumed (in addition to the axial pressure stresses). The loads applied to DM welds documented in this

report bound those documented in a NRC hot leg flaw evaluation summary [19]. Sensitivity studies are included to explore more extreme loading conditions.

Welding residual stresses are modeled stochastically. Uncertainty is incorporated into the calculation of welding residual stresses by setting distributions for parameters used to characterize and constrain the WRS profiles (Equations [A-9] through [A-16] present the constraint equations for the axial and circumferential WRS profiles). For the axial stress profile, the distributed inputs are the ID stress, the through-wall depth where the stress changes sign (from tensile to compressive) and ratio of the OD stress to ID stress. For the hoop stress profile, the distributed inputs are the ID stress, the location of the minimum stress, the ratio of the minimum stress to the ID stress, and the ratio of the OD stress to the ID stress.

The distributions for the parameters of the axial and hoop stress profiles are included in Table A-3. The distributions for the axial stress profile parameters are taken from the xLPR pilot study. The distributions for the hoop stress profile parameters were determined iteratively by using random sampling to generate a family of curves which adequately captured the uncertainty in the data as well as uncertainty due to missing data [18]. The truncation limits are used to prevent the use of unrealistic stress profiles.

Table A-2
Summary of General Inputs

Symbol	Description	Source	Units	Parameter Type	DMW Base Case
[redacted]	Total number of trials	Convergence Study	# trials	[redacted]	1.00E+07
[redacted]	Number of operating cycles	Selected to yield desired cumulative operating time	-	RVON	53
				RVIN	53
	Nominal cycle length	Representative cycle length at Westinghouse plant	years	RVON	1.5
				RVIN	1.5
CF	Operating capacity factor	Representative capacity factor for U.S. PWR	-	RVON	0.97
				RVIN	0.97
[redacted]	Cycle of first UT inspection	Based on typical operating reactor service histories	Cycle number	RVON	14
				RVIN	15
	Pre-peening UT inspection interval	ASME Code Case N-770-1	# cycles	RVON	3
				RVIN	4
T	Operating temperature of RVON–DMW	Maximum Westinghouse hot leg operating temperature	°F	type	Normal
				mean	625.0
				stdev	4.6
				min	597.4
				max	652.6
	Operating temperature of RVIN–DMW	Maximum Westinghouse cold leg operating temperature	°F	type	Normal
				mean	563.0
				stdev	0.9
				min	557.5
				max	568.5
t	Wall thickness of RVON-DMW	Representative component thickness for Westinghouse plants	in.	RVON	2.75
	Wall thickness of RVIN-DMW			RVIN	2.75
D_o	Outer diameter of RVON-DWM	Representative component OD for Westinghouse plants	in.	RVON	35.5
	Outer diameter of RVIN-DWM			RVIN	35.5
w	Width of RVON-DMW	Representative weld width for Westinghouse plants	in.	RVON	1.75
	Width of RVIN-DMW			RVIN	1.75

Table A-3
Summary of Loading Inputs for DMW Model

Symbol	Description	Source	Units	Parameter Type	DMW Base Case
P_{op}	Normal operating pressure	Representative of U.S. PWRs	ksi		2.248
F_x	Effective loads for RVON-DMW (including deadweight, thermal expansion, and thermal stratification loading)	Representative reactor vessel nozzle loads for Westinghouse plant	kips		100
M_x			in-kips		0
M_y			in-kips		40000
M_z			in-kips		0
F_x	Effective loads for RVIN-DMW (including deadweight, thermal expansion, and thermal stratification loading)	Representative reactor vessel nozzle loads for Westinghouse plant	kips		100
M_x			in-kips		0
M_y			in-kips		40000
M_z			in-kips		0
σ_{0WRSa}	Weld residual axial stress on ID surface	xLPR Pilot Study	ksi	type	Normal
				mean	43.55
				stdev	15.95
				min	21.75
				max	79.91
X_c	Fractional through-thickness at which weld residual axial stress profile crosses zero	xLPR Pilot Study	-	type	Normal
				mean	0.25
				stdev	0.05
				min	0.125
				max	0.50
f_{WRSa}	Random scaling factor for weld residual axial stress on OD surface	xLPR Input	-	type	Uniform
				min	0.5
				max	1.0
σ_{0WRSh}	Weld residual hoop stress on ID surface	xLPR Pilot Study	ksi	type	Normal
				mean	43.55
				stdev	15.95
				min	21.75
				max	79.91
f_{WRSh1}	Random scaling factor for minimum weld residual hoop stress	Iterative random sampling, see Section A.8.1.4	-	type	Normal
				mean	0.50
				stdev	0.10
				min	0.25
				max	0.75
f_{WRSh2}	Random scaling factor for weld residual hoop stress on OD surface	Iterative random sampling, see Section A.8.1.4	-	type	Normal
				mean	1.00
				stdev	0.075
				min	0.80
				max	1.20
X_{min}	Fractional through-thickness at which weld residual hoop stress is minimum	Iterative random sampling, see Section A.8.1.4	-	type	Normal
				mean	0.50
				stdev	0.075
				min	0.40
				max	0.75

A.8.2 Crack Initiation Model

The set of inputs for the DM weld PWSCC initiation model is described in Table A-4 at the end of this section. Various inputs are detailed in the following subsections.

A.8.2.1 Industry Inspection Data used to Develop Initiation Model

The following plant inspection data for piping to nozzle DM welds fabricated from Alloys 82 and 182 were used in the Weibull initiation model development:

- Pressurizer safety/relief nozzles, spray nozzles, surge nozzles;
- Reactor hot leg piping surge nozzles, decay heat nozzles, drain nozzles, reactor vessel outlet nozzles, steam generator inlet nozzles, and shutdown cooling nozzles;
- Reactor cold leg piping letdown drain nozzles, core flood nozzles, high-pressure injection nozzles, reactor coolant pump (RCP) suction and discharge nozzles, inlet nozzles, and safety injection nozzles.

Table A-5 shows the list of PWR piping DM welds in which indications of cracking were detected that was used for this analysis. The data were compiled from industry documents (primarily documents from the NRC website such as LERs) using Table E-1 of MRP-216 [20] as a guide. Please note the following regarding Table A-5:

- All of the data are for U.S. plants
- No exhaustive effort was made to include all inspections of PWR piping DM welds that resulted in no indications being reported. This conservatively results in a higher probability of crack initiation than would have been the case if additional inspections were considered.
- The 20 welds given in Table A-5 were evaluated in detail and are considered either to be representative of service-induced cracking or it was not possible to rule out the presence of service-induced cracking (as opposed to fabrication-related defects, etc.). The remaining nozzles without indications are treated as suspended items [6] in the Weibull analysis.

Size data for PWSCC indications presented in Table A-5 were collected from the following sources:

- Table E-1 in MRP-216, Rev. 1 [20]
- Licensee Event Reports to the NRC
- Other documents from the NRC (such as ASME Code Section Flaw Evaluations, Special Inspections, Issuance of Relief from Code Requirements, etc.)

Operating EFPYs at the time of inspection were taken from the EPRI steam generator degradation database, and operating temperatures were based on various sources.

Some of the welds inspected were without indications of cracking and are treated as suspended items. Specifically, a given weld that was found not to have any indications of cracking during its most recent inspection is modeled to have been removed from the statistical population at the time of the most recent inspection. The inspection data given in Table A-5 represent a summary of the detected flaws, which are part of what is known as a censored sample. For a Weibull distribution with a censored sample (i.e., failure data plus suspension data), it is necessary to account for the suspension times within the data set. Using the censored data set, it is possible to include the effect of the effective operating times of the uncracked components.

A.8.2.2 Weibull Fitting Procedure for Time of First Initiation

After adjusting the operating time data for the effect of operating temperature using the Arrhenius adjustment, the values of the Weibull parameters, β and θ, were determined using a maximum likelihood estimator (MLE) statistical procedure [6] fit to the PWR dissimilar metal

weld experience. The MLE procedure is preferred over a least-squares fitting procedure in the case that limited cracking experience is available.

For the particular case of a Weibull distribution with a censored sample (i.e., failure data plus suspension data), the maximum likelihood estimates of the Weibull parameters β and θ may be determined by simultaneously solving the following equations:

$$\frac{\sum_{i=1}^{n} x_i^{\beta^*} \ln x_i}{\sum_{i=1}^{n} x_i^{\beta^*}} - \frac{1}{r}\sum_{i=1}^{r} \ln x_i - \frac{1}{\beta^*} = 0 \qquad \text{[A-45]}$$

$$\theta^* = \left(\frac{\sum_{i=1}^{n} x_i^{\beta^*}}{r} \right)^{\frac{1}{\beta^*}} \qquad \text{[A-46]}$$

where

β^* = maximum likelihood estimate of β

θ^* = maximum likelihood estimate of θ

x_i = operating time of component i

n = number of components in the population

r = number of failures

Components censored at times t_i are assigned values $x_{r+i}=t_i$. Thus, the second term in Equation [A-45] sums the logarithms of the failure times only. The values of β^* and θ^* may be found using an iterative procedure.

A least squares fitting procedure may also be used to determine the values of the Weibull slope and characteristic time parameters. This procedure consists of fitting the available data to the linearized representation of the Weibull distribution (see Equation [A-47]) using a least squares analysis.

$$\ln\left(-\ln(1-F)\right) = \beta \ln(t) - \beta \ln(\theta) \qquad \text{[A-47]}$$

$$y = mx + c$$

Specifically, a plot of F versus t on a double log-log plot yields a line with slope β. The value of θ may then be determined using the values of β and the vertical intercept (referred to here as c) obtained from the fit.

A.8.2.3 Analysis Results for Time of First Initiation

Figure A-10 shows an example MLE Weibull distribution fit to the industry experience with DM welds fabricated form Alloys 82 and 182 given in Table A-5. The failure and suspension times were adjusted to a common reference temperature of 600°F (315°C) using a thermal activation energy of 44.0 kcal/mole (184 kJ/mole) (the mean value given in Section A.8.2.10).

Table A-7 summarizes the MLE fit parameters of the Weibull analysis. Also included in Table A-7 are the standard errors in the Weibull fit parameter, β, and the vertical intercept of the linearized model determined from the linear least squares fit (which is used to determine the value of θ).

It is noted that for simplicity, the standard errors of the linear least squares parameters are presented instead of the MLE parameter values. It is also noted that the standard error in the vertical intercept of the linearized Weibull fit (referred to here as σ_c) is presented because it is used during runtime to account for the uncertainty in the value of the anchor point time, t_1, as discussed later.

A.8.2.4 Uncertainty in First Initiation Time Weibull Slope

The uncertainty in the Weibull slope, β, is modeled with a normal distribution having the mean and standard deviation given in Table A-7. The mean was selected as the value calculated using the MLE fitting procedure and for simplicity, the standard deviation was selected as the standard parameter error determined using the least squares fitting procedure. Based on the similarity of the Weibull slopes calculated using the two methods, this simplification is considered reasonable.

A.8.2.5 Uncertainty in Anchor Point Time (t_1)

Based on data presented in Figure A-10, a value of 0.01 was selected as the value of the arbitrary failure fraction, F_1. Figure A-10 shows that this failure fraction provides a reasonable representation of the earlier failures observed in the field, which will provide a more realistic set of Weibull curves defined by random sampling during the Monte Carlo analysis. That is, appropriately selecting the value of F_1 (which in combination with the Weibull slope and characteristic life determines the mean value of the anchor point time, t_1) will reduce the probability that the initiation model will greatly under-predict or over-predict (relative to observed plant experience) the initiation time of the first flaw during a given Monte Carlo realization.

The value of t_1 is determined by solving Equation [A-30] for time at a failure fraction of F_1 and the mean vales of the Weibull parameters, β and θ, given in Table A-7.

Uncertainty in the anchor point time is incorporated for each Monte Carlo realization using the following procedure:

- Determine the characteristic time, θ, using the value of F_1 and the deterministic values of β and t_1.
- Determine the mean intercept parameter, c, using the deterministic value of β and the value of θ determined in the previous step.

- Sample the value of c from a normal distribution using the mean intercept parameter determined in the previous step and the standard error (σ_c) given in Table A-7.
- Determine the anchor point time for the current trial using the sampled value from the previous step and the deterministic value of β.

A.8.2.6 Uncertainty in the Multiple Flaw Weibull Model

As discussed in the modeling section, a second Weibull model is used to predict the initiation of multiple flaws on a single component. The key inputs to this model are the Weibull slope and the empirical stress exponent.

Based on analysis of laboratory data, an empirical stress exponent, n, of about 4 is often assumed to describe the stress dependence of the initiation of PWSCC in Alloy 600 [21]. For this study, this exponent value is inherited for modeling PWSCC initiation in Alloy 82/182. A normal distribution with a mean of 4.0 standard deviation of 1.0 is employed to incorporate the uncertainties due to material and manufacturing disparities. A lower truncation bound of 0.0 is used to prevent the unphysical trend of earlier initiation for lower tensile surface stresses.

The Weibull slope of the multiple flaw model, β_{flaw}, quantifies the rate at which flaws occur after the initiation of the first flaw. An analytical data fitting procedure, as done for the first initiation time model, was not considered appropriate to fit β_{flaw} given the modeling complexities involved in sampling multiple flaw initiation times. Instead, a mean value of 2.0 was selected for β_{flaw}. This value has a precedent in probabilistic modeling of SCC in steam generators [21]. A normal distribution with a mean of 2.0 and a standard deviation of 0.5 is employed to incorporate uncertainties due to material and manufacturing disparities. A lower truncation bound of 1.0 was selected to prevent a multiple flaw Weibull model in which the PWSCC initiation rate decreases over all time.

A numerical experiment was run with a value of 2.0 for β_{flaw} in order to demonstrate the resulting number of cracks per component, given the parameter and stress distributions discussed throughout this Section A.8. Figure A-11 depicts the resulting distribution of number of flaws in components with at least a single flaw, at 20 EFPY, given an operating temperature of 625°F. The average number of flaws at 20 EFPY, given that at least a single flaw exists, is 3.3.

Industry experience listed in Table A-5 shows that there have been up to five detected cracking indications on a single hot leg DMW component, with the average close to 1.5 indications per component with at least a single flaw. These values are regarded as low given the existence of small cracks that have not been identified. Accordingly, the results given in the numerical study are not considered excessively conservative.

A.8.2.7 Uncertainty in Flaw Orientation

Flaw orientation is not directly controlled with a probability distribution. Rather, the stress adjustment together with the surface stress distributions dictates the ratio of flaw orientations.

A.8.2.8 Uncertainty in Initial Flaw Depth

In the same manner as for xLPR Version 2.0, the initial flaw modeled within the simulation is assumed to be of engineering scale. The initial flaw is the result of both initiation processes and

early growth processes (for which growth is driven by stress intensity factor). This approach bypasses the early stages of growth when coalescence of micro-fissures is especially important. Moreover, the initiation predictions are based on empirical plant experience for detected flaws, which are all of engineering scale, i.e., at least 1 to 2 millimeters in depth.

A log-normal distribution with a median of 5% of through-wall was selected to model the uncertainty in the initial flaw depth. The log-normal distribution conservatively provides greater weight for the upper end of the initial depth distribution (i.e., a long tail). The 95% confidence bound of the distribution was set to an initial depth of 9% through-wall. The log-normal standard deviation was determined using the median and 95% confidence bound values specified above.

A lower truncation limit was defined to prevent the initiation of very small flaws for which the stress intensity factor (based on the input distributions of the surface welding residual stress and other sources of normal operating stress) would be significantly less than the lower bound of stress intensity factors (about 20 MPa-$m^{1/2}$ or 18 ksi-$in^{1/2}$) evaluated in the laboratory studies used to define the flaw propagation models given in MRP-115 [7] for Alloys 82 and 182.

The sensitivity results section presents a study in which the flaw through-wall fraction distribution is scaled down such that cracks initiate approximately 10 times smaller. This is included to assess the potential effect on leakage probability of smaller cracks not being identified during inspections prior to entering the relaxed inspection schedule after peening.

A.8.2.9 Uncertainty in Flaw Aspect Ratio

The distributions of the initial aspect ratios of axial and circumferential flaws were determined from the population of in-service inspection data discussed in A.8.2.1. The aspect ratio of a given flaw was calculated by dividing its total length by its depth. These data were used to determine approximate distributions of the axial and circumferential initial aspect ratios.

A log-normal distribution was selected to model the uncertainty in the initial aspect ratio of both circumferential and axial flaws because they provide reasonable fits to the aspect ratio data given in Table A-6. The parameter values defining these distributions are given in Table A-4.

A.8.2.10Uncertainty in Temperature Effect

Uncertainty in the apparent activation energy for PWSCC crack initiation is treated by defining a distributed input. As shown in Table A-4, a normal distribution is assumed to describe the uncertainty in the activation energy.

An activation energy of 209.4 kJ/mole is a standard value applied for the initiation of PWSCC in Alloy 600 components [22]. This value is based on evaluations of PWSCC in Alloy 600 steam generator tubing [23]. A lower, experimentally determined value of 184.2 kJ/mole (44 kcal/mole) was determined for Alloy 600 CRDM nozzle (i.e., thick-wall) material [24]. Activation energies ranging from 125.6 kJ/mole (30 kcal/mole) to 201.0 kJ/mole (48 kcal/mole) were reported in a review of laboratory and field data [23]. Due to similarities in the compositions of Alloy 82/182 and Alloy 600 wrought material, 184.2 kJ/mole was selected as the mean of the distribution and the standard deviation was selected such that the 95% confidence bound of the distribution would be 209.4 kJ/mole (50 kcal/mole).

Table A-4
Summary of Inputs for DM Weld Initiation Model

Symbol	Description	Source	Units	Parameter Type	DMW Base Case
t_1	Time at which failure fraction F_1 is reached	See Section A.8.2.5	EDY	type	Normal
				mean	11.40
				stdev	0.304
				min	3.14
				max	41.10
σ_c	Standard error in intercept of linearized Weibull fit	See Section A.8.2.3	ln(EDY)		0.304
F_1	Arbitrary failure fraction selected to define Weibull PWSCC initiation function	See Section A.8.2.5	-		0.010
β	Weibull slope for PWSCC flaw initiation	See Section A.8.2.3	-	type	Normal
				mean	1.419
				stdev	0.082
				min	0.927
				max	1.911
N_{crack}	Number of circumferential locations for crack initiation	xLPR Pilot Study	-		19
β_{flaw}	Weibull slope for PWSCC multiple flaw initiation	Based on representative value for formation of PWSCC at multiple locations in industry SGs	-	type	Normal
				mean	2.0
				stdev	0.5
				min	1.0
				max	5.0
ρ_{weld}	Correlation coefficient between PWSCC initiation and propagation rates for all cracks in Alloy 82/182 weld	xLPR Input	-		0.0
ρ_{ww}	Correlation coefficient between PWSCC initiation and propagation rates for indicidual crack	xLPR Input	-		0.0

Table A-4 (continued)
Summary of Inputs for DM Weld Initiation Model

Symbol	Description	Source	Units	Parameter Type	DMW Base Case
Q_i	Thermal activation energy for PWSCC flaw initiation	Distribution based on laboratory data and experience with Weibull analysis	kcal/mole	type	Normal
				mean	44.03
				stdev	3.06
				min	25.65
				max	62.41
$T_{ref,i}$	Reference temperature to normalize PWSCC flaw initiation data	Temperature used to adjust flaw initiation data assessed in this report	°R		1060
n	Exponent for surface stress adjustment to initiation time	EPRI TR-104030	-	type	Normal
				mean	4.0
				stdev	1.0
				min	0.0
				max	10.0
a_0/t	Initial depth assigned to newly initiated flaw	Based on expected performance of UT inspection technique	-	type	Log-Normal
				linear μ	0.053
				median	0.050
				log-norm μ	-3.00
				log-norm σ	0.35
				min	0.01
				max	0.42
AR_{circ}	Initial aspect ratio assigned to newly initiated circumferential flaw	Flaw initiation data from operating experience	-	type	Log-Normal
				linear μ	11.28
				median	8.66
				log-norm μ	2.159
				log-norm σ	0.727
				min	0.110
				max	679.7
AR_{ax}	Initial aspect ratio assigned to newly initiated axial flaw	Flaw initiation data from operating experience	-	type	Log-Normal
				linear μ	3.44
				median	1.74
				log-norm μ	0.554
				log-norm σ	1.167
				min	0.0016
				max	1912.2

Table A-5
Summary of PWSCC Experience in U.S. PWR Piping Nozzle Dissimilar Metal Welds

							Largest Axial PWSCC Indication					Largest Circumferential PWSCC Indication			
Plant	Component Type	Inspection Operating Time (EFPY)	Operating Temp. (°F)	Orientation	Wall Thickness (in.)	Number of Axial PWSCC Indications	Axial Indication Depth (a, in.)	Axial Indication Total Length (2c, in.)	Axial Indication a/t	Axial Indication Aspect Ratio (2c/a)	Number of Circ PWSCC Indications	Circ Indication Depth (a, in.)	Circ Indication Total Length (2c, in.)	Circ Indication a/t	Circ Indication Aspect Ratio (2c/a)
Plant A	Safety Relief	23.1	653	Axial	1.3	1	0.10	0.60	8%	6.00					
Plant B	Safety Relief	19.2	653	Axial	1.40	1	1.23	0.40	88%	0.32					
Plant C	Surge	21.9	653	Axial+Circ	1.5	1	0.31	0.50	20%	1.61	1	0.51	~3	33.0%	5.88
Plant D	Spray	13.9	653	Axial	0.89	1	0.21	0.25	24%	1.17					
Plant E	Relief (Note 1)	10.0	643	Circ	0.44						1	0.44	3.50	100.0%	7.99
Plant F	Surge	17.9	653	Circ	1.5						3	0.45	4.03	31.0%	8.97
Plant F	Safety Relief	17.9	653	Circ	1.3						1	0.30	2.51	22.5%	8.44
Plant F	Safety Relief	17.9	653	Circ	1.4						1	0.34	7.69	25.8%	22.61
Plant A	HL Surge	23.1	597	Circ	1.6						1	0.40	2.40	25.0%	6.00
Plant G	HL Surge	19.2	601	Axial	1.3	1	0.59	(Note 2)	45%	(Note 2)					
Plant A	HL Drain	23.1	597	Circ	0.5						1	0.10	0.45	19.0%	4.50
Plant H	HL Drain	21.7	597	Axial	0.6	2	0.39	(Note 3)	70%	(Note 3)					
Plant I	Decay Heat	21.6	601	Circ	1.3						1	0.90	10.00	68.6%	11.11
Plant J	Decay Heat	19.2	605	Axial	1.3	1	1.25	1.75	100%	1.40					
Plant K	RPV Outlet	20.2	605	Circ	2.62						1	0.63	2.06	24.2%	3.25
Plant L	RPV Outlet	16.5	621	Axial	2.9	2	0.6	0.96	21%	1.6					
Plant M	RPV Outlet	15.6	621	Axial	~2.5	1	2.5	2.5	100%	1.0	1	0.20	2.00	8%	10.00
Plant N	SG Inlet	26.6	620	Axial	4.66	5	4.1	2.0	88%	0.5					
Plant H	CL Drain	21.7	545	Circ	0.6						1	0.06	0.63	10%	11.21
Plant J	CL Drain	17.6	555	Axial	0.6	1	0.06	≥ 0.25	7%	≥ 4.46					

Notes:
(1) PWSCC indication was located in heat affected zone of an Alloy 600 safe end.
(2) Indication reported to extend over the width of weld metal.
(3) Indication length not available

Table A-6
Summary of PWSCC Experience in U.S. PWR Piping Nozzle Dissimilar Metal Welds Used to Define Initial Flaw Aspect Ratio

Plant	Component Type	Inspection Operating Time (EFPY)	Operating Temp. (°F)	Orientation	Wall Thickness (in.)	Number of PWSCC Indications	Indication Depth (a, in.)	Indication Total Length (2c, in.)	Indication a/t	Indication Aspect Ratio (2c/a)
Plant A	Safety Relief	23.1	653	Axial	1.3	1	0.10	0.60	8%	6.00
Plant C	Surge	21.9	653	Circ	1.5	1	0.51	~3	33.0%	5.88
Plant D	Spray	13.9	653	Axial	0.89	1	0.21	0.25	24%	1.17
Plant F	Surge	17.9	653	Circ	1.5	3 (1)	0.45	4.03	31.0%	8.97
Plant F	Surge	17.9	653	Circ	1.5	3 (2)	0.36	2.22	25.0%	6.17
Plant F	Safety Relief	17.9	653	Circ	1.3	1	0.30	2.51	22.5%	8.44
Plant F	Safety Relief	17.9	653	Circ	1.4	1	0.34	7.69	25.8%	22.61
Plant A	HL Surge	23.1	597	Circ	1.6	1	0.40	2.40	25.0%	6.00
Plant I	Decay Heat	21.6	601	Circ	1.3	1	0.90	10.00	68.6%	11.11
Plant L	RPV Outlet	16.5	621	Axial	2.9	2	0.6	0.96	21%	1.6
Plant M	RPV Outlet	15.6	621	Circ	~2.5	1	0.20	2.00	8%	10.00
Plant H	CL Drain	21.7	545	Circ	0.6	1	0.06	0.63	10%	11.21

Table A-7
Summary of Weibull Distribution Parameter Fitting Results for DMW Analysis

Fitting Method	β	θ (EDY)	Standard Error in Weibull Slope	Standard Error in Vertical Intercept (ln(EDY))
Maximum Likelihood	1.42	291		
Linearized Least Squares	1.32	331	0.082	0.304

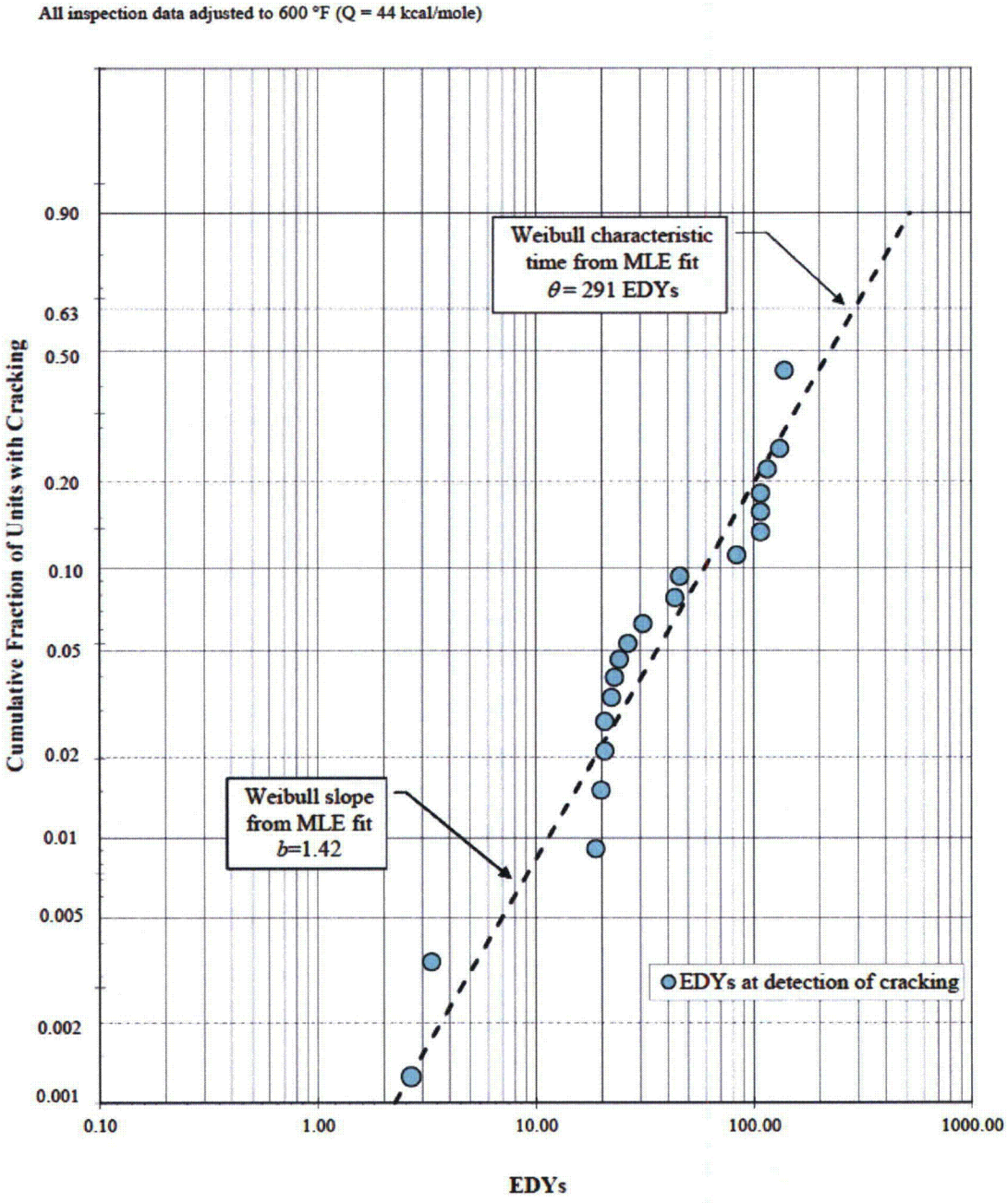

Figure A-10
Example MLE Weibull Probability Distribution for Alloy 82/182 Piping to Nozzle Butt Welds

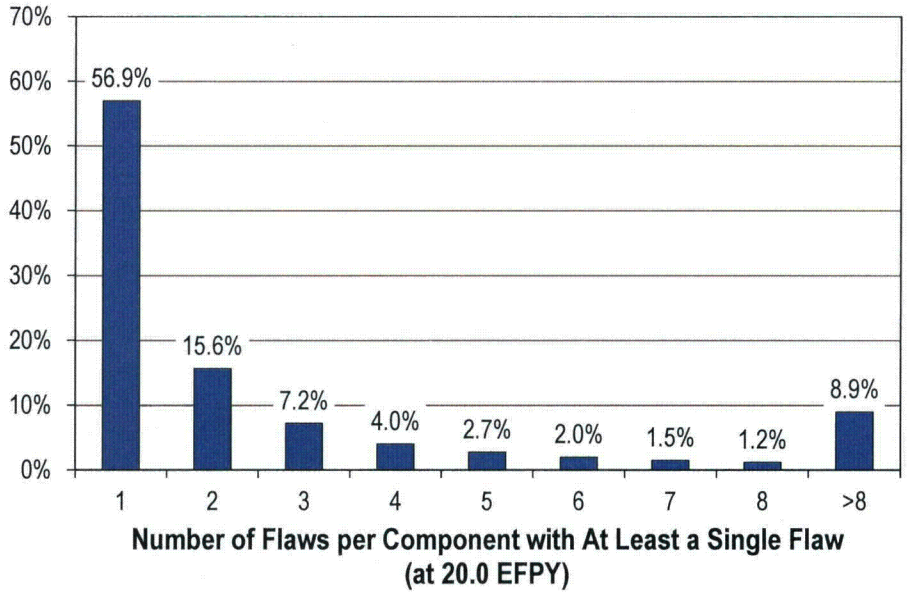

Figure A-11
Result for DM Weld Numerical Study: Distribution of Number of Flaws per Component with at Least a Single Flaw

A.8.3 Crack Growth Model

The set of inputs for the PWSCC propagation model is described in Table A-8 at the end of this section, including deterministic and distributed inputs. Various inputs are detailed in the following subsections.

A.8.3.1 Empirical Growth Parameters

The general flaw propagation rate equation used in this study is given in Equation [A-40]. The flaw propagation rate constant for growth in Alloy 82/182, α_{weld}, is based on MRP-115 and is taken as a deterministic input. Likewise, the stress intensity factor threshold and propagation rate stress intensity factor exponent (for growth in Alloy 82/182) are based on MRP-115 and are taken as deterministic inputs.

A.8.3.2 Growth Variation Factors

The uncertainty in the probabilistically calculated flaw propagation is principally characterized by the f_{weld} and f_{ww} parameters in the MRP-115 flaw propagation rate equations described Section A.5.3.

The f_{weld} parameter is a common factor applied to all specimens fabricated from the same weld to account for effects of the weld wire/stick heat processing and of weld fabrication. For this study, the log-normal distribution fit to the weld factors for the set of laboratory test welds assessed in MRP-115 is used (see Figure A-12).

A "within weld factor" (f_{ww}) is included to describe the variability in flaw propagation rate for different weld specimens fabricated from the same test weld. Log-normal distributions were

developed and are shown in Figure A-13 to describe the variability in f_{ww} observed for the data generated in MRP-115. The f_{ww} distribution describes the scatter in the flaw propagation rate model that remains after all effects addressed by the model are considered including the particular f_{weld} parameter calculated for each test weld.

Because there is a physical upper limit to the rate at which PWSCC crack propagation can proceed, an upper truncation limit is applied when sampling f_{weld} or f_{ww}. The f_{weld} or f_{ww} upper bound is set to the maximum of: the 95th percentile of the respective distribution and the maximum calculated f_{weld} or f_{ww}, respectively. The lower bound is imposed in a similar manner as the minimum of the 5th percentile of the respective distribution and the minimum calculated f_{weld} or f_{ww}, respectively.

Note that when an f_{ww} factor is applied in addition to the f_{weld} factor, the product of the two corresponding upper truncation limits proscribes the maximum flaw propagation rate that can be applied within the flaw propagation model. That maximum flaw propagation rate is assured to be greater than the maximum flaw propagation rate actually observed in any of the laboratory tests used to develop the f_{weld} and f_{ww} distributions when the conditions for each test are applied to the applicable flaw propagation rate equation.

A.8.3.3 Uncertainty in Temperature Effect

The temperature dependence of the flaw propagation process is modeled using a thermal activation energy. As shown in Table A-8, a normal distribution is used to describe the uncertainty in the activation energy. The standard deviation assumed corresponds to 5 kJ/mole, relative to the 130 kJ/mole mean activation energy value for PWSCC growth, and is based on the range of PWSCC flaw propagation activation energy values reported by various investigators for Alloy 600 wrought material [7].

A reference temperature of 617°F is chosen as the reference temperature for the crack growth model. The uncertainty in the activation energy accounts for the uncertainty in the temperature effect between 617°F and the operating temperature.

A.8.3.4 Correlation in Relating Flaw Initiation and Propagation

As discussed in A.5.3, it is generally accepted by PWSCC experts [7] that components that are more susceptible to PWSCC flaw initiation than other components tend to have higher flaw propagation rates than those other components. The main challenge in correlating the time to initiation and the flaw propagation rate in a probabilistic PWSCC assessment is that there is a general lack of data with which to choose an appropriate correlation coefficient. In the absence of data to select an appropriate correlation coefficient, this correlation is examined in a sensitivity study. The correlation coefficient was therefore set to zero for the base case analysis.

A.8.3.5 Crack Coalescence Factor

Crack coalescence modeling requires a distance threshold at which coalescence occurs. In this study, this threshold is modeled by some deterministic ratio of the maximum depth of the two cracks for which coalescence is assessed (that ratio being $1/F_{coalescence}$). For the base case result, the $F_{coalescence}$ parameter is inputted as an arbitrarily large number such that cracks must abut for coalescence to occur.

Table A-8
Summary of Inputs for DM Weld Flaw Propagation Model

Symbol	Description	Source	Units	Parameter Type	DMW Base Case
$1/\Delta t$	Number of time steps per year for crack size increment	The value chosen provides sufficient convergence	1/yr		12
f_{weld}	Weld-to-weld factor: common factor applied to all specimens fabricated from the same weld to account for weld wire/stick heat processing and for weld fabrication	Fit to weld-to-weld variation data from MRP-115	-	type	Log-Normal
				linear μ	1.19
				median	1.00
				75%ile	1.49
				log-norm μ	0.000
				log-norm σ	0.589
				min	0.313
				max	2.64
f_{ww}	Within-weld factor: factor accounting for the variability in crack growth rate for different specimens fabricated from the same weld	Fit to within-weld variation from MRP-115 data after normalizing for weld-to-weld variation factor	-	type	Log-Normal
				linear μ	1.12
				median	1.00
				log-norm μ	0.000
				log-norm σ	0.481
				min	0.309
				max	3.24
α_{weld}	Flaw propagation rate equation power law constant for Alloy 182 weld	MRP-115	$(in/hr)/(ksi\text{-}in.^{0.5})^{1.6}$		1.62E-07
Q_g	Thermal activation energy for PWSCC flaw propagation	MRP-115	kcal/mole	type	Normal
				mean	31.07
				stdev	1.20
				min	23.90
				max	38.24
$T_{ref,g}$	Absolute reference temperature to normalize PWSCC flaw propagation data	MRP-115	°R		1077
$K_{I,th}$	K_I Stress intensity factor threshold	MRP-115	$ksi\text{-}in.^{0.5}$		0.0
$K_{I,min}$	Minimum allowable value for K_I	No technical basis for non-zero value	$ksi\text{-}in.^{0.5}$		0.0
b	Flaw propagation rate equation power law exponent for Alloy 82/182 weld	MRP-115	-		1.6
$1/F_{coalescence}$	Ratio of maximum crack depth that is used to evaluate the critical separation distance for coalescence	Set arbitrarily small such that coalescence occurs only once two cracks overlap	-		1.0E-06
	Flag indicating if crack growth will be predicted considering the effect of crack closure	Crack closure effects are neglected for base case	Logical		FALSE
	Flag indicating if cracks may grow in length without the effect of peening stresses	Sub-surface balloon growth of crack conservatively included for base case	Logical		TRUE

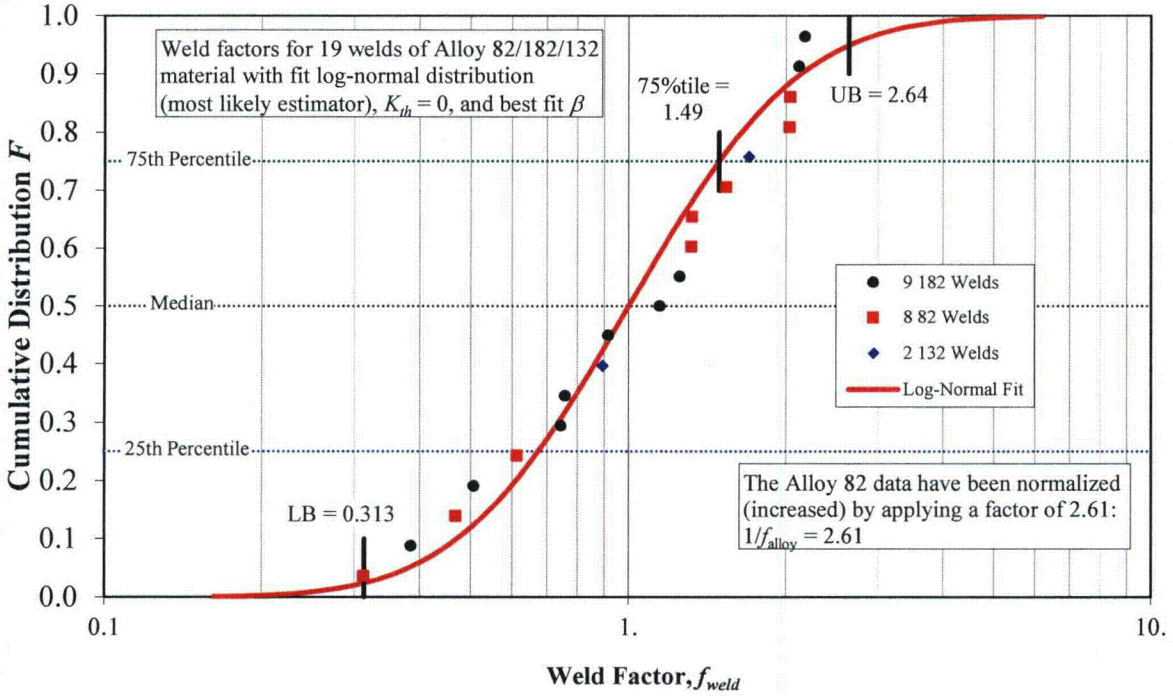

Figure A-12
MRP-115 Weld Factor f_{weld} Distribution [7] with Log-Normal Fit for Alloy 82/182/132

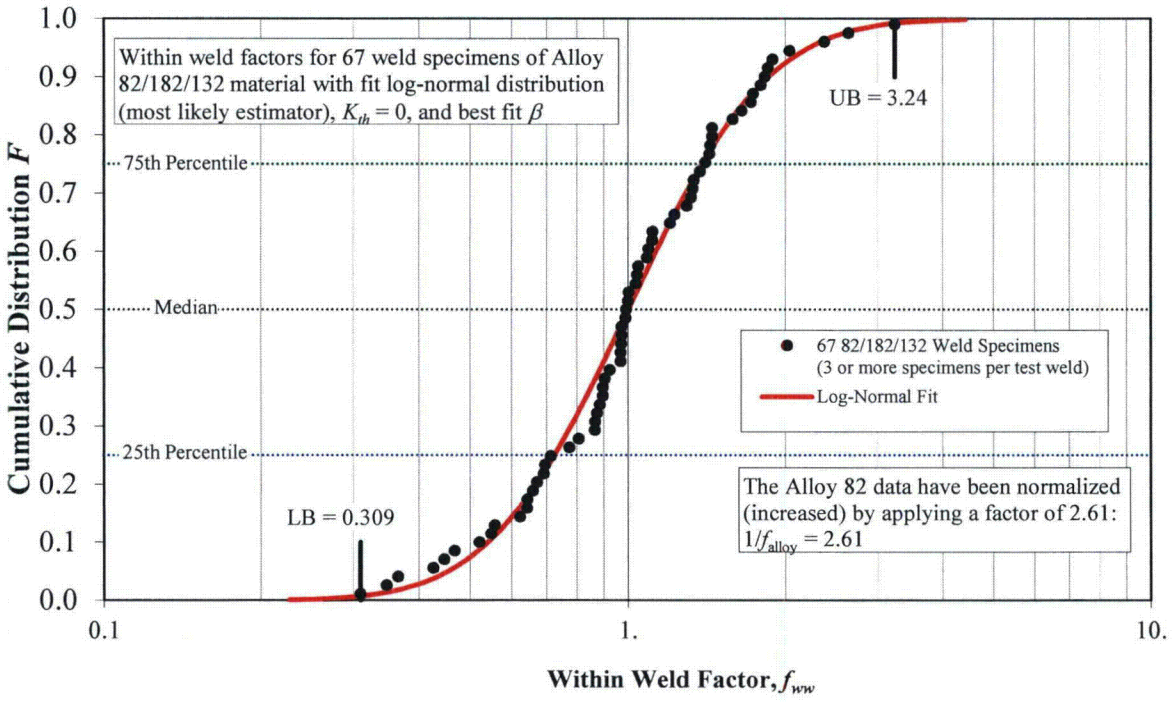

Figure A-13
MRP-115 Within-Weld Factor f_{ww} Distribution [7] with Log-Normal Fit for Alloy 82/182/132

A.8.4 Flaw Inspection and Detection Model

The set of inputs for the flaw examination models is described in Table A-9 at the end of this section, including deterministic and distributed inputs. Various inputs are detailed in the following subsections.

A.8.4.1 Examination Scheduling

As mentioned in the modeling section, UT inspection scheduling prior to peening for DM welds is based on ASME Code Case N-770-1 [15]. Accordingly, a UT inspection is simulated once every three cycles for the RVON and once every four cycles for the RVIN. The first PDI qualified UT inspection is modeled as occurring after the 14th simulated cycle for the RVON and after the 15th simulated cycle for the RVIN. These dates correspond with the units that were used to develop the operating timeline, and geometry inputs discussed in Section A.8.1.

In cases where peening is scheduled, the follow-up and in-service inspection intervals are varied to generate comparative results. The follow-up interval is varied between 1, 2, or 3 cycles for the RVON and between 1, 2, 3, or 6 cycles for the RVIN. The in-service inspection interval is varied from 3 cycles (same as the unmitigated component ISI) to the total plant service life for the RVON and from 4 cycles to the total plant service life for the RVIN.

A.8.4.2 UT Probability of Detection

The UT POD model for DM welds is described by Equation [A-44]. Based on the study of UT qualification data published in MRP-262, Revision 1 [16], the uncertainty of the detection model parameters, β_1 and β_2, can be accurately captured using a bivariate normal distribution. The distribution parameters for POD of DM weld cracking on RVONs from this study are given in Table A-9. Note that these parameters are also applied for the RVIN case given that the two nozzles have a similar geometry in Westinghouse plants.

As discussed in the modeling section, the study used to derive the UT POD curve discussed above did not include axial cracks. Experience indicates a decreased capability to detect axial cracks relative to circumferential cracks using UT. Accordingly, a deterministic reduction factor of 0.8 is conservatively applied to the POD predicted by the model from MRP-262, Revision 1 [16] in order to model detection of axial flaws by UT. This assumption is examined in a sensitivity study, in which both axial and circumferential POD curves are decreased by an additional 20%.

A correlation coefficient relating the results of the next inspection to the results of the previous inspection can be included to take into account the increasing likelihood of non-detection if a crack has already been missed in a previous inspection. Because this value has not been experimentally determined, a modest correlation coefficient of 0.5 is used for the base case input.

Table A-9
Summary of Inputs for DM Weld Examination Model

Symbol	Description	Source	Units	Parameter Type	DMW Base Case
	The through-wall fraction below which the small-flaw contingency (POD = 0) is used	Smallest flaw size used in UT mockup testing			0.10
ρ_{insp}	Correlation coefficient for successive UT inspection	Conservative assumption	-		0.50
$\beta_{1\,(B1)}$	POD model for 0th order logistic equation parameter for Category B1 components: RV Inlet and Outlet	Table 12-3 of MRP-262	-	type	Normal
				mean	3.244
				stdev	0.549
$\beta_{2\,(B1)}$	POD model for 1st order logistic equation parameter for Category B1 components: RV Inlet and Outlet	Table 12-3 of MRP-262	-	type	Normal
				mean	1.06
				stdev	1.32
$\rho_{\beta\,(B1)}$	Correlation coefficient for Category B1 component POD model parameters	MRP-262 Appendix B Wald Model Results	-		-0.8698
$f_{UT,axial}$	Reduction factor applied to POD predicted from circumferential crack detection data	See Section A.8.4.2	-		0.80

A.8.5 Effect of Peening on Residual Stress

The set of inputs related to peening considerations is described in Table A-10 at the end of this section, including deterministic and distributed inputs. Various inputs are detailed in the following subsections.

A.8.5.1 Peening Application Scheduling

For both the RVON and RVIN base cases, the peening application is scheduled for the outage coinciding with the second UT inspection. Given the first inspection times and inspection intervals defined in Section A.8.1.2, the time of peening application for the RVON is EOC 17 and the time of peening application for the RVIN is EOC 19.

A.8.5.2 Post-Peening Residual Stresses

The parameterized model for post-peening residual stress profiles are described in Equations [A-17] through [A-21].

For piping DM welds, the residual plus normal operating stress is modeled to remain compressive for all wetted surfaces along the susceptible material, as defined in Section 4. Thus, the peening compressive stress at the surface is set to result in a total (operating plus residual) stress of zero at the circumferential location and for the principal stress direction with the maximum operating stress.

The peening compressive residual stress depth for the DM weld ID is modeled with a normal distribution. This distribution is given a mean of 1.0 mm (0.039 inch). This value is the minimum allowable compressive residual stress depth defined in Section 4. A standard deviation of 0.25 mm (0.010 inch) is conservatively assumed. The non-realistic case of negative penetration depth is prevented by using a lower truncation bound of 0.0 mm (0.0 inch).

To define the transition from the compressive surface layer to the pre-peening stress profile, two characteristic lengths are required (as detailed in Section A.3.3 and Figure A-3). The first length, $x_{2,PPRS}$, defines the distance from the peened surface to the point where the pre-peening WRS profile is regained. The second length, $x_{3,PPRS}$, defines the distance from the peened surface to the point where the post-peening, stress-balanced WRS profile is regained. These lengths are defined with deterministic ratios:

$$x_{3,PPRS} = f_{1,PPRS} x_{1,PPRS}$$
$$x_{2,PPRS} = x_{1,PPRS} + f_{2,PPRS}(x_{3,PPRS} - x_{1,PPRS}) \quad \text{[A-48]}$$

These ratios were defined based on a review of the peening residual stress profiles in MRP-267R1 [4]. Their values are given in Table A-8.

A.8.5.3 Thermal and Load Cycling

The base case probabilistic inputs do not include any stress relaxation effects; the peening residual stress inputs are based on the bounding stresses permitted by the performance criteria of Section 4 for the remaining service life of the component. The inputs described in this section are used in a sensitivity case.

To estimate the stress relaxation occurring in a peened component over a plant service life, experimental data monitoring residual surface stress measurements on a peened surface as a function of time were analyzed. Specifically, measurements were available for three Alloy 182 specimens treated with WJP by Hitachi-GE [4]. These data are shown in Figure A-14.

To accelerate the stress relaxation, the experiments were performed at a temperature of 842°F (450°C) for 1000 hr, which is much higher than typical component temperatures during operation. This temperature and duration were converted to an equivalent operating time at 625°F (329°C) using an Arrhenius relationship with an activation energy of 188 kJ/mol (44.9 kcal/mol), which corresponds to the lower bound of an activation energy range for creep of Alloy 600 in primary water determined by Was et al. [25]. This results in a total equivalent operating time of approximately 59.5 EFPY at 625°F (329°C).

After linearizing the exponential model defined in Section A.3.4, a best-fit value of the stress relaxation exponent was calculated with linear least squares regression. A value of 5.1×10^{-3} $EFPY^{-1}$ was estimated. This results in a stress relaxation vs. time that is nearly linear between 0 and 80 years (77.6 EFPY).

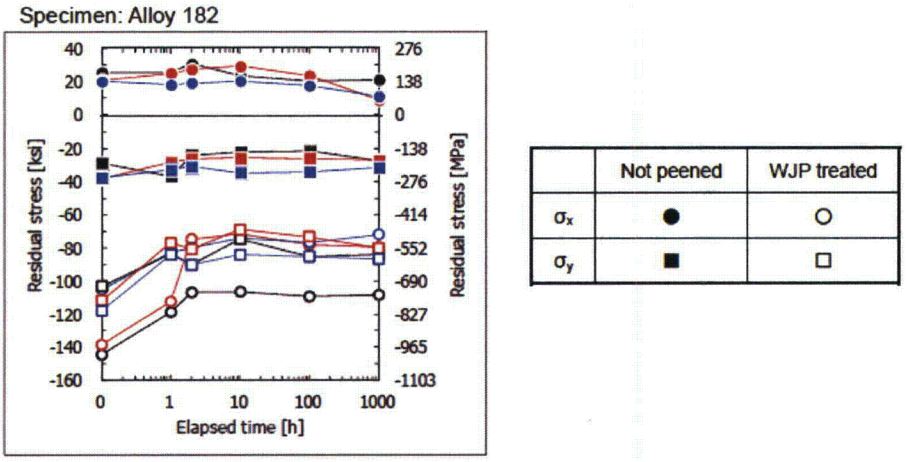

Figure A-14
Experimental Data used to Estimate Thermal Residual Stress Relaxation Factor

A.8.5.4 Effect of Peening on Growth

For the base case probabilistic model results, growth of cracks is simulated without consideration for crack closure. This effect is considered as a sensitivity case.

Also for the baseline results, full credit is given to growth of the length of a crack under the peening surface. As discussed in Section A.5.5, this is done by using the "balloon" growth approximation – neglecting peening stresses for the calculation of length growth. The "balloon" growth approximation is lifted for a sensitivity study.

Table A-10
Summary of Peening-Specific Inputs for DM Weld Model

Symbol	Description	Source	Units	Parameter Type	DMW Base Case
[redacted]	Outage of peening application	Scheduled at next outage coinciding with a UT inspection	Cycle number	RVON	17
				RVIN	19
	Number of cycles between peening application and follow-up	Section 4	# cycles	RVON	2
				RVIN	6
	Inspection interval after peening	Section 4	# cycles	RVON	6
				RVIN	None
	Flag indicating if a UT pre-peening exam is performed	Section 4	-	[redacted]	TRUE
$\sigma_{0,PPRS}$ ($t=0$)	Sum of post-peening residual plus normal operating stress on ID surface	Bounds minimum value from performance criteria (Section 4)	ksi	[redacted]	0.0
$x_{1,PPRS}$	Depth of compressive residual stress layer from ID surface	Bounds minimum value from performance criteria (Section 4)	in.	type	Normal
				mean	0.039
				stdev	0.010
				min	0.000
				max	0.098
$f_{1,PPRS}$	Ratio of minimally-affected depth to peening penetration depth	See Section A.3.3	-	[redacted]	2.0
$f_{2,PPRS}$	Fraction of depth between peening penetration depth and minimally-affected depth where peening results in no effect	See Section A.3.3	-	[redacted]	0.7
m	Empirical stress relaxation exponent	Unused in base case, sensitivity case using best-fit value; Section A.8.5.3	$EFPY^{-1}$	[redacted]	0.0

A.9 Results of Probabilistic Cases

This section presents results generated using the integrated probabilistic model described in Sections A.2 through A.6, with particular focus on the prediction of the leakage criterion described in Section A.7. Using the inputs described in Section A.8, this section presents predictions for the RVON and RVIN base cases without peening mitigation (Section A.9.1) and with peening mitigation (Section A.9.2).

Section A.9.3 presents the results of sensitivity studies wherein one or more inputs or modeling methodologies were varied from those described in Sections A.2 through A.8. The aim of these sensitivity studies is to demonstrate the relative change in the predicted leakage risk for a DM weld component when an input or modeling assumption is varied.

The primary statistics used to assess and compare the results of the probabilistic model are defined below:

- Incremental leakage frequency (ILF) is defined as the average number of new leaking reactor vessel outlet/inlet nozzles per year. A simulated flaw causes leakage if it propagates through the entire material thickness before it is detected and repaired. This statistic is derived for any given operational cycle by averaging the predicted number of new leaking nozzles for that operational cycle across all MC realizations. This is adjusted to a probability per year by dividing by the number of calendar years per cycle.

$$ILF = \frac{\text{(Number of new leaks predicted during cycle across all realizations)}}{\text{(Number of realizations)(Calendar years per cycle)}} \quad \text{[A-49]}$$

- Average leakage frequency (ALF) is the time-average of the ILFs following the hypothetical time of peening until the end of the operational service period of the plant. This statistic is averaged over the number of MC realizations that are active (have not yet leaked) following the hypothetical time of peening. Using this subset of realizations provides no credit to realizations where the component leaks and is removed from the modeled population prior to the hypothetical time of peening.

$$ALF = \frac{\sum_{i=i_{peen}}^{N_{cycle}} \text{(Number of new leaking nozzles predicted during cycle across all realizations)}}{\text{(Number of realizations)(Calendar years per cycle)}(N_{cycle} - i_{peen})} \quad \text{[A-50]}$$

where:

N_{cycle} = number of cycles in operational service period
i_{peen} = cycle number associated with the hypothetical time of peening

- Cumulative probability of leakage (CPL) is defined as the fraction of reactor vessel inlet/outlet nozzles with a predicted leak across all active MC realizations across all cycles of interest. This document reports two versions of this statistic: (1) cumulated from the start of operation to a given cycle and (2) cumulated from the hypothetical time of peening to the end of plant operation. When calculating the CPL after the hypothetical time of peening, realizations in which leakage occurs prior to the time of peening are discarded and are not included in the reported statistic.

$$CPL = \frac{\text{(Total number of realizations with at least one predicted leak)}}{\text{(Number of realizations)}} \quad \text{[A-51]}$$

These probabilistic results are used to compare the risk associated with peened welds examined on a relaxed schedule versus the risk for unmitigated welds examined per the standard intervals. This comparative approach has the advantage of minimizing any potential for bias introduced by the various modeling assumptions.

A.9.1 Results for the Unmitigated Case

Using the inputs specified in Section A.8, predictions were made for the RVON and RVIN base cases without any peening mitigation; leakage probability vs. time predictions are given in Figure A-15 and Figure A-16, respectively. For these cases, inspections were scheduled based on N-770-1 for unmitigated components.

For reference, the hypothetical time of peening is shown on these plots. As discussed in the inputs section, this time of peening has been set to coincide with the second modeled UT inspection. Between the hypothetical time of peening and 80 calendar years (77.6 EFPY), the model predicts a cumulative probability of leakage of 1.5×10^{-1} for the RVON and 2.1×10^{-3} for

the RVIN. These values will be important for assessing the performance of peening with respect to leakage mitigation in the following section.

A.9.2 Results with Peening Mitigation

As discussed previously, a follow-up inspection is expected to be conducted either one, two, three, or six cycles after peening, and after the follow-up inspection, a new in-service inspection interval is expected to be utilized through the end of plant service life. Various combinations of follow-up inspection time and in-service inspection frequency were used to make leakage risk predictions after peening. These results are summarized in Figure A-17 and Figure A-18 for the RVON and RVIN, respectively. It is emphasized that no surface examinations are modeled at the pre-peening inspection for these results.

For both the hot and cold DM weld components, the predicted likelihood of cracks existing after the pre-peening inspection is very low; less than 2.6×10^{-3}.

For the RVON, it was predicted that the cumulative probability of leakage after peening would be reduced by a factor between 60 and 150, (compared to cumulative leakage probabilities on same span of time for an unmitigated RVON), depending on the post-peening follow-up examination and ISI scheduling. While there is some small trend with respect to follow-up time, in general the degree of improvement is not significantly influenced by the follow-up time or the ISI frequency. The former is the result of the fact that most of the cracks that go undetected at the pre-peening inspection are small, and accordingly grow slowly after peening (see deterministic calculations that demonstrate this in Section 5.2); the latter is a result of the fact that nearly all cracks are detected during the pre-peening or follow-up inspection and no new cracks are expected to initiate after peening.

For the RVIN, it was predicted that the cumulative probability of leakage after peening is reduced by a factor between 8 and 24, (compared to cumulative leakage probabilities on same span of time for an unmitigated RVIN), depending on the post-peening follow-up examination and ISI scheduling. This degree of improvement is smaller than that predicted for the RVON because the inspection schedule for an unmitigated RVIN conservatively takes little credit for its reduced temperature in comparison to that for hot-leg locations.

For both the RVON and RVIN peening base cases, the probability of leaking after the follow-up inspection is very low, as can be seen in Figure A-15 and Figure A-16. Furthermore, Figure A-19 demonstrates the decaying nature of leakage probability vs. time after peening, for both the hot and cold components with relaxed UT inspection intervals.

A.9.3 Results for Sensitivity Cases

Various sensitivity studies were conducted with the DM weld probabilistic model in order to demonstrate the relative change in the predicted results given one or more changes to modeling or input assumptions. Each sensitivity case has been classified as either a Model Sensitivity (in which an approximated input or model characteristic is varied) or an Inspection Scheduling Sensitivity (in which a controllable inspection option is varied). These sensitivity cases are described in Table A-11 and Table A-12.

Figure A-20 (RVON) and Figure A-25 (RVIN) compare the cumulative probability of leakage from the hypothetical time of peening to end of plant operation for peened and unmitigated components for Inspection Scheduling Sensitivity cases.

Figure A-21 through Figure A-24 compare the cumulative probability of leakage from the hypothetical time of peening to the end of the operational service period of the plant for peened (Figure A-21 and Figure A-22) and unmitigated (Figure A-23 and Figure A-24) RVON Model Sensitivity cases, respectively. Figure A-26 through Figure A-29 provide the equivalent comparison for RVIN cases.

All sensitivity cases for peened components result in a cumulative probability of leakage substantially below that of the equivalent sensitivity case for an unmitigated component.

The cases of greatest interest are discussed below:

DMW Inspection Scheduling Sensitivity Cases 1 and 2: Skipping Pre-Peening or Follow-Up UT Inspections

The base case included a volumetric (UT) inspection during the pre-peening examination, as well as a follow-up inspection before entering a relaxed in-service inspection schedule. Under the conservative assumption that no credit is taken for the required ET examinations, both the pre-peening and follow-up inspections are key for detecting significant cracks before entering the relaxed inspection schedule. Skipping UT follow-up examinations (Inspection Scheduling Sensitivity Case 1) results in a CPL of 2.5×10^{-3} for the RVON and a CPL of 5.4×10^{-4} for the RVIN. Skipping UT pre-peening inspections (Inspection Scheduling Sensitivity Case 2) results in a CPL of 1.1×10^{-2} for the RVON and a CPL of 9.4×10^{-4} for the RVIN. These sensitivity cases emphasize the importance of pre-peening and follow-up inspections, such that pre-existing cracks that extend beyond the peening compressive layer are detected and corrected.

DMW Model Sensitivity Case 6 – Decreasing UT POD Curves by 20%

The base case POD curves shown in Figure A-9 are a conservatively modified version of the POD model from MRP-262 [16], with a zero POD assumed for flaws less than 10% through–wall. This sensitivity study decreases both UT POD curves by 20%, which results in an increased cumulative probability of leakage. The scaled POD curve results in a CPL of 4.5×10^{-3} for the peened RVON, a CPL of 1.9×10^{-1} for the unmitigated RVON, a CPL of 6.3×10^{-4} for the peened RVIN, and a CPL of 3.7×10^{-3} for the unmitigated RVIN. However, this sensitivity case results in a maximum POD just under 80% for near-through-wall circumferential flaws, which is significantly lower than the best-estimate POD curve derived from personnel and equipment qualification data representative of NDE methods applied in the field. Furthermore, the POD curve for axial flaws applied in this sensitivity case falls below the minimum detection rates (between 0.68 and 0.82) defined in Appendix VIII of ASME Section XI [26] for specimens with a mixture of circumferential and axial flaws.

DMW Model Sensitivity Cases 7 and 8 – NB-3600 [27] Bending Loads

To study the effect of worst-case bending loads on leakage, the high and extreme loads calculated with NB-3600 [27] equations were applied to RVON in DMW Model Sensitivity Case 7.

The extreme bending load calculated using NB-3600 equations is approximately 90% larger than the load used in the base case. These modified loads result in a CPL of 1.1×10^{-3} for the peened RVON, a CPL of 1.9×10^{-1} for the unmitigated RVON, a CPL of 1.6×10^{-4} for the peened RVIN, and a CPL of 2.6×10^{-3} for the unmitigated RVIN. While this resulted in a modest increase in the probability of the leakage for the unmitigated component, it counter-intuitively reduced the probability of leakage for the peened component. This is partially due to the fact that the higher bending results in faster crack growth prior to peening, and thus higher probabilities of detection at the pre-peening inspection.

To compensate for this effect (in Model Sensitivity Case 8), a reduction factor is applied to t_1 of the first crack initiation time model.

$$t_1' = f_{adjust} t_1 \qquad \text{[A-52]}$$

This results in earlier first crack initiation to counteract the reduction in the mean arrival time of multiple crack initiation. The reduction factor is calculated to normalize the initiation times of the extreme bending case:

$$f_{adjust} = \left(\frac{\sigma_{surf,base}}{\sigma_{surf,extreme}} \right)^n \qquad \text{[A-53]}$$

where $\sigma_{surf,base}$ and $\sigma_{surf,extreme}$ are the nominal surface stresses at the point of maximum bending for the base case and the extreme loading case, respectively. The modified loads and initiation model result in a CPL of 3.2×10^{-3} for the peened RVON, a CPL of 3.7×10^{-1} for the unmitigated RVON, a CPL of 5.7×10^{-4} for the peened RVIN, and a CPL of 9.0×10^{-3} for the unmitigated RVIN. This suggests that the faster rate of growth due to the larger bending load outweighs the larger POD at the pre-peening inspection.

DMW Model Sensitivity Case 10: Time-Dependent Residual Stress Relaxation

As an alternative to the bounding peening performance criteria defined in Section 4, an example peening surface stress was combined with a time-dependent residual stress relaxation for DMW Model Sensitivity Case 10.

As demonstrated in Figure A-21, the relative change caused by applying this model was negligible. The modified stress profile results in a CPL of 1.6×10^{-3} for the peened RVON, and a CPL of 2.2×10^{-4} for the peened RVIN. Both of these results are statistically equivalent to the respective peening base cases. This case supports the conclusion that the majority of the benefit of peening comes from preventing further cracks from initiating and arresting shallow flaws within the compressive stress region.

DMW Model Sensitivity Case 13: Earlier Initiation of First PWSCC

This model sensitivity case explored the effect of shifting the initiation time model such that initiations are predicted earlier in general. This provides an alternative approach to accounting for the fact that the initiation model used for the base case was fit to data for detected cracks; hypothetically, if undetected cracks could be included to fit the initiation model, the initiation time distribution would be shifted toward earlier times. (On the other hand, some detections used

to fit the initiation model may not reflect actual PWSCC.) Conservatively, the parameter t_1 of the first crack initiation model, which quantifies the time at which 1% of DM weld components are expected to initiate PWSCC, was reduced by a factor 3 for this sensitivity case.

The modified initiation model results in a CPL of 6.2×10^{-3} for the peened RVON, a CPL of 3.2×10^{-1} for the unmitigated RVON, a CPL of 1.4×10^{-3} for the peened RVIN, and a CPL of 1.2×10^{-2} for the unmitigated RVIN. This sensitivity case results in the largest CPL of all modeling sensitivity cases for the mitigated RVON, mitigated RVIN, and unmitigated RVIN.

It is noted that cumulative probability of leakage for an unmitigated RVON, predicted at 23 EFPY, for this sensitivity case, was approximately 28%. This is a higher probability than indicated by the incidence rate in U.S. PWRs.

DMW Model Sensitivity Case 15: Correlation of Initiation and Growth

DMW Model Sensitivity Case 15 explored the generally accepted tendency for cracks that initiate earlier to grow faster; specifically it explored this tendency's impact on the leakage probability predictions. This tendency is implemented by adding a negative correlation between the time of first crack initiation on DM weld component, t_{ref}, and the weld-to-weld variation factor, f_{weld}, as well as between each multiple crack initiation time, $t_{ref,i}$, and the sampled within-weld variation, $f_{ww,i}$, for each crack. The base case used zero correlation because cases in which relative material susceptibility to both initiation and growth are available are rare, precluding development of a proper correlation coefficient. Instead, this sensitivity case uses a medium/strong (-0.8) correlation coefficient for the correlations described above.

Applying a correlation between initiation and growth results in a CPL of 7.7×10^{-4} for the peened RVON, a CPL of 2.7×10^{-1} for the unmitigated RVON, a CPL of 1.2×10^{-4} for the peened RVIN, and a CPL of 1.0×10^{-2} for the unmitigated RVIN. For the peened component, adding correlation results in a decrease in the probability of leakage after peening because it causes generally larger cracks at the time of the pre-peening inspection which fosters detection before the relaxed inspection scheduled. However, for the unmitigated component, adding correlation results in an increase in probability of leakage because cracks that initiate during the operating lifetime of a DM weld component are considered early (for the corresponding chemical and material conditions) and thus grow faster.

DMW Model Sensitivity Cases 18 and 19: Reduced Initial Crack Depth

The base case inputs used to make predictions for the RVON assumed an initial crack depth with a 5th percentile of roughly 2 mm (3% TW), a median of 3.5 mm (5% TW), and a 95th percentile of roughly 6 mm (9% TW). In reality, the initiation depth of PWSCC can be on the micro- or nano-scale, arising from manufacturing processes, other forms of corrosion, cavitation, etc. The rationale behind selecting a much larger initiation depth is that the initiation time model is based on data for detected cracks, and so it does not account for micro- or nano-scale cracks, of which there are likely many more incidences. Furthermore, the prediction of crack growth rate with the methods presented in the modeling section is compromised as the depth of the crack to be analyzed becomes smaller than approximately 0.1 mm.

Because of the importance of detection during the pre-peening and follow-up inspections, it may be non-conservative to assume cracks with large initial depths. Such cracks may more easily be detected at the pre-peening or follow-up inspections, resulting in fewer active cracks during the

post-peening ISI schedule. DMW Model Sensitivity Cases 18 and 19 assessed this possibility by using an initial crack depth distribution with a median depth 10 times less than that used for the base case, resulting in an initial crack depth with a 5th percentile of roughly 0.2 mm (0.3% TW), a median of 0.35 mm (0.5% TW), and a 95th percentile of roughly 0.6 mm (0.9% TW). This is investigated in combination with utilizing crack closure methodology (Model Sensitivity Case 18) and by applying a minimum K_I value (Model Sensitivity Case 19).

Applying a reduced initial crack depth and imposing a minimum stress intensity factor (Model Sensitivity Case 19) results in a CPL of 2.8×10^{-3} for the peened RVON, a CPL of 1.4×10^{-1} for the unmitigated RVON, a CPL of 4.8×10^{-4} for the peened RVIN, and a CPL of 2.0×10^{-3} for the unmitigated RVIN. The reduction in initial depth with a minimum K_I results in increased leakage likelihood for DMWs. Nonetheless, the leakage likelihood for peened DMWs with a relaxed in-service inspection schedule remains well below that predicted for unpeened components inspected in accordance with the applicable requirements for unmitigated DMWs.

Applying a reduced initial crack depth and crack closure (Model Sensitivity Case 18) results in a CPL of 3.1×10^{-3} for the peened RVON, a CPL of 1.4×10^{-1} for the unmitigated RVON, a CPL of 4.9×10^{-4} for the peened RVIN, and a CPL of 2.0×10^{-3} for the unmitigated RVIN.

The application of the partial crack closure methodology with the reduction in initial depth has a rather small effect on the leakage predictions. This is because flaws generally reside in one of two states at the time of peening: i) shallower than the compressive stress layer resulting from peening and therefore fully closed and arrested or ii) appreciably deeper (e.g., two times or more) than the compressive stress layer and therefore largely unaffected. The fraction of flaws between these states — i.e., the fraction of flaws for which partial crack closure may be important — is small for peening. Partial crack closure has been found to be more important for deeper stress improvement methods like mechanical stress improvement.

Table A-11
Description of Modified Inputs for DMW Model Sensitivity Cases

Sensitivity Case	Description	Symbol	Units	Parameter Type	Base Case Value	Sensitivity Case Value
M1	Reduce Operating Capacity Factor	CF	-	RVON	0.97	0.92
				RVIN	0.97	0.92
M2	Reject trials with detections before given cycle		Cycle number	RVON	0	16
				RVIN	0	18
M3	Halve growth integration time step	$1/\Delta t$	1/yr		12	24
M4	Remove correlation between UT inspections	ρ_{insp}	-		0.5	0.0
M5	Linearly extraplolate POD to zero below 10% TW		-		Assume POD = 0 below 10% TW	Linearly extrapolate
M6	Decrease POD by 20%	$\beta_{1\,(BI)}$	-	mean	3.244	1.242
				stdev	0.549	0.210
		$\beta_{2\,(BI)}$	-	mean	1.06	0.055
				stdev	1.32	0.069
M7	Increase effective bending load per NB-3600 Eq. 10	M_y	in.-kips	RVON	40000	75987
		M_y	in.-kips	RVIN	40000	75987
M8	Increase effective bending load per NB-3600 Eq. 10 and decrease initiation characteristic time	M_y	in.-kips	RVON	40000	75987
		M_y	in.-kips	RVIN	40000	75987
		t_1	EDY	type	Normal	Normal
				mean	11.40	5.18
				stdev	0.304	0.304
				min	3.14	1.43
				max	41.10	18.68
M9	Decrease effective load to match Case C of ML112160169	M_y	in.-kips	RVON	40000	14721
		M_y	in.-kips	RVIN	40000	14721
M10	Include time-dependent stress relaxation	$\sigma_{0,PPRS}$ $(t=0)$	ksi		Normal operating plus residual stress is zero ksi	Residual stress is 30.75 ksi compressive
		m	$EFPY^{-1}$		0	5.10E-03
M11	Double standard deviation of peening penetration depth	$x_{1,PPRS}$	in.	type	Normal	Normal
				mean	0.039	0.039
				stdev	0.010	0.020
				min	0.000	0.000
				max	0.098	0.157
M12	Increase peening compressive surface stress and penetration depth	$\sigma_{0,PPRS}$ $(t=0)$	ksi		Normal operating plus residual stress is zero ksi	Residual stress is 100 ksi compressive
		$x_{1,PPRS}$	in.	type	Normal	Normal
				mean	0.039	0.118
				stdev	0.010	0.059
				min	0.000	0.000
				max	0.098	0.295
M13	Decrease initiation characteristic time by factor of 3	t_1	EDY	type	Normal	Normal
				mean	11.40	3.80
				stdev	0.304	0.304
				min	3.14	1.047
				max	41.10	13.70
M14	Increase multiple flaw initiation model slope	β_{flaw}	-	type	Normal	Normal
				mean	2.0	3.0
				stdev	0.5	0.5
				min	1.0	1.0
				max	5.0	6.0
M15	Include initiation-growth correlation	ρ_{weld}	-		0.0	-0.8
		ρ_{ww}	-		0.0	-0.8

Table A-11 (continued)
Description of Modified Inputs for DMW Model Sensitivity Cases

Sensitivity Case	Description	Symbol	Units	Parameter Type	Base Case Value	Sensitivity Case Value
M16	Increase initiation activation energy to N-729-1 value	Q_i	kcal/mole	type	Normal	Normal
				mean	44.03	50.00
				stdev	3.06	3.06
				min	25.65	31.62
				max	62.41	68.38
M17	Remove stress adjustment of initiation times	n	-	type	Normal	Constant
				mean	4.0	0.0
				stdev	1.0	-
				min	0.0	-
				max	10.0	-
M18	Utilize crack closure methodology and decrease initial flaw depth		-		Do not utilize crack closure	Utilize crack closure
		a_0/t	-	type	Log-Normal	Log-Normal
				linear μ	0.053	0.0053
				median	0.050	0.0050
				log-norm μ	-3.00	-5.30
				log-norm σ	0.35	0.35
				min	0.01	0.001
				max	0.42	0.42
M19	Decrease median initial crack depth and impose minimum K value	a_0/t	-	type	Log-Normal	Log-Normal
				linear μ	0.053	0.005
				median	0.050	0.005
				log-norm μ	-3.00	-5.30
				log-norm σ	0.35	0.35
				min	0.01	0.001
				max	0.42	0.42
		$K_{I,min}$	ksi-in.$^{0.5}$		0.00	10.9
M20	Increase growth activation energy	Q_g	kcal/mole	type	Normal	Normal
				mean	31.07	33.46
				stdev	1.195	1.195
				min	23.90	26.29
				max	38.24	40.63
M21	Increase coalescence distance threshold	$1/F_{coalescence}$	-		1.0E-06	0.5
M22	Utilize crack closure methodology		-		Do not utilize crack closure	Utilize crack closure
M23	Prevent balloon growth		-		Prevent balloon growth	Allow balloon growth
M24	Increase peening compressive surface stress and penetration depth	$\sigma_{0,PPRS}$ $(t=0)$	ksi		Normal operating plus residual stress is zero ksi	Residual stress is 100 ksi compressive
		$x_{1,PPRS}$	in.	type	Normal	Normal
				mean	0.039	0.118
				stdev	0.010	0.059
				min	0.000	0.000
				max	0.098	0.295
	Utilize crack closure methodology		-		Do not utilize crack closure	Utilize crack closure
	Prevent balloon growth		-		Prevent balloon growth	Allow balloon growth

Table A-12
Summary of Modified Inputs for DMW Inspection Scheduling Sensitivity Cases

Sensitivity Case	Description	Symbol	Units	Parameter Type	Base Case Value	Sensitivity Case Value
S1	Skip follow-up inspection and enter post peening ISI schedule	[redacted]	-	RVON	Perform follow-up UT 2nd cycle after peening	Skip follow-up UT inspection; first ISI after .6 cycles
				RVIN	Perform follow-up UT 6th cycle after peening	Do not perform UT inspection after peening
S2	Skip UT during pre-peening inspection	[redacted]	-	[redacted]	Perform UT during pre-peening inspection	Skip UT during pre-peening inspection

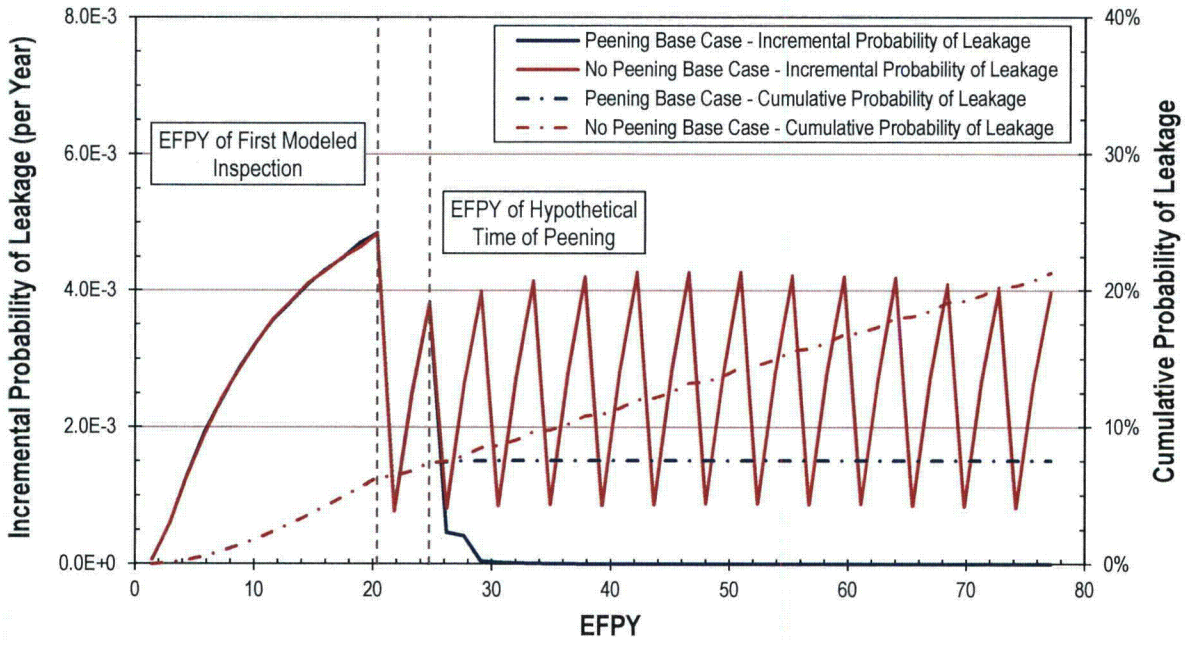

Figure A-15
Prediction of Leakage vs. Time for RVON

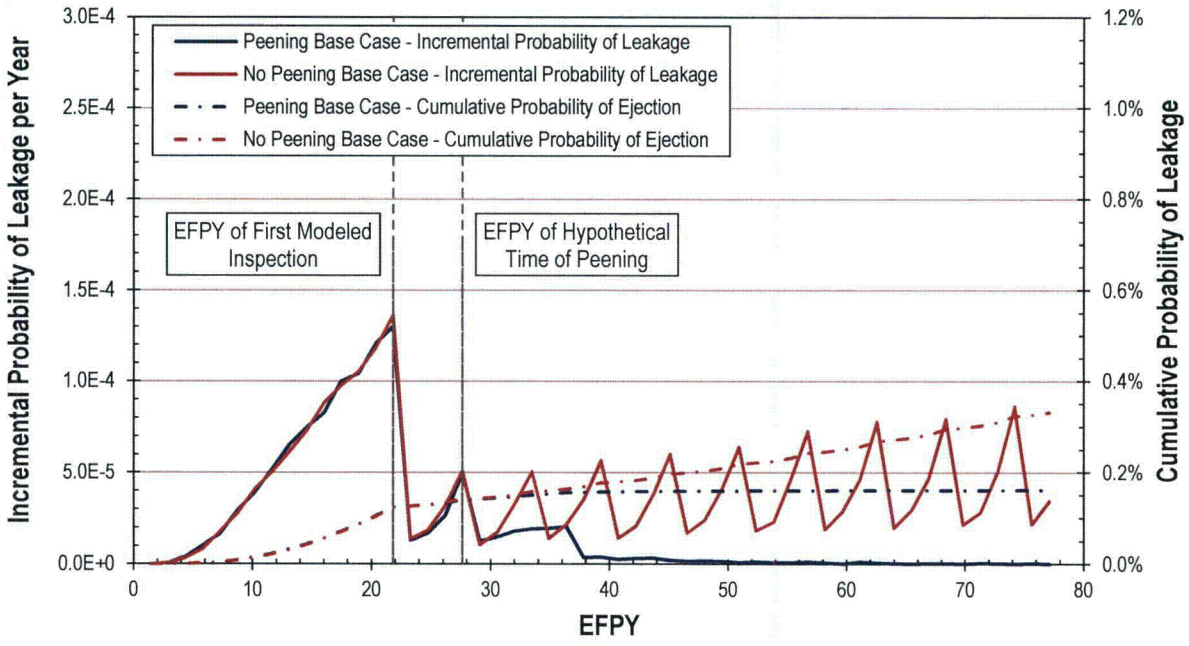

Figure A-16
Prediction of Leakage vs. Time for RVIN

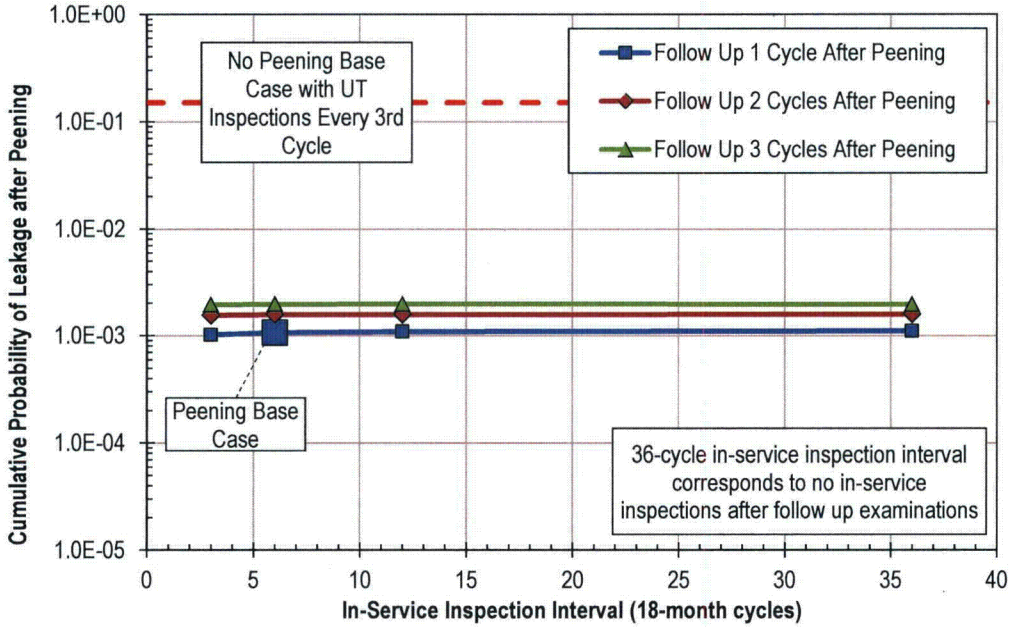

Figure A-17
Cumulative Probability of Leakage from Hypothetical Time of Peening to End of Operational Service Period vs. ISI Frequency for a RVON

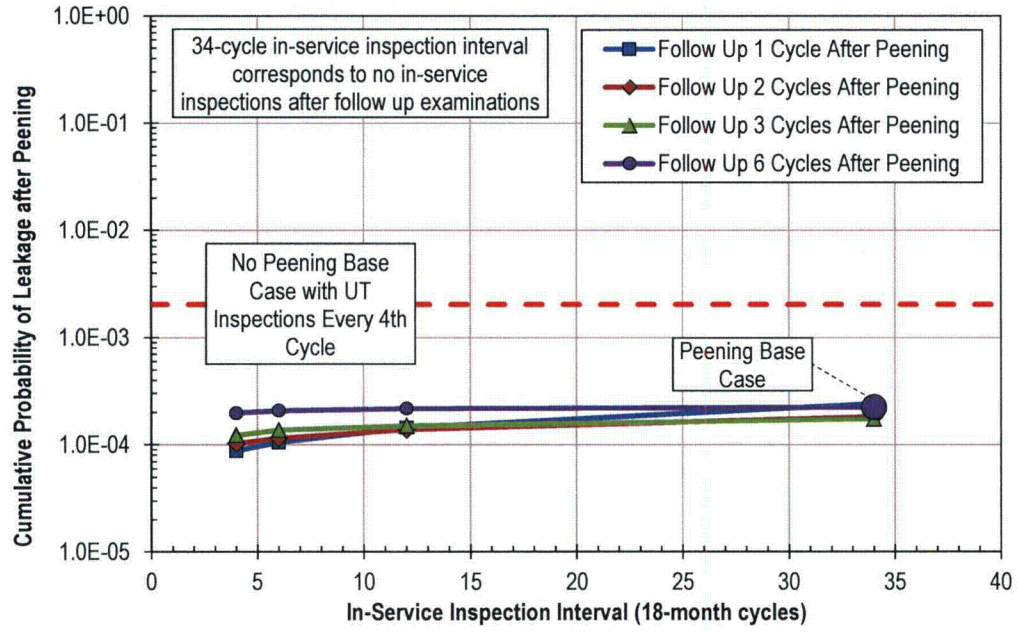

Figure A-18
Cumulative Probability of Leakage from Hypothetical Time of Peening to End of Operational Service Period vs. ISI Frequency for a RVIN

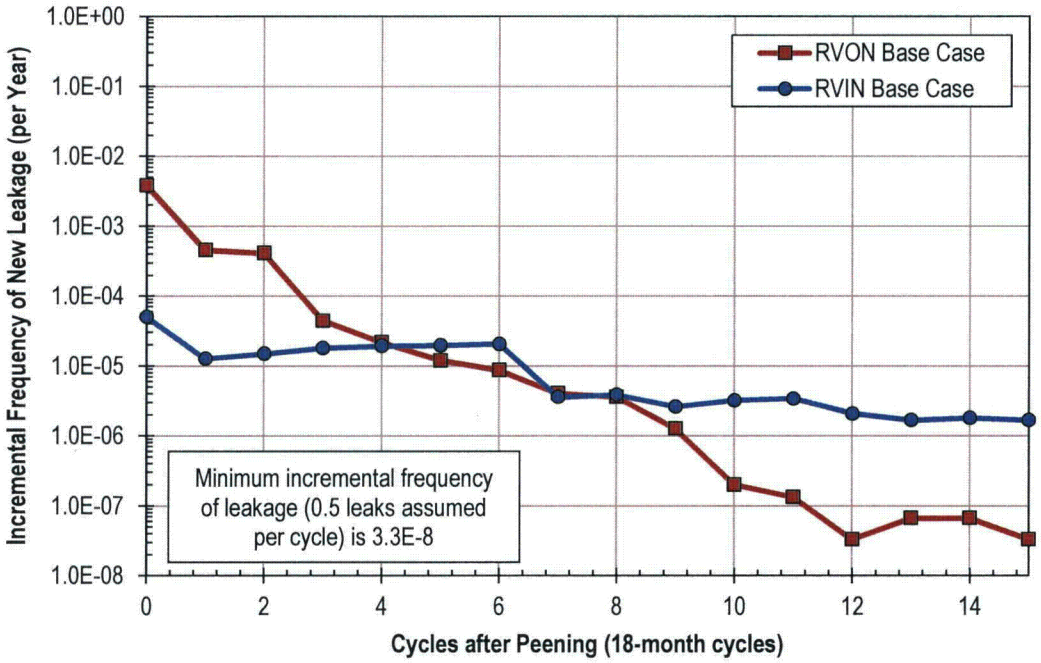

Figure A-19
Incremental Leakage Frequency after Peening with Relaxed ISI Intervals

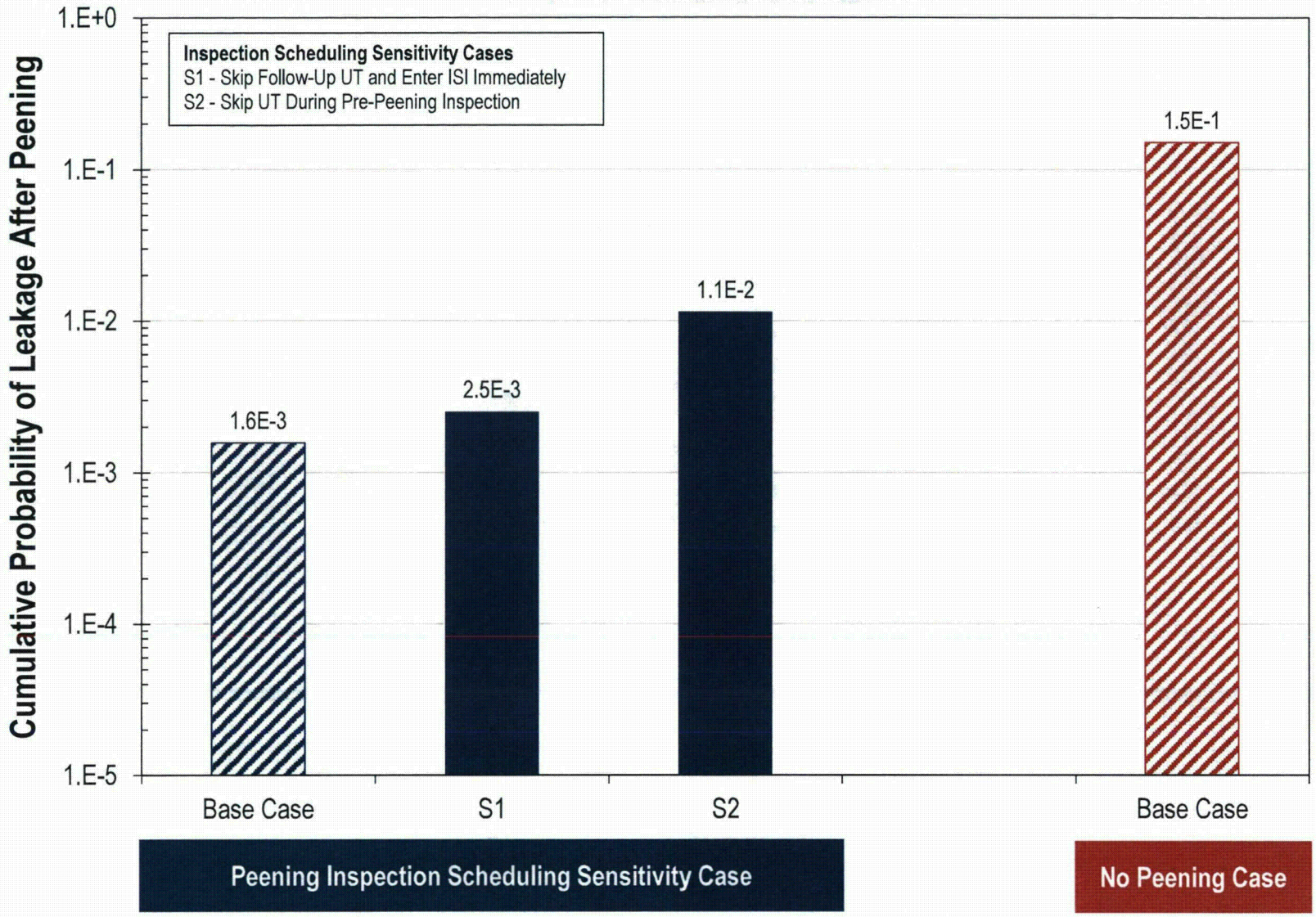

Figure A-20
Summary for Inspection Scheduling Sensitivity Results for RVON Probabilistic Model with Peening

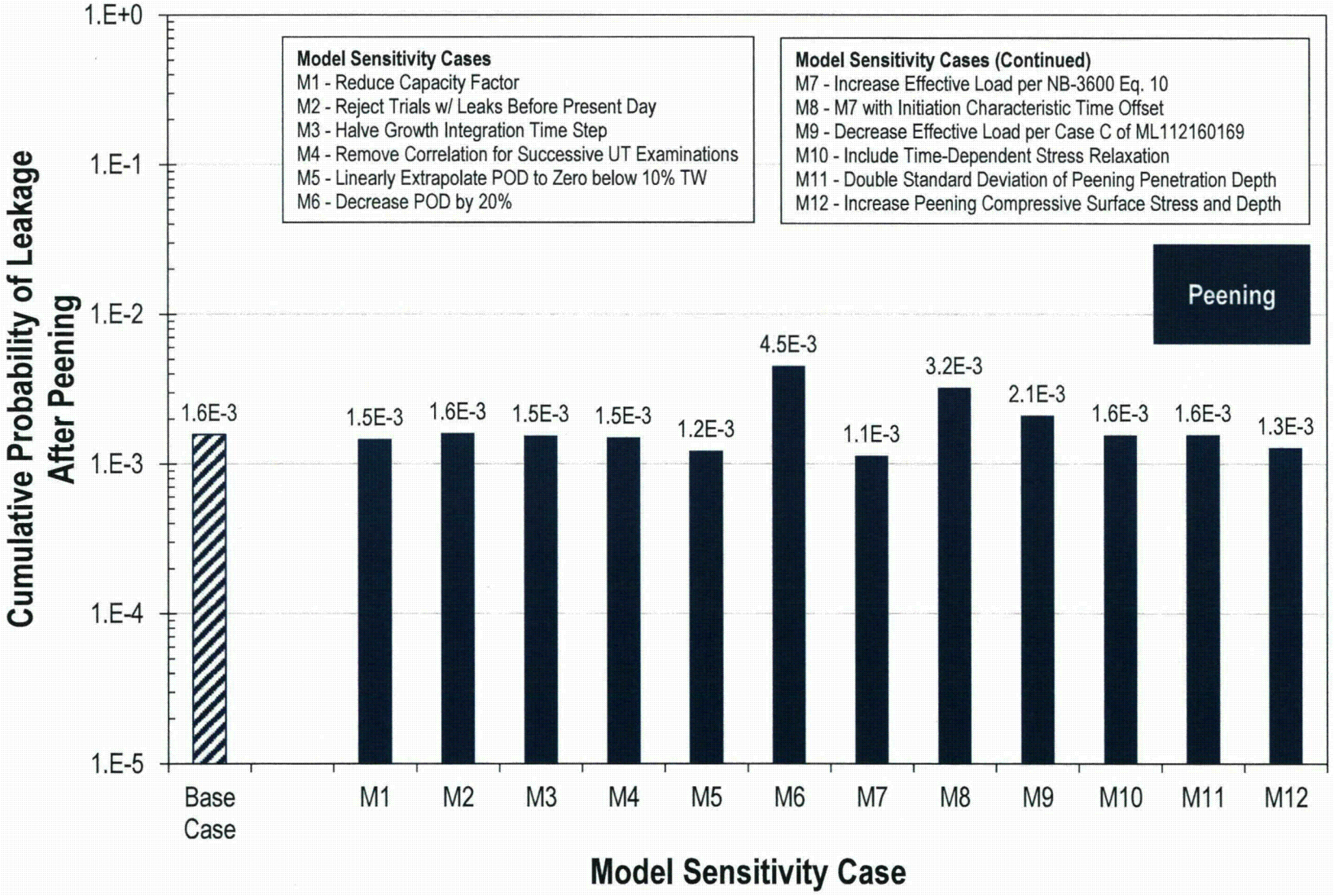

Figure A-21
Summary of Model Sensitivity Results for RVON Probabilistic Model with Peening

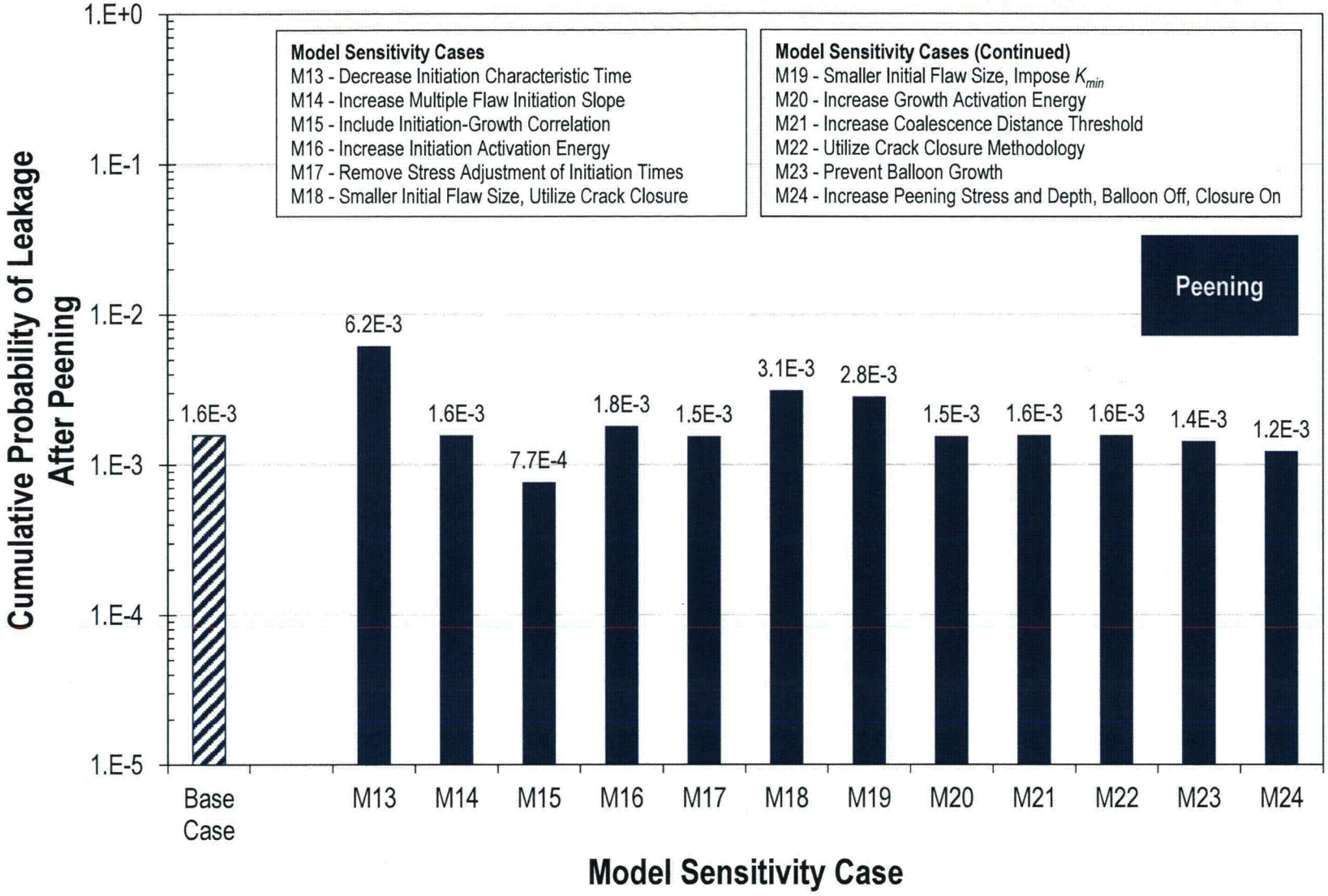

Figure A-22
Summary of Model Sensitivity Results for RVON Probabilistic Model with Peening (continued)

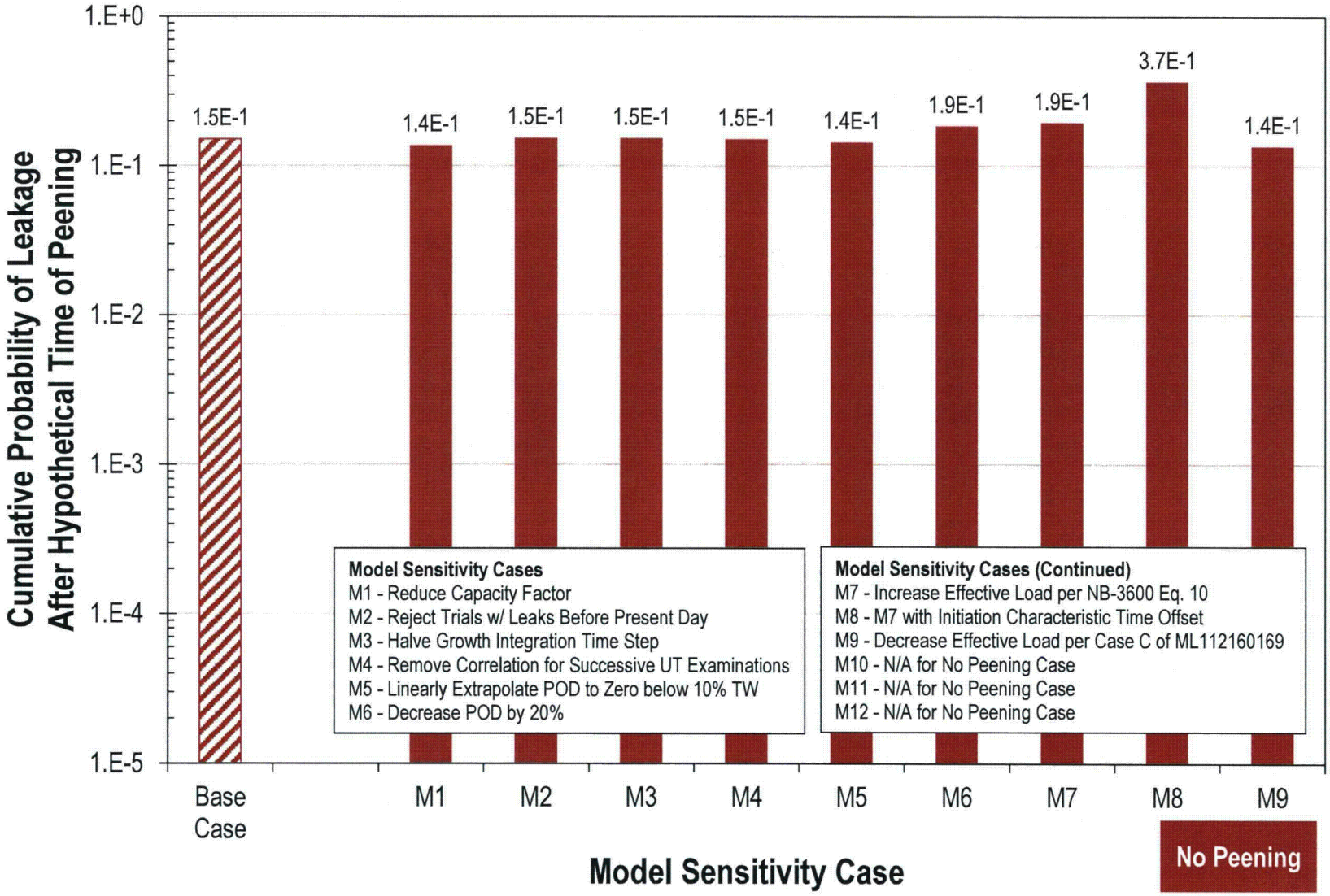

Figure A-23
Summary of Model Sensitivity Results for RVON Probabilistic Model without Peening

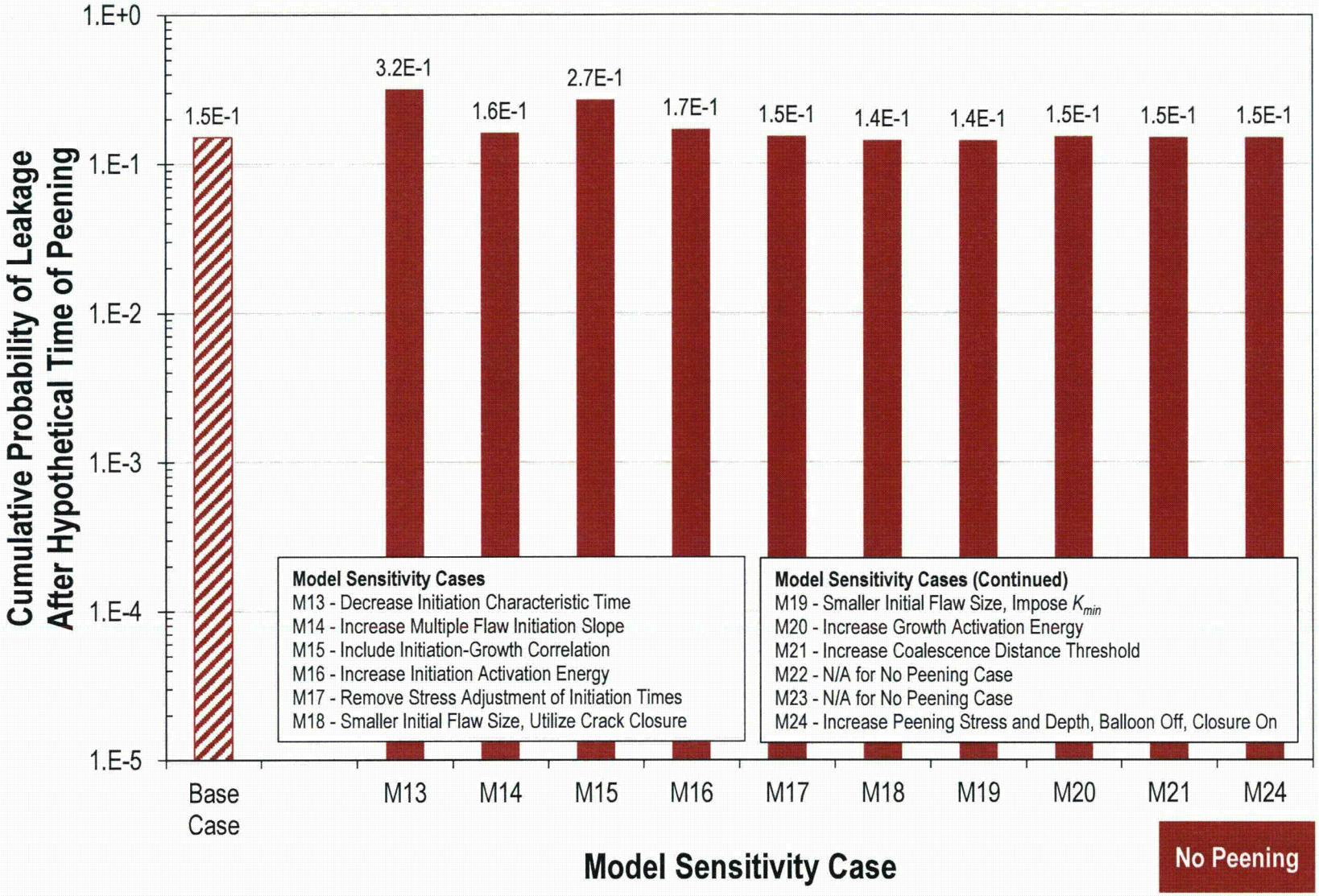

Figure A-24
Summary of Model Sensitivity Results for RVON Probabilistic Model without Peening (continued)

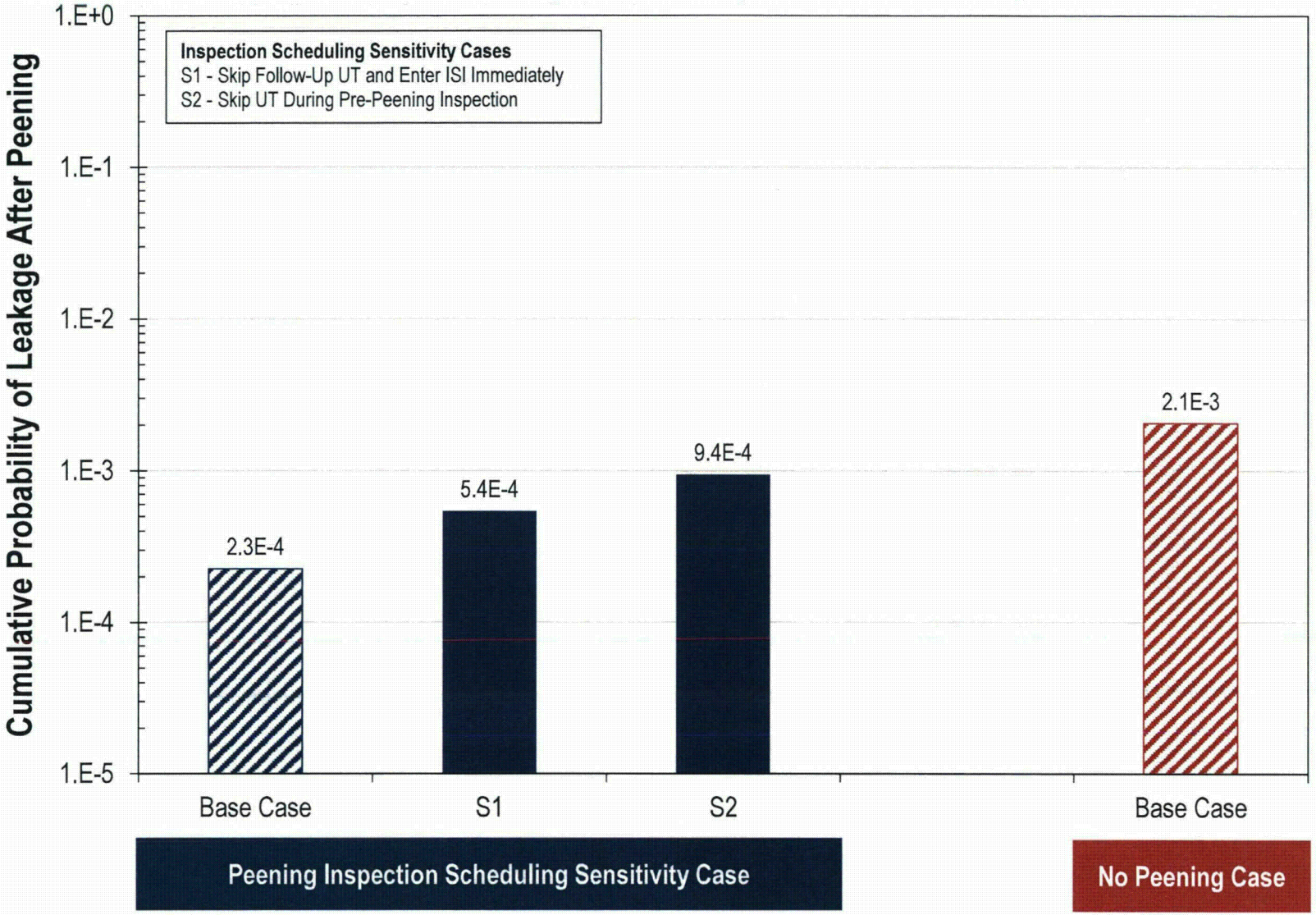

Figure A-25
Summary for Inspection Scheduling Sensitivity Results for RVIN Probabilistic Model with Peening

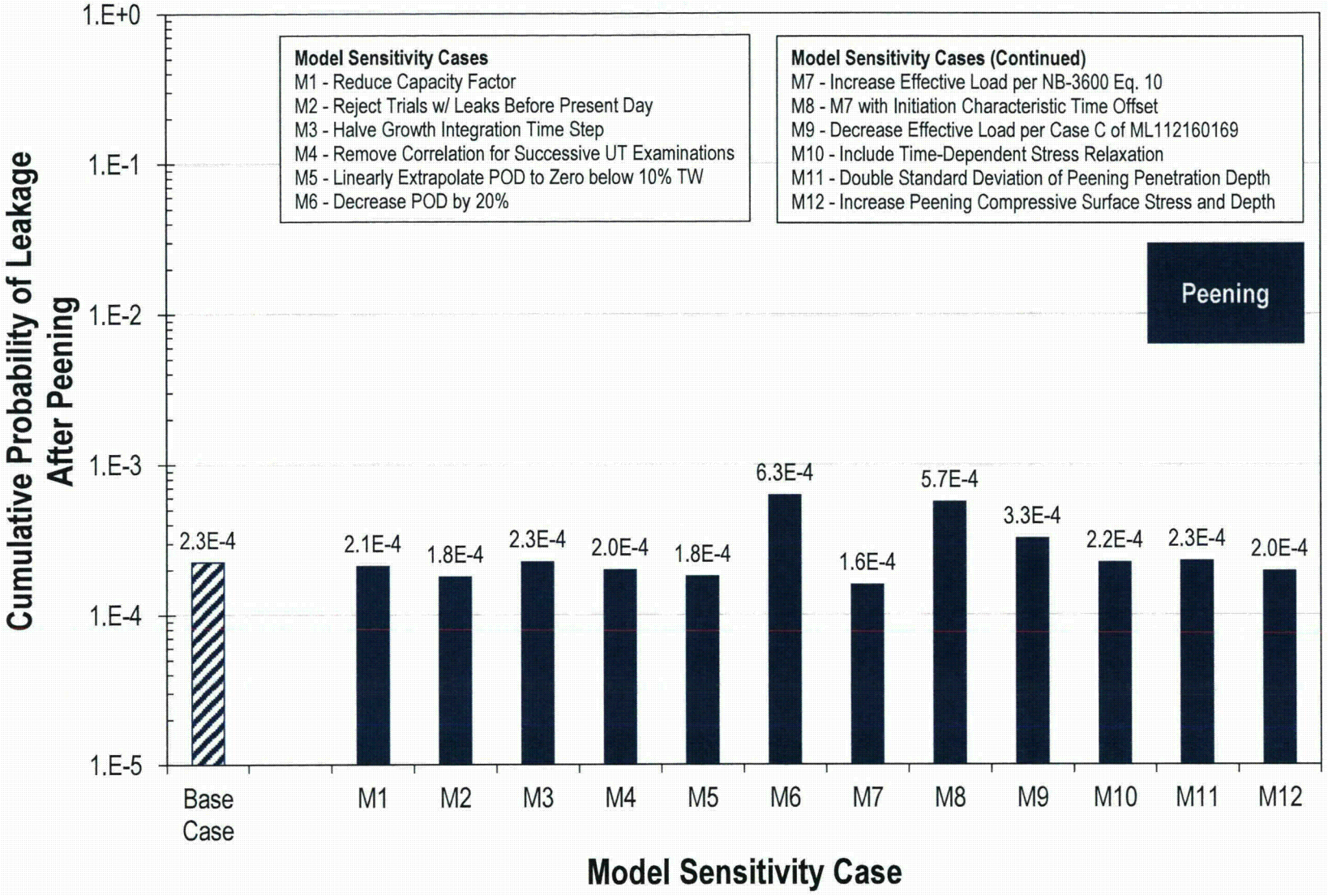

Figure A-26
Summary of Model Sensitivity Results for RVIN Probabilistic Model with Peening

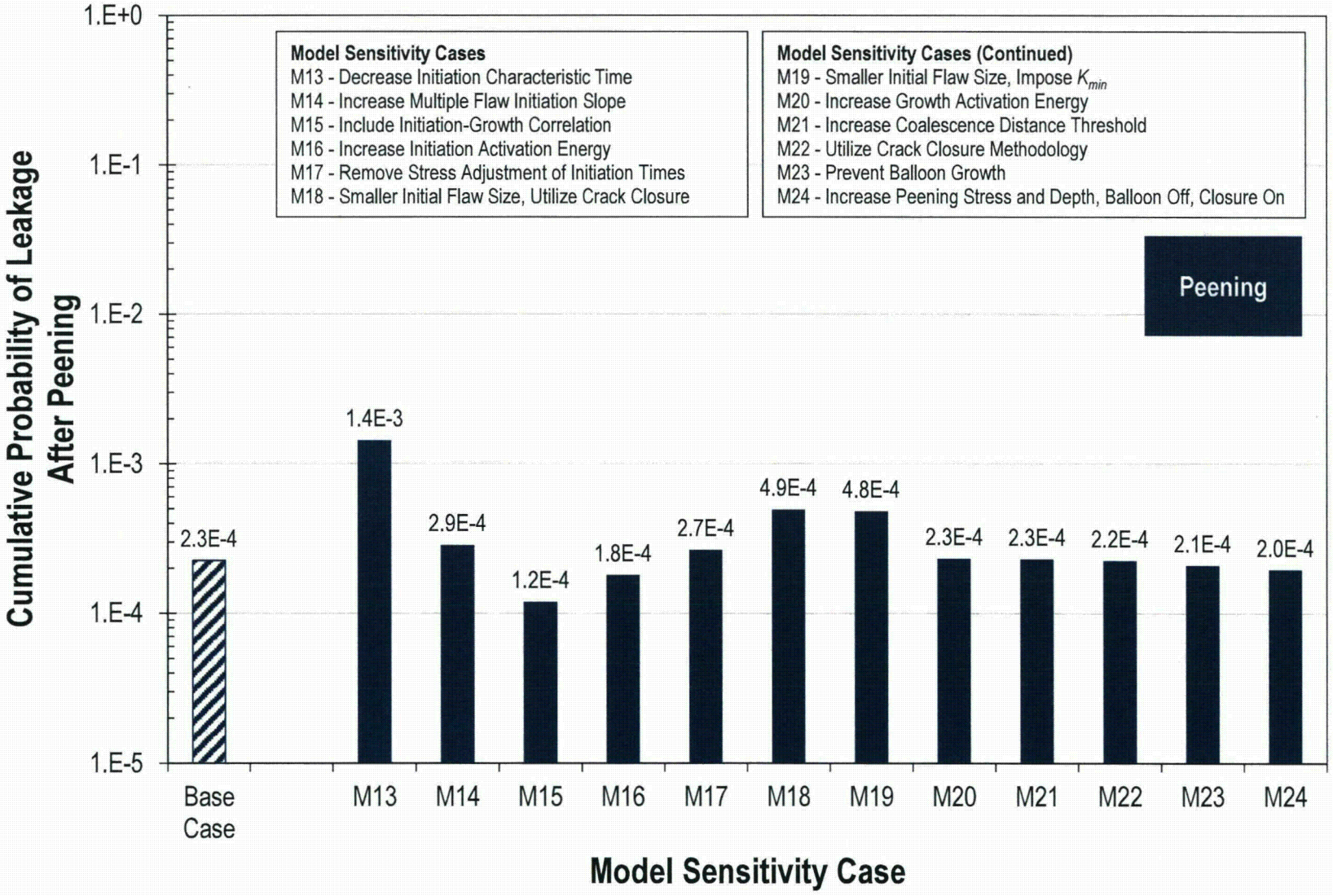

Figure A-27
Summary of Model Sensitivity Results for RVIN Probabilistic Model with Peening (continued)

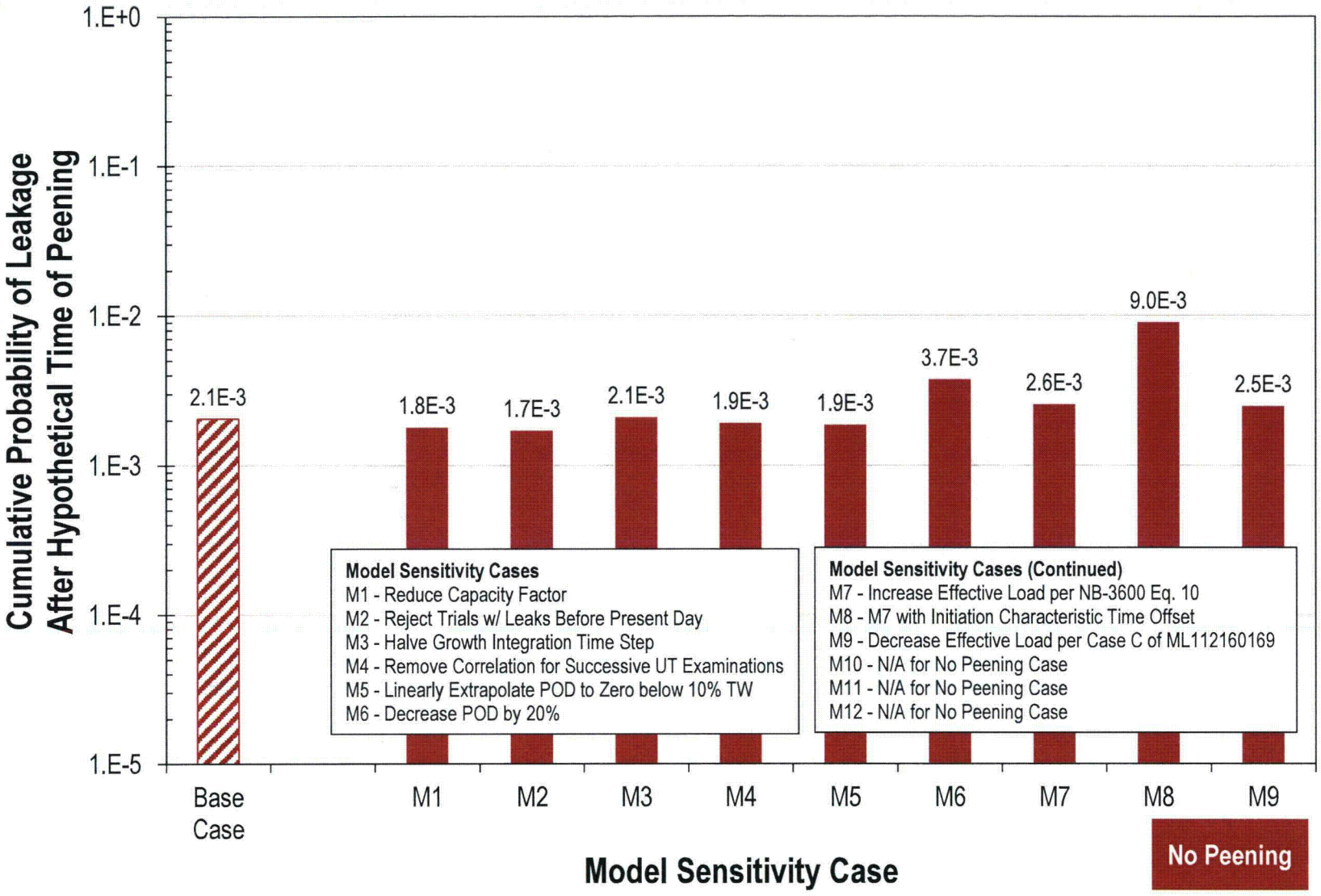

Figure A-28
Summary of Model Sensitivity Results for RVIN Probabilistic Model without Peening

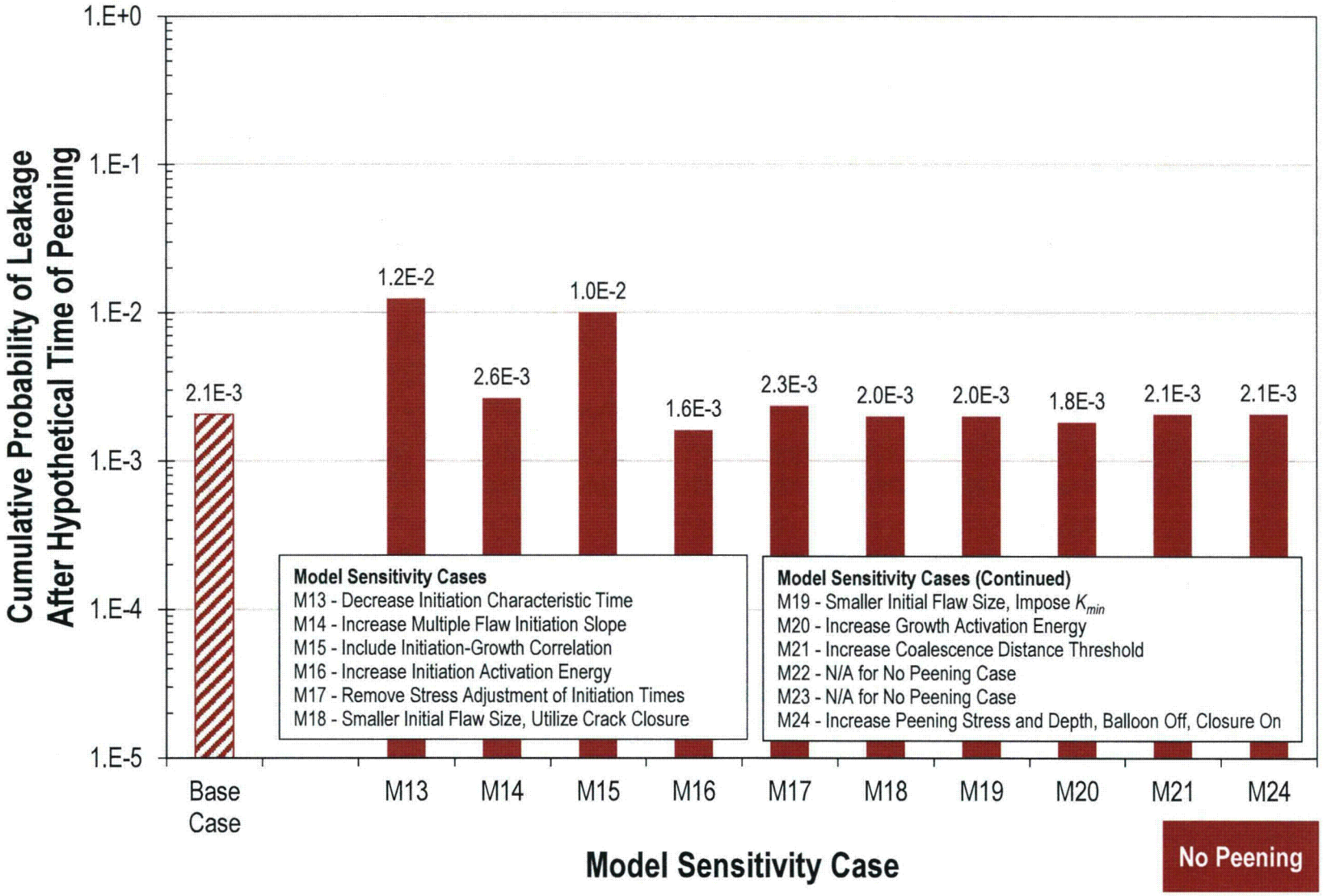

Figure A-29
Summary of Model Sensitivity Results for RVIN Probabilistic Model without Peening (continued)

A.10 Conclusions Regarding Appropriate In-Service Examination Requirements for DMWs in Primary System Piping Mitigated by Peening

The results of the probabilistic analysis of PWSCC on a general RVON support the relaxed UT inspection schedules prescribed in Section 4 of this report. Specifically, the cumulative leakage probability after the hypothetical time of peening is predicted to be reduced by:

- A factor of approximately 142 when the follow-up UT inspection is scheduled one cycle after peening and subsequent UT inspections are scheduled every 10 years (every interval)
- A factor of approximately 97 when the follow-up UT inspection is scheduled two cycles after peening and subsequent UT inspections are scheduled every 10 years (every interval)

The results of the probabilistic analysis of PWSCC on a general RVIN support the relaxed UT inspection schedules prescribed in Section 4 of this report. Specifically, the cumulative leakage probability after the hypothetical time of peening is predicted to be reduced by:

- A factor of approximately 11 when the follow-up UT inspection is scheduled two cycles after peening and no subsequent UT inspections are scheduled after follow-up examinations are performed
- A factor of approximately 12 when the follow-up UT inspection is scheduled three cycles after peening and no subsequent UT inspections are scheduled after follow-up examinations are performed
- A factor of approximately 9 when the follow-up UT inspection is scheduled six cycles after peening and no subsequent UT inspections are scheduled after follow-up examinations are performed

Many key input or modeling assumptions have been varied for Model Sensitivity Cases. While the leakage probability predictions are shown to vary for many of these cases, no case negates the prediction that a peened RVON or RVIN can maintain a lower probability of leakage with a relaxed inspection schedule (as compared to the unmitigated component). This is due primarily to the large margin of improvement predicted for the base cases.

Two Inspection Scheduling Sensitivity Cases investigate the impact of optional alterations to the inspection schedule/scope. Inspection Scheduling Sensitivity Case 2 demonstrates the importance of a pre-peening UT inspection.

A.11 References

1. D. Rudland, et al., "Development of Computational Framework and Architecture for Extremely Low Probability of Rupture (xLPR) Code," *Proceedings of the ASME 2010 Pressure Vessels & Piping Division / K-PVP Conference: PVP2010*, Bellevue, Washington, July 2010.
2. *xLPR Pilot Study Report.* U.S. NRC-RES, Washington, DC, and EPRI, Palo Alto, CA: NUREG-2110 and EPRI 1022860. 2012. [NRC ADAMS Accession No.: ML12145A470]
3. W. H. Press, S. A. Teukolsky, W. T. Vetterling, B. P. Flannery, *Numerical Recipes. The Art of Scientific Computing. Third Edition.* Cambridge University Press, Cambridge, MA, 2007.
4. *Materials Reliability Program: Technical Basis for Primary Water Stress Corrosion Cracking Mitigation by Surface Stress Improvement (MRP-267, Revision 1)*, EPRI, Palo Alto, CA: 2012. 1025839. [Freely Available at www.epri.com]
5. *Materials Reliability Program Generic Evaluation of Examination Coverage Requirements for Reactor Pressure Vessel Head Penetration Nozzles, Revision 1 (MRP-95R1NP)*, EPRI, Palo Alto, CA: 2004. 1011225. [NRC ADAMS Accession No.: ML043200602]
6. R. B. Abernethy, *The New Weibull Handbook, Second Edition*, Robert B. Abernethy, North Palm Beach, Florida, 1996.
7. *Materials Reliability Program: Crack Growth Rates for Evaluating Primary Water Stress Corrosion Cracking (PWSCC) of Alloy 82, 182, and 132 Welds (MRP-115)*, EPRI, Palo Alto, CA: 2004. 1006696. [Freely Available at www.epri.com]
8. T. L. Anderson, et al., "Development of Stress Intensity Factor Solutions for Surface and Embedded Cracks in API 579," *Welding Research Council Bulletin 471*, May 2002.
9. S. Marie, et al., "French RSE-M and RCC-MR code appendices for flaw analysis: Presentation of the fracture parameters calculation – Part III: Cracked Pipes," *International Journal of Pressure Vessels and Piping*, 84, pp. 614-658, 2007.
10. S. Xu, et al., "Technical Basis for Proposed Weight Function Method for Calculation of Stress Intensity Factor for Surface Flaws in ASME Section XI Appendix A," *Proceedings of the ASME 2011 Pressure Vessels & Piping Division / K-PVP Conference: PVP2011*, Baltimore, Maryland, July 2011.
11. *3-D Finite Element Software for Cracks: User's Manual v2.7.* Structural Reliability Technology – FEA Crack.
12. *ASME Boiler and Pressure Vessel Code 2011, Section XI, IWA-3330*, ASME, 2011.
13. M. Beghini and L. Bertini, "Fatigue Crack Propagation Through Residual Stress Fields with Closure Phenomena," *Engineering Fracture Mechanics*, Vol. 36, No. 3, pp. 379-387, 1990.
14. D. Rudland, et al., "PWSCC Crack Growth Mitigation with Inlay," *Proceedings of the ASME 2011 Pressure Vessels & Piping Division Conference: PVP2011*, Baltimore, Maryland, July 2011.
15. Case N-770-1, "Alternative Examination Requirements and Acceptance Standards for Class 1 PWR Piping and Vessel Nozzle Butt Welds Fabricated With UNS N06082 or UNS W86182 Weld Filler Material With or Without Application of Listed Mitigation Activities,"

Section XI, Division 1, American Society of Mechanical Engineers, New York, Approval Date: December 25, 2009.

16. *Materials Reliability Program: Development of Probability of Detection Curves for Ultrasonic Examination of Dissimilar Metal Welds (MRP-262, Revision 1) – Typical PWR Leak-Before-Break Line Locations*, EPRI, Palo Alto, CA: 2009. 1020451. [Freely Available at www.epri.com]
17. *PWR Materials Reliability Project, Interim Alloy 600 Safety Assessments for US PWR Plants (MRP-44): Part 1: Alloy 82/182 Pipe Butt Welds*, EPRI, Palo Alto, CA: 2001. TP-1001491, Part 1.
18. *Materials Reliability Program: Probabilistic Assessment of Chemical Mitigation of Primary Water Stress Corrosion Cracking in Nickel-Base Alloys (MRP-307), Zinc Addition and Hydrogen Optimization Mitigate Primary Water Stress Corrosion Cracking in Westinghouse Reactor Vessel Outlet Nozzles and Babcock & Wilcox Reactor Coolant Pump Nozzles*, EPRI, Palo Alto, CA: 2011. 1022852. [Freely Available at www.epri.com]
19. Memo from A. Csontos (NRC-NRR) to T.R. Lupold (NRC-NRR), "Hot Leg Flaw Evaluation Summary" dated August 18, 2011. [NRC ADAMS Accession No.: ML112160169]
20. *Materials Reliability Program: Advanced FEA Evaluation of Growth of Postulated Circumferential PWSCC Flaws in Pressurizer Nozzle Dissimilar Metal Welds (MRP-216, Rev. 1): Evaluations Specific to Nine Subject Plants*, EPRI, Palo Alto, CA: 2007. 1015400. [Freely Available at www.epri.com]
21. *PWSCC Prediction Guidelines*, EPRI, Palo Alto, CA: 1994. TR-104030. [Freely Available at www.epri.com]
22. J. A. Gorman, et al., "Correlation of Temperature with Steam Generator Tube Corrosion Experience," *Fifth International Symposium on Environmental Degradation of Materials in Nuclear Power Systems – Water Reactors*, E. Simonen and D. Cubicciotti, eds., American Nuclear Society, LaGrange Park, Illinois, 1992.
23. *Statistical Analysis of Steam Generator Tube Degradation*, EPRI, Palo Alto, CA: 1991. NP-7493. [Freely Available at www.epri.com]
24. C. Amzallag, et al., "Stress Corrosion Life Assessment of Alloy 600 PWR Components," *Ninth International Symposium on Environmental Degradation of Materials in Nuclear Power Systems – Water Reactors*, Edited by F.P. Ford et al., The Minerals, Metals & Materials Society (TMS), 1999.
25. Y. Yi and G. S. Was, "Stress and Temperature Dependence of Creep in Alloy 600 in Primary Water," *Metallurgical and Materials Transactions A,* Vol. 32, No. 10, pp. 2553-2560, 2001.
26. ASME Boiler and Pressure Vessel Code 2013, Section XI, Mandatory Appendix VIII, ASME, 2013.
27. ASME Boiler and Pressure Vessel Code 2011, Section III, Division 1, NB-3600, ASME, 2011.

B
PROBABILISTIC ASSESSMENT CASES FOR REACTOR PRESSURE VESSEL HEAD PENETRATION NOZZLES (RPVHPNS)

B.1 Scope of Assessment

There is currently a subpopulation of 24 reactor vessel top heads with Alloy 600 penetration nozzles operating in the U.S. that are potential candidates for peening mitigation. Currently, there are 41 replacement heads with PWSCC-resistant Alloy 690 nozzles in operation at U.S. PWRs, with two additional plants planning to perform head replacement by 2017. Of the 24 remaining Alloy 600 heads in operation, 19 operate at cold-leg temperature (i.e., cold heads) and five operate at a temperature significantly above cold-leg temperature (i.e., non-cold heads).

The probabilistic calculations presented in this section are designed to bound the conditions for all 24 of these heads, such that the conclusions of the probabilistic model are applicable to all U.S. PWRs that may perform peening mitigation of RPVHPNs. As described below, probabilistic calculations are performed for a non-cold head case (i.e., hot head) with an assumed head temperature (605°F) bounding that for the five candidate non-cold heads and for a cold head case with an assumed head temperature (561°F) bounding that for the 19 candidate cold heads.

B.1.1 CRDM and CEDM Nozzles

The design information tabulated in MRP-48 [1] shows that the large majority of RPVHPNs in the 24 heads with Alloy 600 penetration nozzles (1822 of 1890) are CRDM or CEDM nozzles. The basic geometry of CRDM/CEDM nozzles is illustrated in Figure B-1. All CRDM nozzles have the same basic nozzle tube dimensions (OD = 4.00 inches, ID = 2.75 inches, and wall thickness = 0.625 inch), while CEDM nozzles have roughly similar dimensions that vary among different plants designed by Combustion Engineering. The base case calculations presented in this section are based on the standard CRDM nozzle dimensions, while sensitivity cases are used to investigate the specific CEDM nozzle dimensions for two CE-designed heads.

B.1.2 Other RPVHPNs

A relatively small number of the Alloy 600 RPVHPNs currently operating in U.S. PWRs are nozzle types other than CRDM or CEDM nozzles (68 of 1890):

- 16 in-core instrumentation (ICI) nozzles in two CE-designed heads
- 22 J-groove head vent nozzles in 22 heads
- 8 J-groove auxiliary head adapter (AHA) nozzles in two Westinghouse-designed cold heads

- 2 "butt-weld" type head vent nozzles in two Westinghouse-designed heads
- 20 "butt-weld" type auxiliary head adapter (AHA) nozzles in five Westinghouse-designed cold heads

MRP-44 Part 2 [2] includes sketches illustrating each of these nozzles types. Because of their relatively small number, these other nozzles types were not explicitly included in the probabilistic calculations. Furthermore, the last two "butt-weld" type nozzles are not within the scope of Code Case N-729-1 [4] because they are not attached to the head with a partial-penetration (i.e., J-groove) weld. The conclusions of the probabilistic calculations are considered to extend to the full set of RPVHPNs attached using J-groove (i.e., partial penetration) welds for the following reasons:

- The greater diameter of the ICI nozzles results in a larger crack growth distance required for nozzle ejection compared to the case for a CRDM nozzle. Furthermore, there have not been any reported cases of PWSCC detected in ICI nozzles [3]. Thus, the ICI nozzles are conservatively represented with CRDM nozzle dimensions in the probabilistic calculations.
- For the same reasons as for the case of ICI nozzles, the J-groove type AHA nozzles are represented by CRDM nozzle dimensions in the probabilistic calculations.
- As was the case for the MRP-105 [5] probabilistic calculations forming a key part of the basis for inspection requirements for unmitigated RPVHPNs, the J-groove type head vent nozzles are not included in the probabilistic modeling. There is no more than one such nozzle in each head, it represents a much smaller potential break size than CRDM nozzles (about 1-inch diameter break compared to 2.75-inch ID typical for CRDM nozzles), and an ejection of a head vent nozzle would not result in an ejected control rod. It is considered that the head vent nozzle has a negligible effect on the probabilistic assessment of the set of RPVHPNs in a particular head.

Finally, the small number of "butt-weld" type nozzles noted above were not assessed as part of this study. These nozzles explicitly fall outside of the scope of ASME Code Case N-729-1 [4]. Thus, the technical basis of this report for inspection requirements for use with peening is not applicable to such nozzles not attached to the head with J-groove (i.e., partial penetration) welds.

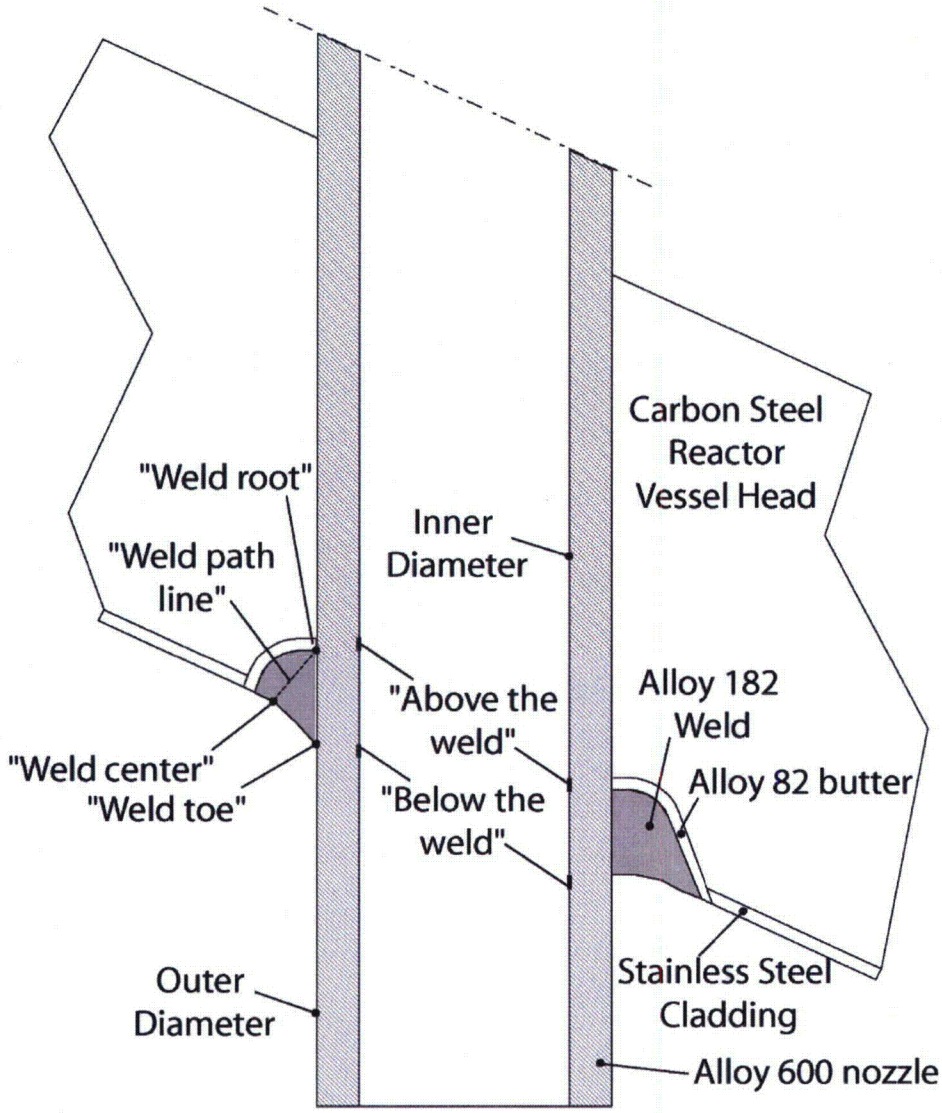

Figure B-1
Summary of General RPVHPN Geometry

B.2 Overall Modeling Methodology

The probabilistic model that was developed to study PWSCC in RPVHPNs was derived from the DM weld probabilistic model that is fully detailed in Appendix A. While the two models share a similar simulation framework, and several sub-models, there are many significant differences that will be discussed in this appendix. For conciseness, this appendix will reference portions of Appendix A where large overlap exists between the two models. To facilitate comprehension, this appendix has been organized analogously to Appendix A, in as much as possible.

A full description of the RPVHPN probabilistic modeling framework is given in the Section B.2.1. This is followed by Section B.2.2, which introduces the specific cracking modes (e.g., type, location, orientation, etc.) for which PWSCC initiation and growth are modeled; these modes will be referenced frequently throughout this appendix.

B.2.1 Probabilistic Modeling Methodology

The integrated probabilistic modeling framework that is used to study the effect of peening on RPVHPN PWSCC combines the individual models discussed in Sections B.3 through B.6. Namely, the probabilistic modeling framework is used to predict ejection criterion statistics, as discussed in Section B.7. Results generated with this model, using the inputs and uncertainties discussed in Section B.8, are given in Section B.9.

The RPVHPN probabilistic model applies a framework similar to the DM weld probabilistic model. In summary:

- Uncertainty propagation is handled by sampling input and parameter values from appropriately selected probability distributions (with appropriately selected bounds) in the main model loop, prior to the time looping structure. Important correlations are included.
- Event scheduling for a given weld, including operating, mitigation, inspection, and PWSCC initiation times, is developed in the main loop prior to entering the time looping structure.
- If one or more of the predicted PWSCC initiation times, adjusted for differences in temperature, are less than the final operating time and the time of peening (if applied), the time looping structure is entered. Each active flaw is allowed to grow until it reaches the end of the operation, its penetration is repaired, or its penetration nozzle is ejected.
- Initiations, ejections, repairs, among other events, are tracked as a function of operating cycle for each Monte Carlo realization and summary statistics are compiled at the end of each Monte Carlo run.

The central differences between the DM weld and RPVHPN models include:

- The RPVHPN model accounts for flaw initiation and growth on multiple penetrations (between 54 and 98 in a reactor vessel head), while the DM weld model only accounts for a single component, per Monte Carlo realization. Accordingly, a penetration loop exists inside the main loop and contains the time looping structure.
- The RPVHPN model accounts for several diverse modes of PWSCC initiation and growth (as detailed in Section B.2.2) as opposed to just axial and circumferential ID cracks. In fact, the majority of the model augmentation required for the RPVHPN model was to address new crack types and locations.
- In the case of DM welds, through-wall growth (i.e., leakage) is considered the end criteria (at which point simulation ends and summary statistics are compiled). For RPVHPNs, the end criteria is nozzle ejection; when leakage occurs due to a flaw at any location, it is assumed that this flaw immediately transitions to through-wall circumferential crack that grows along the top of the J-groove weld contour until it is repaired or it becomes large enough to fulfill the ejection criterion.
- Visual examination for leakage is modeled.
- There are other technical augmentations or logical revisions to be disclosed fully in the following sections.

A high level presentation of the main loop of the probabilistic model for a given weld is presented in Figure B-2 and a more detailed presentation of the time looping structure is given in

Figure B-3. The remainder of this section provides an end-to-end description of a single RPVHPN Monte Carlo run. Contrary to the rest of this appendix, this description is comprehensive and may have substantial overlap with Appendix A.

The initial conditions for the run are defined prior to entering the main loop. These initial conditions include all input parameters that remain constant throughout the run, such as the number and length of operating cycles, the frequency of inspections, certain weld geometry attributes, and the times of mitigation.

Following the definition of the initial conditions, the main loop is entered. The main loop is cycled for each Monte Carlo realization and is exited once all of the user-specified Monte Carlo realizations have been completed. After exiting the main loop, the program evaluates the results of the run, outputs certain information relevant to the study, and terminates the run.

At the beginning of each Monte Carlo realization, the values of reactor vessel head-specific distributed inputs are determined by random sampling. The distributions for each of the distributed inputs are user-defined. Then, the first flaw initiation model (detailed in Section B.4) is called to predict the initiation reference time for the reactor vessel head; the average time of the first PWSCC initiation in the head.

Following the definition of the head-specific values, the penetration loop is entered. This loop is cycled until PWSCC initiation and growth has been simulated for each penetration in the head. Upon exiting the penetration loop, the penetration results are cumulated to form penetration-specific and head-specific results.

At the beginning of each penetration cycle, penetration-specific distributed inputs are determined by random sampling. Then, the program invokes the multiple flaw initiation model (detailed in Section B.4) to predict the initiation times at all potential flaw sites. The flaw initiation times are compared to the "initiation end time": the final operating time, or, if peening is scheduled, the peening application time. The current penetration cycle is terminated if all of the predicted initiation times exceed the "initiation end time." If not, the initiation model assigns initiation conditions to each flaw with an initiation time occurring before the "initiation end time".

After determining that there are flaws that will initiate during the initiation time window in the current penetration, the program calls the load models (detailed in Section B.3) to determine the relevant loads at the various crack sites (including peening loads if peening is scheduled before the end of plant operation). This is different from, and more computationally efficient than, the DM weld model, which calculates load prior to initiation. The DM weld initiation model utilizes load information to incorporate a functional dependence of initiation time versus surface stress; the RPVHPN model does not; i.e., it is assumed that all locations on a given nozzle are equally likely to initiate PWSCC.

After attaining the stresses at locations of interest, the program enters the time looping structure for the current penetration.

The time looping structure is composed of an outer cycle-by-cycle loop with a nested within-cycle loop. The cycle-by-cycle loop may be terminated if the penetration is repaired or ejected. If this occurs, the program stores relevant information and cycles to the next penetration.

The within-cycle loop is entered if there is an active flaw on the current penetration whose initiation time is less than the time of the end of the current operating cycle. Immediately prior to

entering the within-cycle loop, any peening application that is scheduled for the current cycle is invoked resulting in new stress profiles utilized to predict crack growth.

If no flaw initiations occur prior to the end of the current sub-step in the within-cycle loop, the sub-step is skipped. Otherwise, at the beginning of the sub-step, the stress intensity factor for each active flaw is calculated based on the location of the flaw, the geometry of the flaw and its respective stress profile at the beginning of the sub-step. During each sub-step, all active flaws are grown using the flaw propagation model (detailed in Section B.5) that determines the flaw propagation rate and increases the depth and length of the flaw at a constant rate for the duration of the sub-step.

Before completing a given sub-step, the program checks if any flaw has reached through-wall (or through-weld in the case of the weld location), and if so, the cycle number is stored for a statistical summary generated at the end of the Monte Carlo run. Flaws that grow through-wall may or may not cause a leak (e.g., flaws that grow through-wall below the weld do not produce a leak). If a flaw does cause a leak, it is assumed to transition immediately to a circumferential through-wall crack that grows along the top of the J-groove weld contour. Flaws that are below the weld must grow in length to the nozzle OD annulus (i.e., the weld toe) before they are considered to leak.

At the end of each sub-step, any through-wall circumferential flaws are evaluated to predict if, cumulatively, they occupy enough of the nozzle circumference to cause ejection (detailed in B.7). The user can define an operating time at which an inspection has been performed by which time no nozzle ejections and no nozzle repairs had occurred. If ejection is predicted to occur (and the ejection time does not contradict the results of a user-defined assumed past inspection), the penetration is removed from service, the cycle number is stored for a statistical summary generated at the end of the Monte Carlo simulation, the current penetration simulation is terminated, and the program moves on to the next penetration. If the ejection result does contradict the results of the assumed past inspection, the code exits the penetration loop without saving any results and restarts the current Monte Carlo realization from the beginning of the main loop.

When all sub-steps of a given cycle have been completed, the program determines if an examination is to be performed at the end of the current cycle, and if the examination is to be ultrasonic (UT), bare-metal visual (BMV), or some combination of the two. If so, the inspection models (discussed in Section B.6) are called appropriately. If any flaw is detected (and its detection time does not contradict the results of an assumed user-defined past inspection) it is repaired, the cycle number is stored for a statistical summary generated at the end of the Monte Carlo simulation, the current penetration simulation is terminated, and the program moves on to the next penetration. In a similar fashion to an ejection occurrence, if the detection result contradicts the results of the assumed past inspection, the code exits the penetration loop without saving any results and restarts the current Monte Carlo realization from the beginning of the main loop. If a flaw is not detected, it remains active. After all scheduled inspections, the code returns to the cycle-by-cycle loop and continues to the next cycle or returns to the penetration loop if the cycle-by-cycle loop is complete.

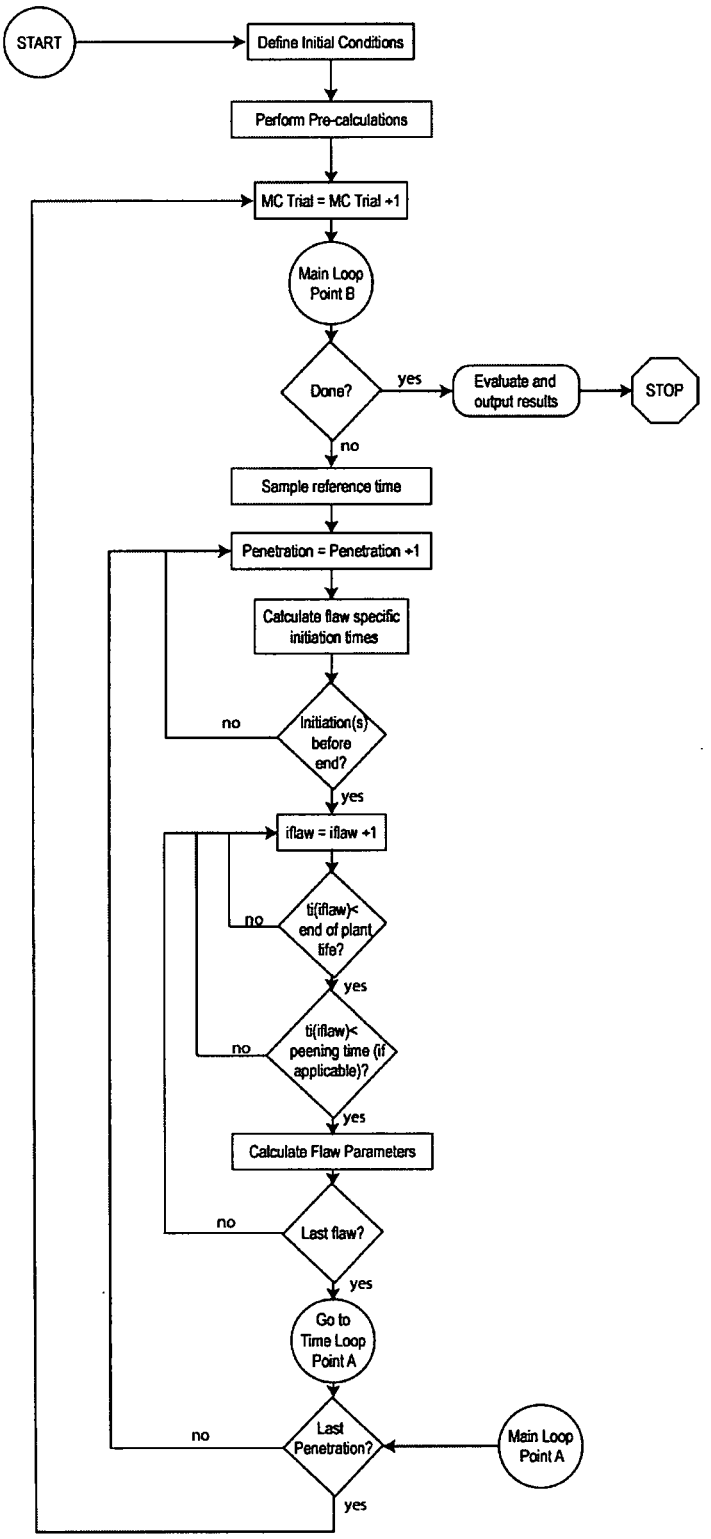

Figure B-2
RPVHPN Probabilistic Model Flow Chart: Main Loop

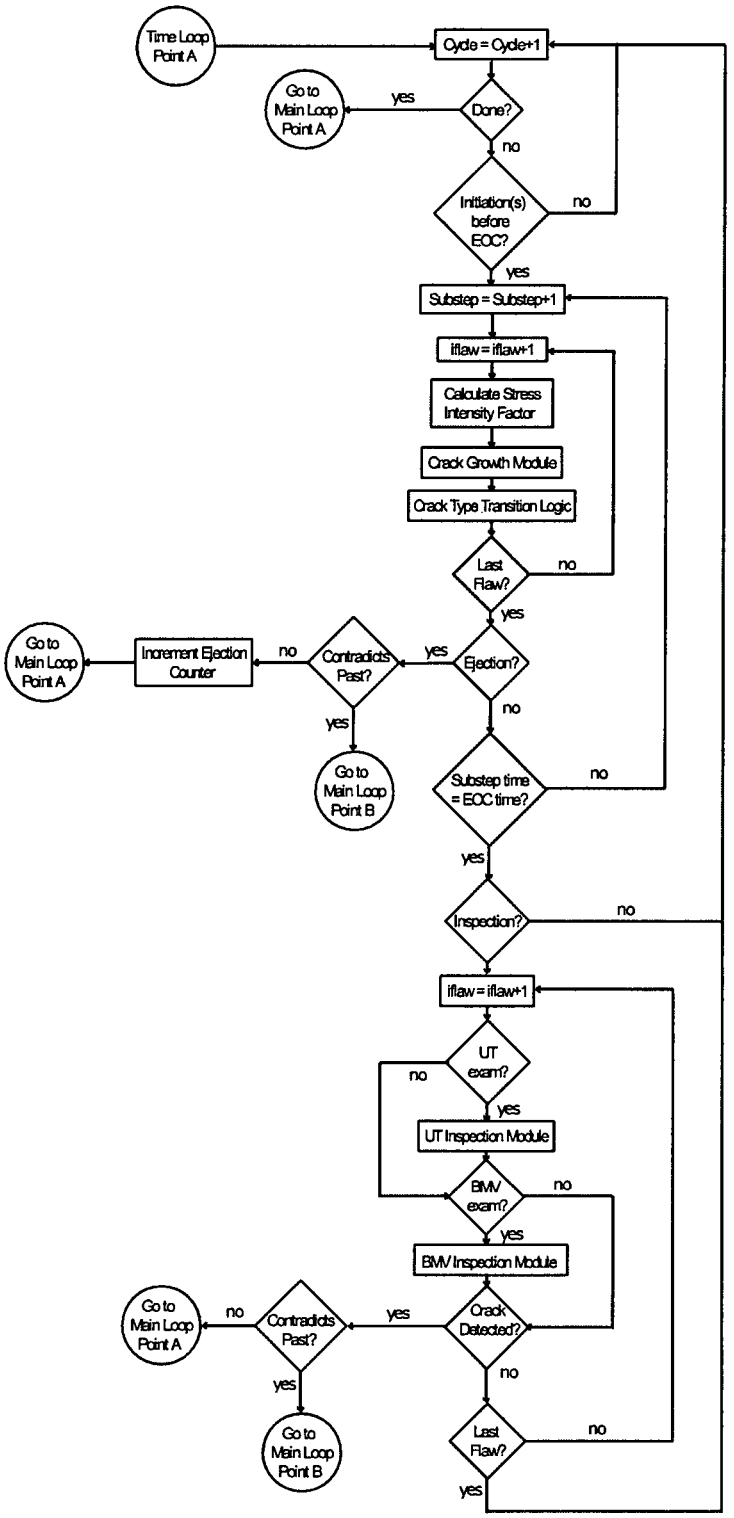

Figure B-3
RPVHPN Probabilistic Model Flow Chart: Time Loop